The Pennsylvania State University

The Graduate School

Department of Geosciences

LATE ORDOVICIAN OCEAN-CLIMATE SYSTEM AND PALEOBIOGEOGRAPHY

A Thesis in

Geosciences

by

Achim D. Herrmann

Submitted in Partial Fulfillment
of the Requirements
for the Degree of

Doctor of Philosophy

May 2004

The thesis of Achim D. Herrmann was reviewed and approved* by the following:

Mark E. Patzkowsky
Associate Professor of Geosciences
Thesis Advisor
Chair of Committee

Rudy L. Slingerland
Professor of Geosciences

Michael A. Arthur
Professor of Geosciences

Raymond Najjar
Associate Professor of Meteorology

David Pollard
Senior Research Associate

Peter Deines
Professor of Geochemistry
Associate Head for Graduate Programs and Research

*Signatures are on file in the Graduate School

ABSTRACT

The Ordovician was a time of extensive diversification and radiation of marine life. The end of the Ordovician is marked by a major mass extinction that is generally attributed to environmental perturbations associated with an extensive yet short-lived glaciation. The understanding of the climate dynamics during this crucial time period for the evolution of life is still fragmental.

I used an atmospheric general circulation model (AGCM) and an ocean general circulation model (OGCM) to study the climate system in the Caradoc (~454 Ma) and the Ashgill (~545 Ma). Specifically, I investigated the response to changes in paleogeography, atmospheric pCO_2, solar insolation cycles (obliquity), poleward ocean heat transport, and sea level. I also used a 3-dimensional ice sheet model to explore the necessary boundary conditions for ice sheet formation.

The AGCM results indicate that, assuming that pCO_2 did not fall below 8x PAL (a minimum value for this time period), a drop in pCO_2 and the paleogeographic evolution can only be regarded as preconditioning factors in the glaciation. In order for ice sheets to form, other factors must have changed such as a drop in sea level from its generally high Late Ordovician levels and/or a reduction in poleward ocean heat transport.

In all OGCM simulations, a drop in sea level led to a reduction in poleward ocean heat transport. This indicates a possible positive feedback that could have led to enhanced global cooling in response to pre-glaciation sea level drop. Continental drift could explain the observed global cooling trend in the Late Ordovician through a combined reduction in poleward ocean heat transport and increased ice-albedo effect. The ocean-climate system was also dominated by strong latitudinal temperature gradients and vigorous horizontal and vertical ocean circulation.

Finally, I compared the paleobiogeography of different taxonomic groups to the results of the climate models. The spatial distribution of Caradocian marine organisms is consistent with climatic and oceanographic gradients inferred from coupled ocean-climate models. The paleobiogeographic data thus provide an important evaluation of the global ocean-climate models and lead to a more robust inference of the early Late Ordovician global ecosystem.

TABLE OF CONTENTS

LIST OF FIGURES

LIST OF TABLES

ACKNOWLEDGEMENTS

I thank Dr. Mark E. Patzkowsky for suggesting and supervising this project. He gave me advice and encouragement throughout the duration of this study while at the same time giving me enough academic freedom' to pursue ideas of my own. For his many insightful discussions I am very grateful. I also thank my PhD committee of Drs. R. L. Slingerland, M. A. Arthur, R. Najjar, D. Pollard for their time, patience, and helpful advice. In addition, I thank B. J. Haupt for discussions and assistance in the ocean modeling effort.

In addition to the funding sources mentioned at the end of each chapter, this study was also financially supported by the Pennsylvania State University, Department of Geosciences through the Krynine Fund, an ExxonMobil Doctoral Fellowship, and appointments as research and teaching assistant positions. Funding was also provided by the American Association of Petroleum Geologists and the Geological Society of America (Northeastern Section Travel Funds).

Chapter 1

Introduction

Motivation: Improving the understanding of the Late Ordovician climate system

An extraordinary rise in marine biodiversity occurred in the Ordovician (e.g., Sepkoski, 1996), followed by the second largest mass extinction event of the Phanerozoic (Fig. 1.1). This mass extinction event coincided with a major glaciation. This glaciation was presumably a short-lived climatic fluctuation that interrupted a prolonged greenhouse interval (Brenchley et al., 2003; Sheehan, 2001). Evidence for extraterrestrial bolide impacts is missing (Orth et al., 1986; Robertson et al., 1991; Wang et al., 1992; Wilde et al., 1986), and thus the mass extinction event is generally attributed to climatic and oceanographic changes associated with the glaciation event.

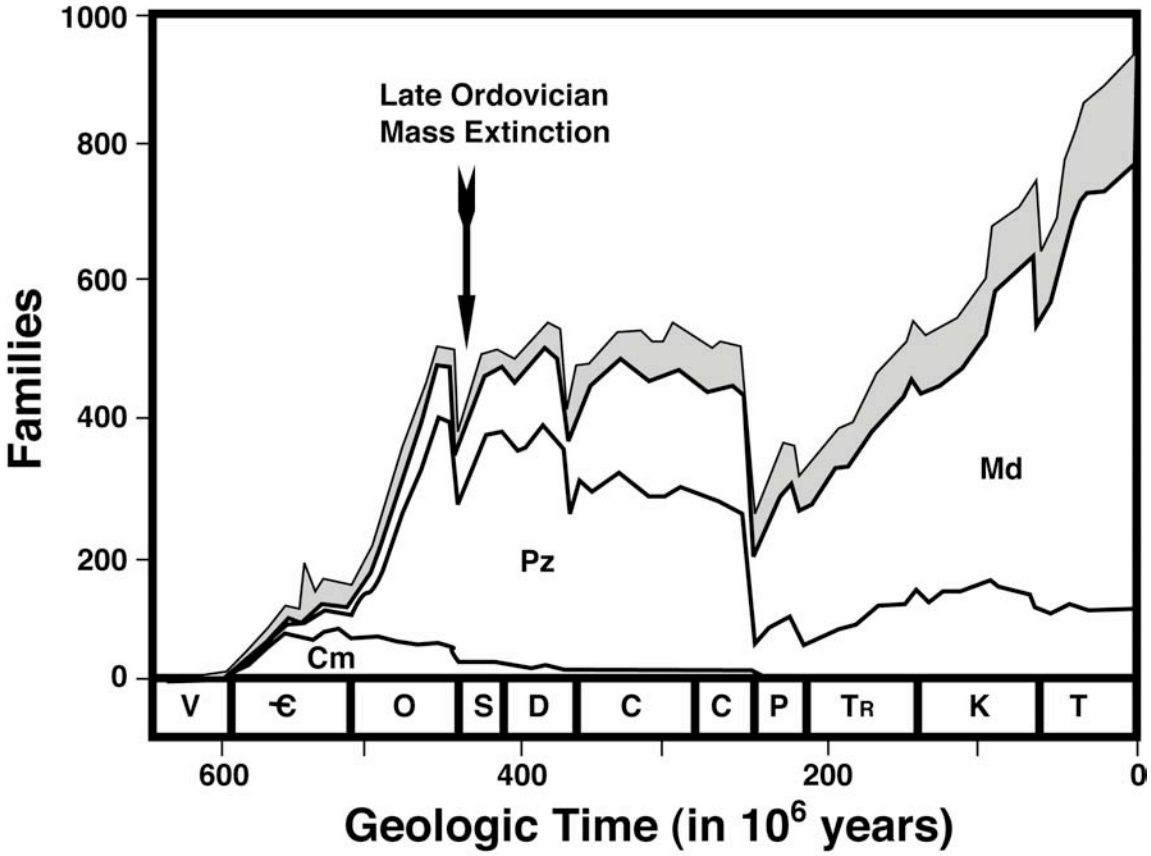

Figure 1.1: Family diversity of marine organisms through the Phanerozoic (after Sepkoski, 1996), showing the location of the Late Ordovician mass extinction. V- Vendian; ∈ - Cambrian; O – Ordovician; S – Silurian; D – Devonian; C – Carboniferous; P – Permian; TR – Triassic; J – Jurassic; K – Cretaceous; T – Tertiary; Cm – Cambrian Evolutionary Fauna (EF); Pz – Paleozoic EF; Md – Modern EF. Gray area indicates poorly skeletonized fossils.

However, our understanding of the Late Ordovician ocean-climate system is still fragmental. Only a few numeric climate studies have been conducted for the last stage of the Ordovician (Crowley and Baum, 1991; Crowley and Baum, 1995; Gibbs et al., 1997). Only one coupled atmosphere-ocean model has been proposed for this time period (Poussart et al., 1999) and the inference of climatic gradients of ocean surface temperatures during the Late Ordovician are mostly based on paleobiogeographic

interpretations. Previous numerical models of the ocean-climate system focused mainly on the perturbation of the global carbon cycle as a cause for the initiation of the glaciation (e.g., Brenchley et al., 2003; 1995; Kump et al., 1999). The ocean general circulation model of Poussart et al (1999) is also at odds with geochemical and stratigraphic data that suggest a sluggish global ocean with deep, saline, anoxic bottom waters (Berry and Wilde, 1978; Railsback et al., 1990). In addition, none of these previous models investigated and evaluated long term trends like sea level changes or continental drift directly by comparing different paleogeographic reconstructions. However, evaluating these changes are important as it is increasingly recognized that the glaciation might not have been as short lived as proposed, as evidence for long term cooling and potential glaciations as early as the Caradoc is mounting (Frakes et al., 1992; Pope and Steffen, 2003). In addition, opposing interpretations exist about the fate of atmospheric pCO_2 during the glaciation. While Kump et al. suggest that pCO_2 increased to near 16x pre-industrial atmospheric levels (PAL), Brenchley et al. (1995; 1994) propose that during the glacial interval, pCO_2 levels were reduced to 7-10x PAL.

In order to better understand the climate dynamics during this crucial time period for the evolution of life, I used numerical models to investigate the response of the Late Ordovician climate system to perturbations at different time scales. In particular, I investigated perturbations of the climate system that included changes in sea level and solar insulation cycles (obliquity cycles), which operated at time scales of thousands of years. I also evaluated the impact of paleogeographic change and atmospheric pCO_2 during the Late Ordovician, which operated at timescales of millions of years. I then compared the results of the ocean general circulation model to the paleobiogeographic

distribution of 490 invertebrate genera to test whether their distribution can be explained with physical factors (e.g., surface temperature or surface circulation patterns) as hindcasted by these models. Early Paleozoic moist land surfaces were probably coated with eubacteria and cyanobacteria in the absence of vascular land plants and land animals (Gray, 1993). Therefore, the atmospheric model results cannot be evaluated with terrestrial biogeographic data.

Structure of this thesis

The results of this study are divided into four chapters. Each one of these four chapters is written independently of one other and three of these (chapter 2, 3, and 4) have been submitted to peer-reviewed journals for publication (Herrmann et al., in press-a; Herrmann et al., 2003; Herrmann et al., in press-b). Chapters 2 and 3 present results from coupled atmospheric general circulation and ice-sheets models for the Late Ordovician. In chapter 4 I discuss the results of ocean general circulation model studies. In chapter 5 I compare the results of the ocean general circulation results to the paleobiogeographic distribution of major taxonomic groups during the Caradoc. The concluding chapter summarizes the results of this research and discusses their implications.

Appendix A contains the Internet locations where the data files for the different climate and ocean models can be downloaded. Appendix B contains the data matrix used in the paleobiogeographic study of chapter 5. Appendix C contains the different

collections of the Paleobiology Database used in the paleobiogeographic study of chapter 5.

Significance of each chapter

Chapter 2 presents results from sensitivity experiments with the atmospheric general circulation model GENESIS and a three-dimensional ice-sheet model on two stages of the Late Ordovician (Caradoc, ~454 Ma; Ashgill, ~446 Ma). This part of the study aimed at testing the hypothesis that changes in atmospheric pCO_2 alone could have been the main driver of the observed global cooling and initiation of the glaciation. To this end, I investigated the necessary boundary conditions for ice sheet formation with pCO_2 values of 8-18x PAL, which is the range of proposed pCO_2 values for this time period (Berner, 1994; Berner and Kothavala, 2001; Yapp and Poths, 1992) (Fig. 1.2). In addition, I performed these simulations with high and low sea levels, and two values of poleward ocean heat transport to determine the importance of these variables on long term global cooling during the Late Ordovician. This study showed that continental drift and a drop in pCO_2 during the Late Ordovician cooled the global climate, and is consistent with the stratigraphic record (Frakes et al., 1992; Pope and Steffen, 2003). However, changes in additional factors, such as a drop in sea level, a reduction in poleward ocean heat transport, or a combination of both, were required to initiate ice sheet formation.

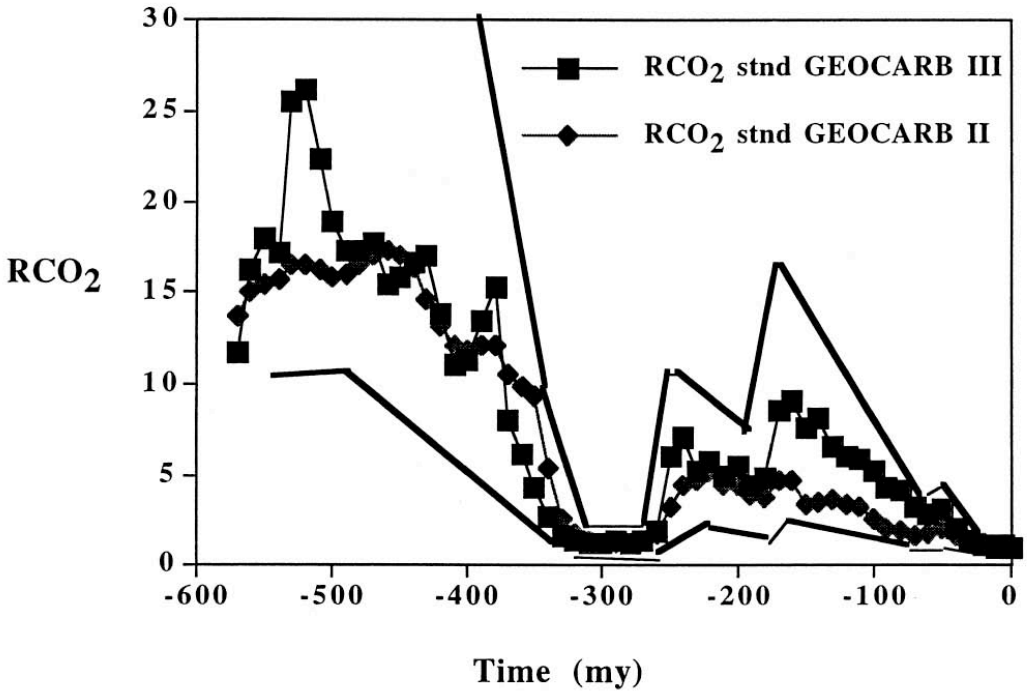

Figure 1.2: Estimates of atmospheric pCO_2 through the Phanerozoic based on geochemical models (from Berner and Kothavala, 2001). RCO_2 is the ratio of atmospheric CO_2 compared to pre-industrial levels of 280 ppm.

Chapter 3 presents results from additional ice-sheet model experiments to investigate the sensitivity of waxing and waning of these ice sheets to changes in atmospheric pCO_2 and orbital forcing at the obliquity timescale (30 to 40 kyr). This study aims at investigating the contradictory proposals of atmospheric pCO_2 levels during the glacial interval (Brenchley et al., 1995; Kump et al., 1999). In addition, the orbital variations used in the climate model in this chapter addresses 'bias' in chapter one where only cold summer orbits were used. These simulations indicate that large ice sheets, grown during extreme periods of low pCO_2 (8x PAL), can subsequently be sustained during periods of higher pCO_2 (9-10x PAL) that would otherwise prevent the growth of ice from ice-free starting conditions. Thus, if atmospheric pCO_2 was one of the main

drivers of climate during the Late Ordovician then atmospheric pCO_2 must have risen to greater than 10x PAL to melt the ice-sheets in the higher southern latitudes and end glaciation. These results support the proposed rise of pCO_2 during the glaciation as put forward by Kump et al. (1999).

Chapter 4 presents results from atmospheric general circulation and ocean general circulation model simulations for the Caradoc and Ashgill. The absence of a dynamical ocean in the atmospheric general circulation model GENESIS prevents the investigation of atmosphere-ocean interactions and potential climate feedbacks of the global ocean. I therefore used the output from the atmospheric general circulation model (chapter 2) to produce the forcing boundary conditions and initial conditions for an ocean general circulation model (MOM v.2.2) in order to investigate oceanic feedbacks to the these perturbations. In particular, I looked into changes in ocean heat transport in response to continental drift, and changes in atmospheric pCO_2 and sea level. The results indicate that the long-term cooling trend can be explained by progressive cooling of the global ocean in response to lower levels of atmospheric pCO_2, but sea level changes and paleogeographic changes were also very important. Sea level changes however had the strongest influence on surface circulation patterns. In addition, these models indicate the presence of strong meridional overturning in all simulations which are at odds with the previous interpretations of saline, deep, anoxic bottom waters (e.g., Berry and Wilde, 1978; Railsback et al., 1990). This has important implications for the Late Ordovician mass extinction event as changes in oxygenation state of the deep ocean is often hypothesized as a kill mechanism (e.g., Brenchley et al., 2003; Brenchley et al., 1995; Brenchley and Newall, 1984).

Chapter 5 presents a comparison of the ocean general circulation model results with a paleobiogeographic study for the Caradoc. The paleobiogeographic study consists of an extensive literature review of previous biogeographic studies as well as an original multivariate analysis of 11,067 occurrences of 490 marine invertebrate genera which were downloaded from the Paleobiology Database. The spatial distribution of these marine organisms is consistent with climatic and oceanographic gradients inferred from coupled ocean-climate models and suggested by earlier biogeographic workers. The paleobiogeographic data thus provide an important corroboration of the global ocean-climate models and lead to a more robust inference of the early Late Ordovician global ecosystem.

References

Berner, R.A., 1994, GEOCARB II: A revised model of atmospheric CO_2 over Phanerozoic time: American Journal of Science, v. 294, p. 56-91.

Berner, R.A., and Kothavala, Z., 2001, GEOCARB III: A revised model of atmospheric CO2 over Phanerozoic time: American Journal of Science, v. 301, p. 182-204.

Berry, W.B.N., and Wilde, P., 1978, Progressive ventilation of the oceans - an explanation for the distribution of the Lower Paleozoic black shales: American Journal of Science, v. 278, p. 257-275.

Brenchley, P.J., Carden, G.A., Hints, L., Kaljo, D., Marshall, J.D., Martma, T., Meidla, T., and Nõlvak, J., 2003, High-resolution stable isotope stratigraphy of Upper

Ordovician sequences: Constraints on the timing of bioevents and environmental changes associated with mass extinction and glaciation: Geological Society of America Bulletin, v. 115, p. 89-104.

Brenchley, P.J., Carden, G.A.F., and Marshall, J.D., 1995, Environmental changes associated with the 'first strike' of the Late Ordovician mass extinction: Modern Geology, v. 22, p. 69-82.

Brenchley, P.J., Marshall, J.D., Carden, G.A.F., Robertson, D.B.R., Long, D.G.F., Meidla, T., Hints, L., and Anderson, T.F., 1994, Bathymetric and isotopic evidence for a short-lived Late Ordovician glaciation in a greenhouse period: Geology, v. 22, p. 295-298.

Brenchley, P.J., and Newall, G., 1984, Late Ordovician environmental changes and their effect on faunas, *in* Bruton, D.L., ed., Aspects of the Ordovician System, Volume 295: Oslo, Universitetsforlaget - Palaeontological Contributions from the University of Oslo, p. 65-79.

Crowley, T.J., and Baum, S.K., 1991, Toward reconciliation of Late Ordovician (~440 Ma) glaciation with very high CO2 levels: Journal of Geophysical Research, v. 96, p. 597-610.

—, 1995, Reconciling Late Ordovician (440 Ma) glaciation with very high CO_2 levels.: Journal of Geophysical Research, v. 100, p. 1093-1101.

Frakes, L.A., Francis, J.E., and Syktus, J.I., 1992, Climate modes of the Phanerozoic: Cambridge, Cambridge University Press, 274 p.

Gibbs, M., Barron, E.J., and Kump, L.R., 1997, An atmospheric pCO_2 threshold for glaciation in the Late Ordovician: Geology, v. 25, p. 447-450.

Gray, J., 1993, Major Paleozoic land plant evolutionary bioevents: Palaeoecology Palaeoclimatology Palaeogeography, v. 104, p. 153-169.

Herrmann, A.D., Haupt, B.J., Patzkowsky, M.E., Slingerland, R.L., and Seidov, D., in press-a, Response of Late Ordovician paleoceanography to changes in sea level, continental drift, and atmospheric pCO_2: potential causes for long-term cooling and glaciation: Palaeoecology Palaeoclimatology Palaeogeography.

Herrmann, A.D., Patzkowsky, M.E., and Pollard, D., 2003, Obliquity forcing with 8-12x pre-industrial levels of atmospheric pCO_2 during the Late Ordovician glaciation: Geology, v. 31, p. 485–488.

—, in press-b, The impact of paleogeography, pCO_2, poleward ocean heat transport and sea level change on global cooling during the Late Ordovician: Palaeogeography, Palaeoclimatology, Palaeoecology.

Kump, L.R., Arthur, M.A., Patzkowsky, M.E., Gibbs, M.T., Pinkus, D.S., and Sheehan, P.M., 1999, A weathering hypothesis for glaciation at high atmospheric pCO_2 during the Late Ordovician: Palaeogeography, Palaeoclimatology, Palaeoecology, v. 152, p. 173-187.

Orth, C.J., Gilmore, J.S., Quitana, L.R., and Sheehan, P.M., 1986, The terminal Ordovician extinction: Geochemical analysis of the Ordovician/Silurian boundary, Anticosti Island, Quebec: Geology, v. 14, p. 433-436.

Pope, M.C., and Steffen, J.B., 2003, Widespread, prolonged late Middle to Late Ordovician upwelling in North America: A proxy record of glaciation?: Geology, v. 31, p. 63-66.

Poussart, P.R., Weaver, A.J., and Barnes, C.R., 1999, Late Ordovician glaciation under high atmospheric CO_2: a coupled model analysis: Paleoceanography, v. 14, p. 542-558.

Railsback, L.B., Ackerly, S.C., Anderson, T.F., and Cisne, J.L., 1990, Palaeontological and isotope evidence for warm saline deep waters in Ordovician oceans: Nature, v. 343, p. 156-159.

Robertson, D.B.R., Brenchley, P.J., and Owen, A.W., 1991, Ecological disruption close to the Ordovician-Silurian boundary: Historical Biology, v. 5, p. 131-144.

Sheehan, P.M., 2001, The Late Ordovician mass extinction: Annual Review of Earth Planetary Sciences, v. 29, p. 331-340.

Wang, K., Chatterton, B.D.E., Attrep, M., and Orth, C.J., 1992, Iridium abundance maxima at the latest Ordovician mass extinction horizon, Yangtze Basin, China: Terrestrial or Extraterrestrial: Geology, v. 20, p. 39-42.

Wilde, P., Berry, W.B.N., Quinby-Hunt, M.S., Orth, C.J., Quitana, L.R., and Gilmore, J.S., 1986, Iridium abundances across the Ordovician-Silurian stratotype: Science, v. 233, p. 339-341.

Yapp, C.H., and Poths, H., 1992, Ancient atmospheric CO_2 inferred from natural geothites: Nature, v. 355, p. 342-344.

Chapter 2

The impact of paleogeography, pCO_2, poleward ocean heat transport and sea level change on global cooling during the Late Ordovician

Abstract

We performed sensitivity experiments with the global climate model GENESIS on two stages of the Upper Ordovician (Caradocian, ~454 Ma; Ashgillian, ~446 Ma) under a range of atmospheric pCO_2 values (8-18x PAL; Pre-industrial Atmospheric Level), high and low sea level, and two values of poleward ocean heat transport in order to determine the importance of these variables on global cooling. We then coupled a 3-dimensional ice sheet model to the global climate model in order to investigate the necessary boundary conditions for ice sheet formation. All simulations with a high sea level and normal heat transport remain free of ice sheets, even with pCO_2 levels as low as 8x PAL. In the Caradocian simulations, ice sheets form in three scenarios: (1) with pCO_2 of 8x PAL and a low sea level and normal poleward ocean heat transport, (2) with pCO_2 of 8x PAL and a high sea level and reduced (50% of normal) poleward ocean heat transport, and (3) with pCO_2 of 15x PAL and a low sea level and reduced poleward ocean heat transport. In the Ashgillian simulations, ice sheets form in only two scenarios: (1) with pCO_2 of 8x PAL and a low sea level and normal poleward ocean heat transport, or (2) with pCO_2 of 8x PAL and a high sea level and reduced poleward ocean heat transport. The ice sheets in the Ashgillian experiments are larger and thicker than the ice sheets in the Caradocian simulations because the southward movement of Gondwana increased

land area in the higher southern latitudes where ice sheets could grow. The threshold for glaciation under Ashgillian paleogeography is 8x PAL and either a low sea level (exposed shelves) or a reduced poleward ocean heat transport. While the paleogeographic evolution and a drop in pCO_2 during the Late Ordovician cooled the global climate, changes in additional factors were required to initiate ice sheet formation, such as a drop in sea level, a reduction in poleward ocean heat transport, or a combination of both.

Introduction

Global environmental changes during the Late Ordovician have been subject to intense research. In particular, the glaciation at the end of the Ordovician has attracted attention not only because of its association with a major extinction event, but also because it required unusual causes due to its apparent short duration during an otherwise warm period in Earth's climate.

Several authors have suggested that the glaciation lasted for less than 1 Myr and was confined to the Hirnantian, which is the uppermost stage of the Ordovician. This hypothesis is supported by data on changes in eustatic sea level (Brenchley et al., 1994), stratigraphy (Paris et al., 1995) and carbon and oxygen isotopes (Qing and Veizer, 1994; Marshall et al., 1997). This time span is presumably too short to allow for tectonic mechanisms, i.e. the southward movement of Gondwana towards the South Pole, as the sole cause for this glaciation (Gibbs et al., 2000). However, evidence also exists for a long-term cooling from the Middle to the Late Ordovician. Isotopic as well as lithologic evidence can be interpreted in terms of progressive cooling of shallow ocean waters

during the Middle to Late Ordovician (Patzkowsky and Holland, 1993; Qing and Veizer, 1994; Lavoie, 1995; Holland and Patzkowsky, 1996, 1997; Pope and Read, 1997; Patzkowsky et al., 1997; Lavoie and Asselin, 1998; Veizer et al., 1999). Based on the temporal and spatial distribution of glacial marine and continental deposits, it has even been argued that the late Middle Ordovician marks the initiation of glaciation (Frakes and Francis, 1988; Frakes et al., 1992). The presence of wide-spread upwelling conditions along the southern margin of Laurentia in the Middle Ordovician also support the interpretation that the initiation of the glaciation occurred during this time period and reached its maximum in the Hirnantian (Pope and Steffen, 2003). An additional problem related to the glaciation is that numerical models of the carbonate-silicate cycle (Berner, 1994; Berner and Kothavala, 2001) as well as geochemical data from paleosols (Yapp and Poths, 1992) indicate that during the Late Ordovician atmospheric pCO_2 was high (~14±6x pre-industrial pCO_2 (PAL)) leading to an overall warm climate.

Recent research has focused on explaining the short duration of the glaciation by a drawdown of atmospheric pCO_2. Brenchley et al. (1994, 1995) proposed that an increase in marine productivity and organic carbon burial led to a rapid drawdown in atmospheric pCO_2. Kump et al. (1999) on the other hand favored a weathering model in which atmospheric pCO_2 values were reduced by increased silicate weathering rates below a threshold value that promoted ice-sheet growth. Several numerical model studies found a high sensitivity of the formation of permanent snow cover, necessary for the formation of ice sheets, with respect to atmospheric pCO_2 values for the Late Ordovician paleogeography (Crowley and Baum, 1991, 1995; Gibbs, 1996; Gibbs et al., 1997, 2000; Poussart et al., 1999).

Although these studies have hypothesized that the paleogeographic evolution during the Late Ordovician contributed to global cooling as a necessary pre-conditioning factor, this influence has never been quantified by directly comparing paleogeographies for different stages of the Late Ordovician. In addition, the previous studies simulated climate with a sea level lowstand that would have occurred only at peak glaciation. None have simulated climate with a sea level highstand, the condition prior to glaciation. Estimates of eustatic sea level highstands prior to maximum glaciation range from ~175 m (Algeo and Seslavinsky, 1995a, b), ~300 m (Vail et al., 1977) to ~600 m (Hallam, 1984) above present sea level. Due to the high sea level, extensive continental areas were flooded. For example, Algeo and Seslavinsky (1995a, b) estimate that 60.9% of Laurentia and 21.7% of Gondwana were flooded during the Late Ordovician. Since previous computer models have not accounted for the smaller continental area exposed during high sea level, they were potentially biased towards colder global temperatures and ice sheet formation. During the Late Ordovician lowstand more landmass was closer to the poles and the exposed land area would have increased the albedo; both factors that enhance ice-sheet formation.

We therefore extend previous sensitivity studies by 1) quantifying the contribution of the movement of Gondwana during the Late Ordovician to global cooling as a pre-conditioning factor by directly comparing Caradocian and Ashgillian paleogeographies under a reasonable range of pCO_2 values, by 2) assessing the effect of the reduced land area at high sea level, which was the condition prior to glaciation, 3) evaluating the influence of reduced poleward ocean heat transport on global climate, and

4) by coupling a 3-dimensional ice sheet model to the global climate model in order to investigate the necessary boundary conditions for glaciation.

We find that under the range of pCO_2 values, high sea level and normal poleward ocean heat transport, ice sheets could not form. However, with lower sea level and thus more exposed land area, global annual average temperatures drop significantly and glaciation can be initiated in the Ashgillian and Caradocian under a pCO_2 level of 8x PAL. In addition, with a reduced poleward ocean heat transport, extensive ice sheets also form in the Ashgillian under a pCO_2 level of 8x PAL and a high sea level, while the Caradocian simulations with these boundary conditions only lead to very small ice sheets.

Previous Ordovician Model Results

Several previous modeling studies have assessed the role of pCO_2 and paleogeography in causing the Late Ordovician glaciation. Crowley et al. (1987) showed that because of the closeness of the coast of the Gondwana supercontinent to the South Pole the ocean's high thermal inertia could cause summertime temperatures at the poles to remain below freezing. This would lead to year-round snow accumulation. Crowley and Baum (1991) and Crowley et al. (1993) tested the hypothesis that the unique paleogeographic position of Gondwana permitted permanent snow cover in parts of Gondwana under high pCO_2 levels. Using an energy balance model, Crowley and Baum (1991) found that a rotation of Gondwana over the pole led to changes in ice area on Gondwana and that ice area peaked when the pole was tangent to the continent. Crowley et al. (1993) supported these results with a general circulation model and subsequently

Crowley and Baum (1995) showed that with an elevated topography, reduced solar luminosity and pCO_2 levels of 14x PAL glaciation was possible in the Late Ordovician.

Gibbs (1996) and Gibbs et al. (1997) performed sensitivity studies with a general circulation model under a range of different pCO_2 levels and found that a reduction from 14x PAL to 10x PAL led to a significant drop in annual average global temperature and more extensive snow accumulation. Using a coupled atmosphere-ocean-sea ice model, Poussart et al. (1999) also showed that permanent snow cover in southern Gondwana could be maintained at 10x PAL.

Gibbs et al. (2000) assessed the role of paleogeography as a precondition for the glaciation by comparing general circulation model results for Late Ordovician and Early Silurian paleogeographies. This study showed that for simulations under low atmospheric pCO_2 values (10x PAL) both paleogeographies led to glaciation, while simulations under high atmospheric pCO_2 values (18x PAL) remained ice-free for both paleogeographies. However, the model indicated that glaciation would be possible under 14x pCO_2 for the Late Ordovician paleogeography, while the Early Silurian remained ice-free. Gibbs et al. (2000) concluded that this was a consequence of Gondwana's position over the pole which preconditioned the earth system for glaciation by making it more susceptible to changes in atmospheric pCO_2. Nevertheless, none of these studies addressed directly the question of how important the paleogeographic evolution during the Late Ordovician was for the timing of the glaciation. Gibbs et al. (2000) only effectively demonstrated that a glaciation could not be sustained for a Silurian paleogeography under high atmospheric pCO_2 values. Moreover, none of these studies have used the climate model output to drive a dynamic ice-sheet model. The only

criterion for establishing the initiation of glaciation was whether permanent snow cover existed during the austral summer in higher Southern latitudes or not, regardless of snow thickness or snow cover extent.

Model Description and Boundary Conditions

The atmospheric general circulation climate model experiments were completed using the Global Environmental and Ecological Simulation of Interactive Systems (GENESIS v. 2.0; Thompson and Pollard, 1997). The GENESIS model has a spectral resolution of ~3.75º x 3.75º (T31) and 18 vertical layers. It includes a 2º x 2º (2X2) land surface model incorporating physical effects of vegetation, a six-layer soil model, a snow model, a three layer thermodynamic sea-ice model and a slab mixed layer ocean (Pollard and Thompson, 1995a, 1995b; Thompson and Pollard, 1997).

The GENESIS climate output was used to drive a high-resolution dynamic ice sheet model. The model is a 3-dimensional model with a 1º x 1º resolution and thermodynamics following Ritz el al. (1997). A 2-km bedrock with vertical heat diffusion is included and the surface mass balance was calculated with a degree-day method. The degree-day parameterization uses empirical relations between observed ablation based on a long history of field studies (mainly on Greenland) and positive degree-days. The degree-day method provides a robust estimate of the mass budgets during the Last Glacial Maximum and modern day for Antarctica and Greenland (Pollard and PMIP Participating Groups, 2000). The net surface balance estimates for modern-day Antarctica and Greenland are well within the observational limits (~15 cm/year)

(Pollard and PMIP Participating Groups, 2000; their figure 1). The averaged last ten years of the stored atmospheric general circulation model climate results were used to drive the ice sheet model for 200,000 years to equilibrium. All previous studies have used permanent summer snow cover to decide whether glaciation occurred or not. However, this can be misleading because the formation of ice sheets depends not only on permanent summer snow cover, but also on snow fraction. Even extensive permanent snow cover during the summer may not lead to ice growth if the snow fraction of the model grid points is less than one. It is therefore important to use the ice sheet model in order to better constrain the initiation of glaciation. Pollard and Thompson (1997) describe the coupling process between GENESIS and the ice sheet model in detail.

The boundary conditions for the experiments include two different paleogeographies, an elevated constant topography, a series of different atmospheric pCO_2 values, reduced solar luminosity, pre-industrial values for greenhouse gases other than CO_2, cold-winter orbital parameters, bare soil, and no vegetation (Table 2.1). In order to focus on the effect of paleogeography and pCO_2, and to facilitate the comparison of our results with previous modeling studies (Crowley and Baum, 1991, 1995; Gibbs, 1996; Gibbs et al., 1997, 2000; Poussart et al., 1999) as many boundary conditions as possible were made the same as or close to the same values as these other studies. In the following subsections, the initial and boundary condition used in this study are discussed in more detail.

Table 2.1: Boundary conditions used for the GENESIS climate-model experiments reported in this study. See text for explanations.

Boundary Condition	**How varied**
Land-Sea distribution	Paleogeography of Scotese and McKerrow (1991); Shoreline position after Scotese (1997)
Topography	250 m for coastal grid points and 500 m for all other land grid points
Orbital Parameters	"Cold-Summer Orbit" eccentricity: 0.06 obliquity: 22. precession: 270. perihelion to N.H. vernal equinox
Solar luminosity	4.5% reduction of present day
Vegetation and soil type	No vegetation with intermediate soil color values
Poleward ocean heat transport	1) Value for normal poleward ocean that replicates the modern climate with GENESIS v.2.0, and 2) 50% of this modern value
Atmospheric pCO_2	5040 ppm (18x PAL); 4200 ppm (15x PAL); 3360 ppm (12x PAL); 2800 ppm (10x PAL); 2240 ppm (8x PAL)

Land-Sea Distribution and Topography

Late Ordovician paleogeographic reconstructions are based on Scotese and McKerrow (1990, 1991) and Scotese (1997). These reconstructions were chosen to provide consistency with most published oceanographic and climate models for the Ordovician (e.g., Wilde, 1991; Gibbs et al., 1997; Carrera and Rigby, 1999; Poussart et al., 1999). In alternative paleogeographic reconstructions it has been proposed that the Taconic orogeny was caused by the collision between North America and South America (e.g., Dalla Salda et al., 1992; Dalziel et al., 1994). This model, which is largely based on the SWEAT hypothesis (sensu Moores, 1991), is possible given the fact that paleomagnetic data provide no longitudinal constraints for the location of continents. However, this model has been rejected based on paleontological and geological reasons (Mac Niocaill et al., 1997; van der Pluijm et al., 1995).

Caradocian to Ashgillian paleogeographic changes in this study include 1) a southward movement of Gondwana towards the South Pole of ~15º, 2) a northward movement of Baltica towards the equator of ~12º (Scotese and McKerrow, 1991), and a northward movement of Siberia of ~10º. Figure 2.1 shows the resulting land-sea distribution at the GENESIS LSX resolution of 2X2. The GENESIS atmospheric resolution of T31 for the atmospheric model was obtained by linearly interpolating the 2X2 base maps.

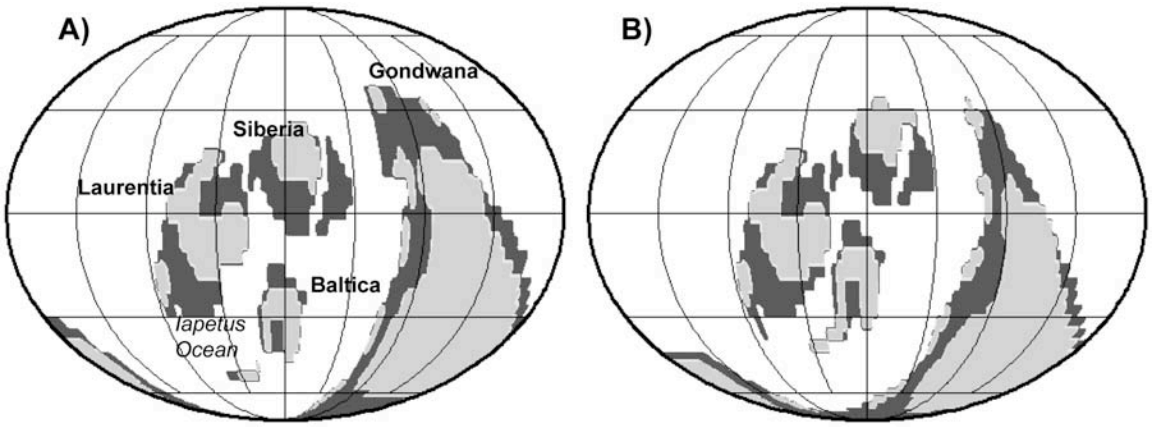

Figure 2.1: Land-sea distribution of the A) Caradocian and B) Ashgillian. Paleogeographic reconstructions based on (Scotese and McKerrow, 1990, 1991; Scotese, 1997). Note that during the last 14 my of the Ordovician 1) Gondwana moved southward towards the South Pole, 2) Baltica moved northward towards the equator narrowing the Iapetus ocean, and 3) Siberia moved northward. Light gray is continental area exposed in the high sea level simulations. Dark gray indicates additional shelf area exposed in the low sea level simulations.

Topographic maps for the Late Ordovician have not been published. The approach of Crowley and Baum (1995) and Gibbs (1996) was followed, who specified a uniform land elevation of 500 m for all land grid points and 250 m for all coastal areas. This is less than the modern-day average surface elevation of ~875 m (Fairbridge, 1968) and should lead to a somewhat warmer surface temperature. Crowley and Baum (1995)

showed that this topography was sufficient to generate permanent summer snow cover which is essential for the formation of ice. However, the elevation of polar land is important for the inception and maintenance of ice sheets. For example, under the present climate, which is considered interglacial, elevated Greenland is glaciated. Future work therefore needs to focus on generating paleoaltitude maps in order to overcome these simplifications. Shoreline positions for the low and high sea level simulations are based on Scotese and McKerrow (1990, 1991) and Scotese (1997). As in previous studies, low sea level has the continental shelfs exposed. At high sea level continental shelfs and significant proportions of continental areas are flooded.

Orbital Parameters

The "cold summer orbit" (CSO) of Berger (1978) was used for all experiments following the studies of Crowley and Baum (1995) and Gibbs (1996). As Gibbs (1996) points out, the initiation of a glaciation is most likely to start during a cold-summer orbit, since a CSO enhances snow survival during summer. Poussart et al. (1999) conducted a sensitivity study on the impact of different orbital parameters in their Late Ordovician climate study. They found that, compared to a CSO, a "hot summer orbit" HSO led to slightly cooler equatorial and tropical surface air temperatures (~0.5ºC) and slightly warmer polar temperatures (~1ºC). Despite these spatial variations in atmospheric temperatures, the annually averaged global atmospheric temperatures for both orbits were not significantly different. Choosing the CSO for the experiments should lead to colder

polar temperatures that bias the model towards the generation of permanent snow cover and freezing temperatures.

Solar Luminosity

The current understanding of stellar evolution implies that the brightness of the sun increases with time (Bahcall and Ulrich, 1988). Endal and Sofia (1981) estimated that the solar luminosity in the Late Ordovician was between 3.5% and 5% lower than today. In this study, a solar luminosity 4.5% lower than today is used following other Late Ordovician climate studies (Crowley and Baum, 1995; Gibbs et al., 1997; Poussart et al., 1999).

Vegetation and Soil Type

The Ordovician is characterized by a lack of vascular land plants. In addition, no information on Late Ordovician soil types is available. Therefore, like in previous studies, bare land surfaces with median soil values were prescribed globally (Gibbs, 1996; Gibbs et al., 1997).

Atmospheric pCO_2

Geochemical evidence from Ordovician paleosols (Yapp and Poths, 1992) and from geochemical modeling (Berner, 1994; Berner and Kothavala, 2001), indicate that Late Ordovician atmospheric CO_2 levels were higher than today, around 14x pre-

industrial pCO_2. Crowley and Baum (1995) showed that with a topography of 500 m, glaciation is just possible at 14x pCO_2. Later studies also found that permanent snow cover started to form between 14x and 10x PAL (Gibbs, 1996, Gibbs et al., 1997, Poussart et al., 1999). In our study, we performed simulations with atmospheric pCO_2 levels at 18x, 15x, 12x, 10x and 8x pre-industrial pCO_2 (280 ppm) to evaluate the sensitivity of the climate system to pCO_2 over the range reported by Berner (1994) and to assess the threshold for the initiation of permanent snow cover for each time period. However, we note that the radiation code in GENESIS does not perform well for pCO_2 levels above 12x PAL and underestimates the climatic effect for those high pCO_2 values. This means that the model tends to predict lower temperatures for higher pCO_2 values potentially biasing the model towards glaciation.

Oceanic heat transport

In GENESIS, a 50-m mixed ocean layer represents a thermodynamic slab, which captures the seasonal heat capacity of the ocean surface mixed layer. As GENESIS lacks a dynamic ocean, the total oceanic heat transport is calculated as linear horizontal diffusion along the gradient of the sea surface temperatures, with the diffusive coefficient being a function of ocean fraction and latitude (Thompson and Pollard, 1997). The oceanic heat transport diffusion coefficient values in the conducted experiments had values that replicate the modern climate. In addition, a heat transport coefficient of 50% of modern values was used in order to investigate the effect of lowered heat transport on the Late Ordovician climate system.

Initial Conditions

The initial conditions for this study were no snow cover on land, no sea ice, a motionless atmosphere and present-day annually averaged zonal temperatures. Except for some boundary conditions specified above, all other boundary conditions are the same as those used by Gibbs (1996). The model integrations were 40 years long and were judged to be close to equilibrium when global annual average surface temperatures did not change significantly over the last five years (Figure 2.2). Equilibrium was assumed when the global annual-average surface temperature did not change significantly over the last ten model years.

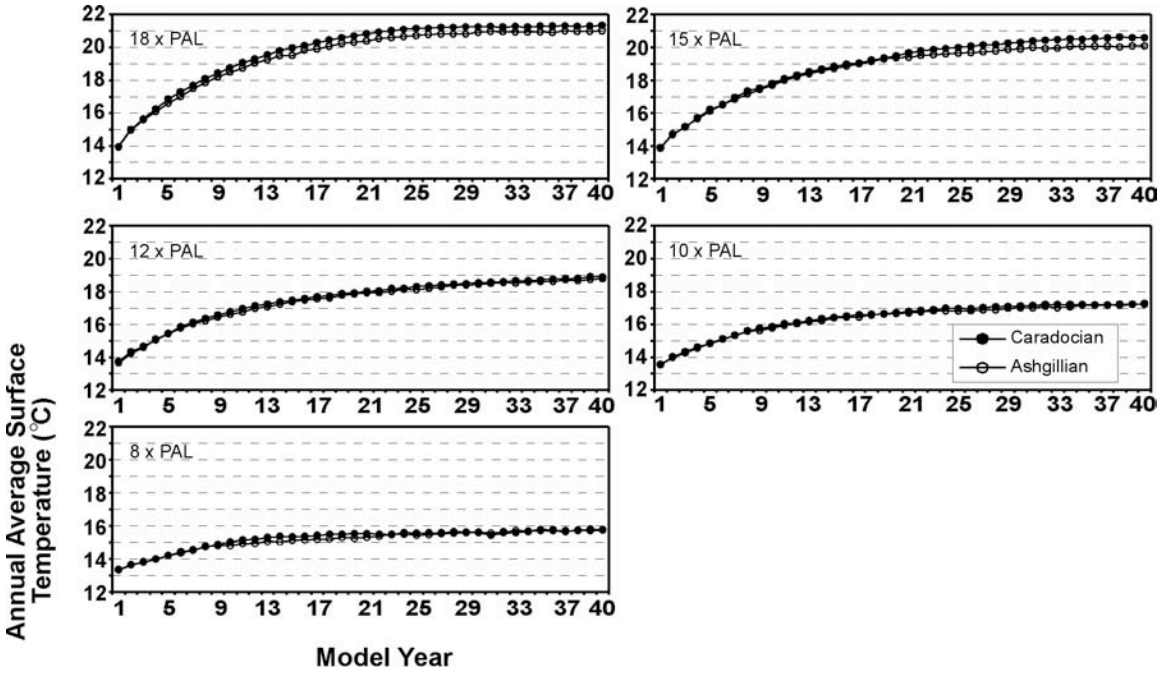

Figure 2.2: Evolution of the global annual-average surface temperature from the 10 climate runs with high sea level and an ocean heat transport diffusion coefficient value that replicates the modern climate.

Results

Atmospheric pCO_2 values, sea level, poleward ocean heat transport, and paleogeography strongly influence the annual global mean temperatures during the Late Ordovician (Fig. 2.2, 2.3, 2.4). As has been demonstrated by other researchers (Crowley and Baum, 1991, 1995; Gibbs, 1996; Gibbs et al., 1997, 2000; Poussart et al., 1999), low pCO_2 values result in lower global mean temperatures. However, in simulations with high sea level changes in pCO_2 values alone cannot lead to glaciation. Lower sea level and/or lower in poleward ocean heat transport are necessary for the initiation of ice sheets in the Late Ordovician (Table 2.2).

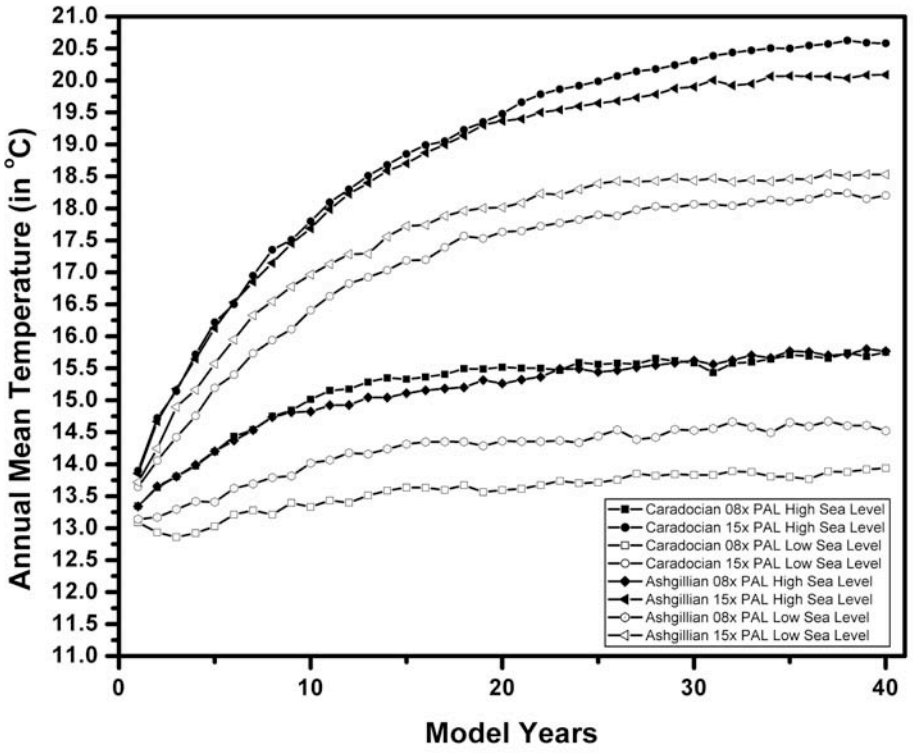

Figure 2.3: Comparison of the evolution of the global annual-average surface temperature for simulations with high and low sea level. All simulations have an ocean heat transport diffusion coefficient value that replicates the modern climate.

Table 2.2: Summary of ice sheet-model results (ice volume in km^3)

Simulation	Caradocian	Ashgillian
18x High sea level normal heat transport	0	0
15x High sea level normal heat transport	0	0
15x Low sea level normal heat transport	0	0
15x Low sea level low heat transport	22,049,561	0
12x High sea level normal heat transport	0	0
10x High sea level normal heat transport	0	0
8x High sea level normal heat transport	0	0
8x Low sea level normal heat transport	58,608,596	168,110,922
8x High sea level low heat transport	67,428	35,989,121

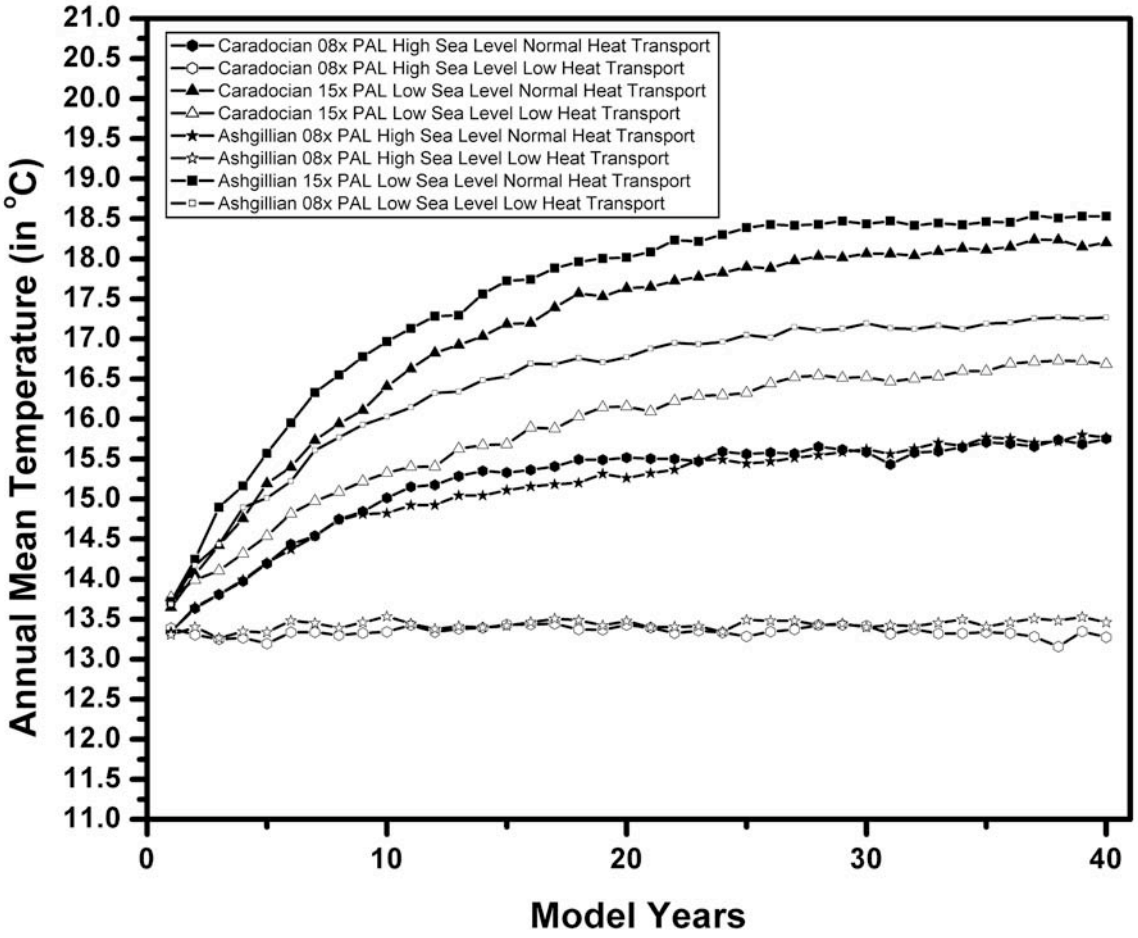

Figure 2.4: Comparison of the evolution of the global annual-average surface temperature for simulations with normal and reduced poleward ocean heat transport.

High Sea Level

At model year 40 there is a 5.6ºC difference in annual global mean temperatures between the 18x Caradocian and the 8x Ashgillian experiment (Fig. 2.2). Simulations with Ashgillian paleogeography have annual global mean temperatures that are 0.3ºC (18x PAL) and 0.5ºC (15x PAL) lower than the simulations with Caradocian paleogeography (Fig. 2.2). Below pCO_2 values of 12x PAL, paleogeography do not lead

to differences in global annual temperatures. Extensive sea ice and snow fields in the Northern and Southern hemispheres in both the Caradocian and Ashgillian simulations may in part contribute to comparable annual mean temperatures for both reconstructions.

Temperatures in Southern Gondwana are colder for Ashgillian experiments compared to Caradocian experiments for pCO_2 values above 12x PAL (Fig. 2.5). Ashgillian annual mean temperatures for Southern Gondwana reach freezing temperatures in the 18x and 15x pCO_2 experiments, whereas Caradocian temperatures remain above freezing for those pCO_2 values (Fig. 2.5). Due to the southward movement of Gondwana, the 10ºC isotherm penetrates further north in the Ashgillian and extends over larger areas of Gondwana.

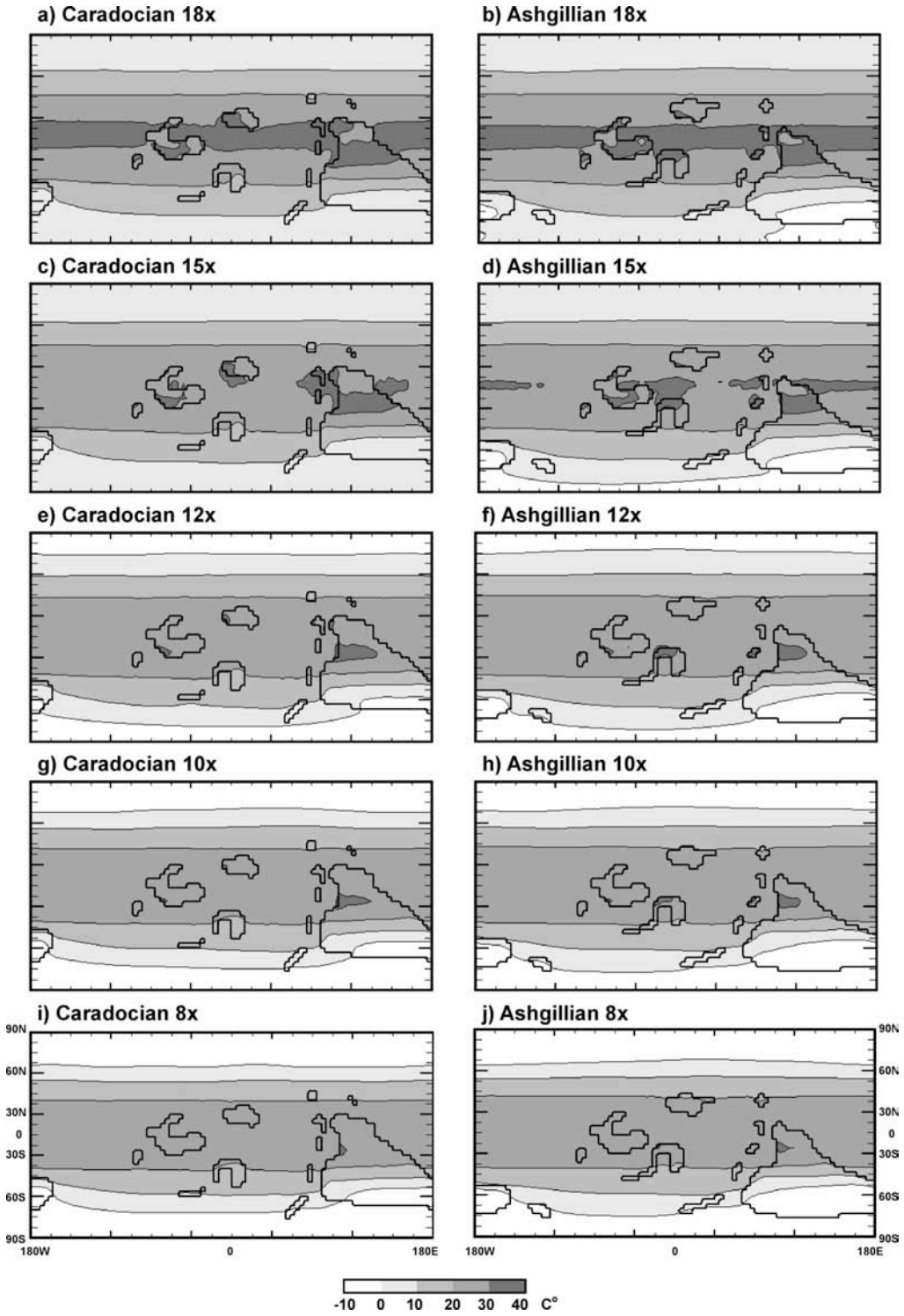

Figure 2.5: Global annual-average surface temperature distribution with high sea level for two time intervals and varying levels of pCO_2. All simulations have an ocean heat transport diffusion coefficient value that replicates the modern climate.

Global mean temperatures in equatorial regions remain above 20ºC for all experiments. In the simulations with 18x PAL, temperatures in the equatorial regions climb above 30ºC. The aerial extent of regions with temperatures above 30ºC decreases in the simulations with 15x PAL and only small areas in Northern Gondwana and Baltica retain temperatures above 30ºC.

The northward movement of Baltica towards the equator leads to generally warmer temperatures on Baltica in the Ashgillian experiments compared to the Caradocian. The Iapetus ocean between Baltica and Laurentia remains above the 20ºC isotherm in all experiments with the northern part of the Iapetus ocean lying above the 30ºC isotherm in experiments with 18x pCO_2.

The global annual mean temperature distribution also determines the location of permanent snow cover during the austral summer months (December, January and February). In the experiments, Gondwana remains snow free only during the austral summer for the 15x and 18x pCO_2 experiments with the Caradocian paleogeography. Snow cover accumulates in areas of Gondwana where annual global mean temperatures are below zero. In addition, sea ice (not shown) forms only in those experiments that also have snow coverage.

Low Sea Level

The increased continental area exposed at low sea level leads to significantly cooler global average annual temperatures. Compared to simulations with high sea level,

Caradocian and Ashgillian simulations with low sea level and 15x PAL have lower temperatures of ~2.4 ºC and ~1.6 ºC respectively (Fig. 2.3).

These lower temperatures also have a profound effect on the accumulation and preservation of permanent snow cover in southern Gondwana. Snow cover increases in size around the South Pole over the exposed continental areas for the Ashgillian simulations. While previous Late Ordovician climate models encountered runaway icehouse conditions at 8-10x PAL for the Ashgillian (Gibbs, 1996), runaway conditions did not occur in these simulations, even with atmospheric pCO_2 values as low as 8x PAL and low sea level when annual global temperatures reach ~14.5 ºC. While previous studies used GENESIS v. 1.02, we used GENESIS v.2.0 with new and improved physics and a higher atmospheric GCM resolution. The two versions give quite similar present day global temperatures; however there are several model differences that might give rise to the differing results. The response to pCO_2 perturbations for example is different in both models. A doubling of pCO_2 for present day results in a 2.1ºC increase in global temperatures in GENESIS v.1, whereas GENESIS v.2 leads to a 2.5ºC global warming response. In addition, in GENESIS v.1 the prescribed ocean heat transport was only about 1/3 of the observed ocean heat transport. In the version that we used, ocean heat transport is about 3/4 of the observed modern values (Thompson and Pollard, 1995; Pollard and Thompson, 1997). These are significant differences and can account for the discrepancies in model results.

Low poleward heat transport

The lower poleward ocean heat transport leads to a significant drop in global annual mean temperatures (Fig. 2.4). For the Ashgillian 8x PAL simulation, the reduced poleward ocean heat transport leads to more snow and sea ice accumulation resulting in a ~2.3 ºC colder climate (Fig. 2.4).

Ice sheet model results

While most simulations with normal poleward heat transport and high sea level have extensive permanent snow cover even during the austral summer, the ice sheet model indicates that a drop in atmospheric pCO_2 to as low as 8x PAL is not sufficient to initiate the formation of ice sheets (Fig. 2.6; Table 2.2). In these cases, the fractional snow cover falls below 1 in the summer and there is not sufficient snow accumulation for the formation of ice sheets. Ice sheets form only when sea level is low and/or poleward ocean heat transport is reduced. This is also the case for the initiation of ice sheet formation in the Caradocian simulation with atmospheric pCO_2 values of 15x PAL, a low sea level, and low poleward ocean heat transport. However, the global annual mean temperature for the corresponding Ashgillian simulation is higher (Fig. 2.4) and so ice sheets do not form.

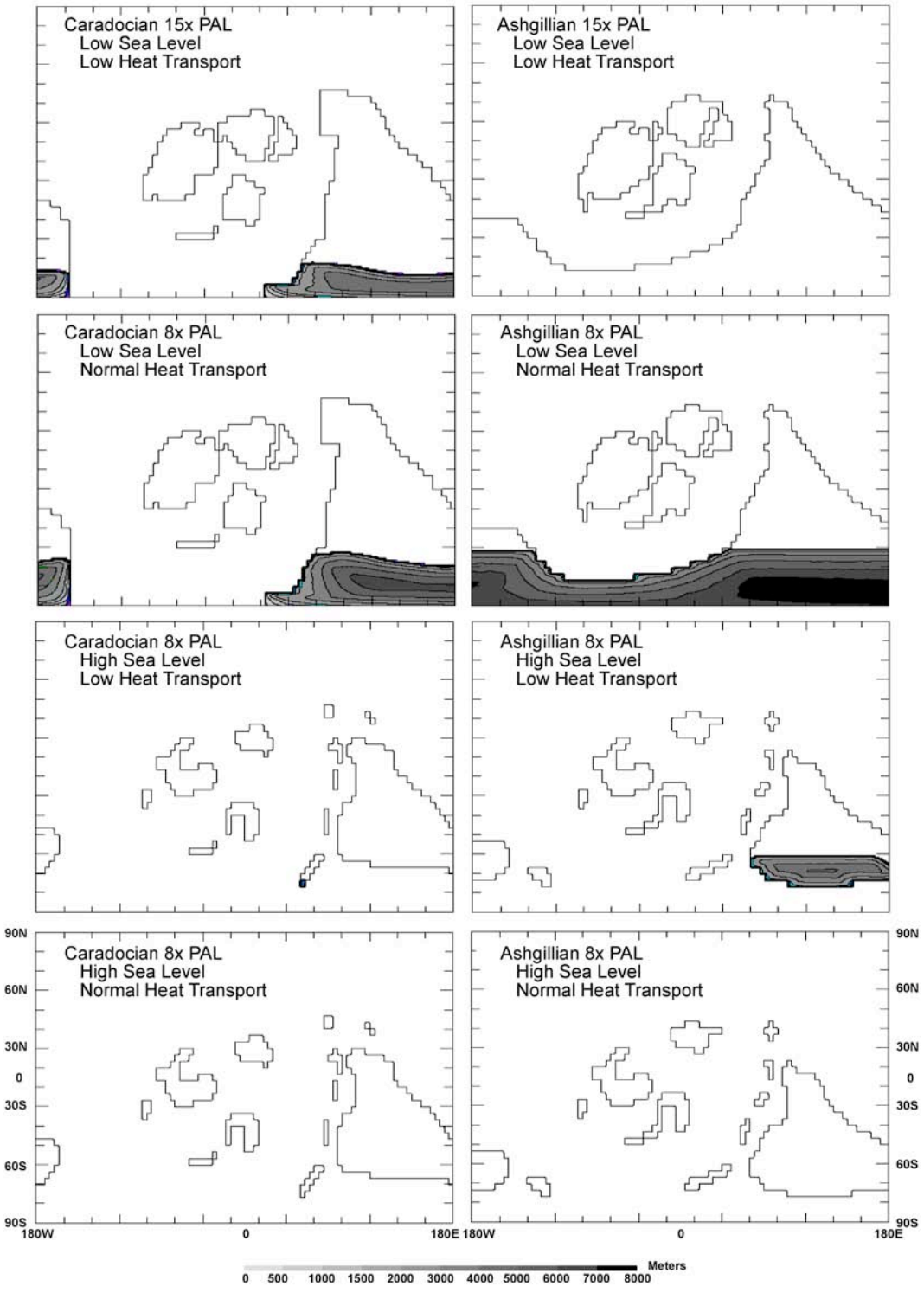

Figure 2.6: Ice sheet model results. Shown is ice thickness in meters.

Discussion

Paleogeography, atmospheric pCO_2, and high sea level

The results of these experiments show that it is not possible to initiate ice sheets in Southern Gondwana with atmospheric pCO_2 levels as low as 8x PAL during the Late Ordovician with a high sea level. Even at 8x PAL pCO_2, when the snow area increases in size and the 0ºC isotherm expands, snow fraction falls below 1 in the summer and ice sheets do not form with the ice sheet model. There are also no temperature differences between the different paleogeographies with atmospheric pCO_2 values of 12x PAL and below. However, above atmospheric pCO_2 values of 12x PAL, the Ashgillian paleogeography leads to lower global annual mean temperatures. This indicates that during times of high pCO_2 (above 12x PAL) and high sea level the paleogeographic evolution could have been an important factor pre-conditioning the global climate system for glaciation. Thus, the observed long-term cooling trend during the Late Ordovician can be regarded as the result of a combination of drawdown of pCO_2 and paleogeographic change, but changes in both of these variables were not sufficient to cause glaciation. The larger ice sheets of the Ashgillian simulations, compared to the Caradocian experiments, also indicate the importance of paleogeographic change during the Late Ordovician for global cooling and the formation of ice sheets. The southward movement of Gondwana increases the land area in the higher southern latitudes and therefore the ice sheets in the Ashgillian experiments can grow larger than the ice sheets in the Caradocian simulations.

Sea level change

Under a high sea level, paleogeographic changes and a drawdown of pCO_2 were only pre-conditioning events which by themselves could not lead to glaciation. However, it is possible to form ice sheets with a low sea level, a normal ocean heat transport and an atmospheric pCO_2 level of 8x PAL. This underlines the potential importance of sea level change as a mechanism to initiate glaciation.

The onset of glaciation using this mechanism depends on the timing of a drop in sea level, i.e., sea level must have dropped prior to the initiation of extensive ice sheets. The position of sea level is critical, but the stratigraphic resolution of the Late Ordovician is not perfect and the record of sea level change remains controversial. While some Late Ordovician sea level curves confine the sea level drop to the Ashgillian (Brenchley and Newall, 1980; Leggett et al., 1981; Lenz, 1982), other authors describe a sea level drop starting before the Ashgillian (Fortey, 1984; McKerrow, 1979; Ross and Ross, 1988, 1992). Evidence exists for early stages of ice formation prior to the Ashgill and glacio-eustatic sea level changes could have occurred during the Caradoc (e.g., Frakes et al., 1992; Pope and Steffen, 2003). In addition, sea level could have dropped due to factors other than glacio-eustacy (e.g., changes in spreading rates: Pitman, 1978) before the Hirnantian glaciation. If indeed there was a sea level drop before the Ashgillian at low pCO_2 values, this could have led to breaching a threshold for the initiation of ice sheets by increasing the available land area for ice sheet growth in the higher southern latitudes.

Poleward ocean heat transport

Since we were unable to simulate glaciation in our initial experiments beginning with a high sea level and varying pCO_2 and paleogeography, we also investigated the role of poleward ocean heat transport as a contributing factor to the Late Ordovician glaciation. Poleward ocean heat transport is an important variable that can control climate (Barron et al., 1993). Generally, higher poleward ocean heat transport keeps the polar region from icing over, resulting in warmer global temperatures. Moreover, changes in pCO_2, paleogeography, and sea level could change poleward ocean heat transport leading to additional cooling at high latitudes and possibly to ice sheet formation. We used two values for poleward ocean heat transport coefficients in this study: (1) a normal ocean heat transport value that replicates the modern climate, and (2) a lower value 50% of normal that should lead to colder polar climates.

One of the simulations that led to ice sheet formation was the simulation with a lowered poleward ocean heat transport, a high sea level, Ashgillian paleogeography, and pCO_2 levels of 8x PAL. The corresponding Caradocian simulation does not lead to the formation of extensive ice sheets, although smaller ice sheets are produced. This indicates that a reduction in poleward ocean heat transport, possibly in response to paleogeographic changes from the Caradocian to the Ashgillian, could have contributed to the initiation of ice sheets at the end of the Ordovician. In addition, the Caradocian simulations with a low sea-level, a pCO_2 value of 15x PAL and a reduced poleward ocean heat transport results in glaciation, while the corresponding Ashgillian simulation has no ice sheets. The results that ice sheets form in the Caradocian but not in the

Ashgillian with otherwise identical parameters further support the fact that both paleogeography and poleward ocean heat transport influence the annual global mean temperatures (Fig. 2.4). Therefore, both parameters are important for the initiation of ice sheets.

The results of Poussart et al. (1999) show that as a consequence of the Late Ordovician paleogeographic configuration, global ocean poleward heat transport in the southern hemisphere may have been higher than present day values. However, our results indicate that in order to initiate glaciation poleward ocean heat transport had to be lower in the Late Ordovician compared to today. This significant discrepancy between Poussart et al. (1999) and our results must be reconciled with further studies that directly calculate poleward ocean heat transport by coupling an ocean general circulation model with an atmospheric general circulation model. With fully coupled ocean models it will be possible to evaluate changes in poleward ocean heat transport with respect to the different paleogeographic settings and changes in atmospheric pCO_2 directly. Our results suggest that poleward heat transport plays an important role for determining the threshold not only for initiation of permanent snow covers, but also for the formation of ice sheets.

The paleogeographic reconfiguration during the Late Ordovician might have led to changes in paleoceanography, modifying the poleward ocean heat transport. Using conceptual models, Wilde (1991) showed how the paleoceanographic conditions during the Ordovician were modified as a result of climatic and paleogeographic changes. Studies with a coupled ocean-atmospheric general circulation model are necessary to assess the impact of paleogeographic changes on the poleward heat transport. If the oceanographic conditions, and therefore the heat transport, changed significantly during

the Late Ordovician due to the southward movement of Gondwana, the drop in atmospheric pCO_2 and southward movement of Gondwana could have been necessary pre-conditioning events that caused the reduced poleward heat transport to cross a threshold value for the start of the glaciation.

Orbital parameters

The boundary conditions used in this study favor cool temperatures in southern high latitudes. The prescribed orbital parameters are the most extreme Pleistocene values for the southern hemisphere (Berger, 1978). Further studies are necessary to evaluate the effects of high frequency orbital perturbations to the Late Ordovician climate system and investigate the role of orbital forcing versus the other forcings addressed in this study.

Conclusions

(1) This study suggests that changes in atmospheric pCO_2 levels and the paleogeographic evolution during the Late Ordovician alone were not responsible for the initiation of the Late Ordovician glaciation. As previous studies have shown, the threshold for glaciation under Ashgillian paleogeography is 8x-10x PAL with a low sea level. However, under the same conditions with high sea level, ice sheets do not form.

(2) Assuming that pCO_2 did not fall below 8x PAL, a drop in pCO_2 and the paleogeographic evolution coupled with an ice-albedo feedback can therefore be regarded as only preconditioning factors for the Late Ordovician glaciation. In order for ice sheets

to form in the Late Ordovician, other factors must have changed such as a drop in sea level from its generally high Late Ordovician levels and/or a reduction in poleward ocean heat transport. A lower sea level, as well as paleogeographic change, leads to more exposed land area where ice sheets can grow.

(3) Further studies need to address the effect of high-frequency orbital perturbation on the Late Ordovician climate system. This is important in order to determine if the ice sheets which are produced in our simulations with a cold summer orbit would survive during warmer orbits. In addition, better paleotopographic reconstructions are required since most glaciers nucleate in higher altitudes. In our simulations the relatively flat topography does not allow glaciers to nucleate in higher altitudes and expand towards lower altitudes. A better understanding of the location of mountain belts in the Ordovician would therefore improve future climate simulations since ice sheets might be able to form in higher altitudes at high pCO_2 values.

Acknowledgements

We thank the Penn State Earth and Mineral Science Environment Institute, NASA Astrobiology Institute (NCC2-1057), and NSF (EAR 00-01918 and EAR 01-06737) for supporting this research. We also thank Lee Kump (Penn State) for comments on the manuscript. We thank P.J. Brenchley, Jozef Syktus, and Finn Surlyk for their helpful reviews.

References Cited

Algeo, T.J., Seslavinsky, K.B, 1995a. The Paleozoic world: Continental flooding, hypsometry, and sea level. American Journal of Science 295, 787-822.

Algeo, T.J., Seslavinsky, K.B., 1995b. Reconstructing epeirogenic and eustatic trends from paleo-continental flooding data. In Haq, B.U., (Ed.), Sequence Stratigraphy and Depositional Response to Eustatic, Tectonic and Climatic Forcing. Kluwer Academic Publishers, Dordrecht, pp. 209-246.

Bahcall, J.N., Ulrich, R.K., 1988. Solar models, neutrino experiments, and helioseismology. Reviews of Modern Physics 60, 297-372.

Barron, E.J., Peterson, W.W., Pollard, D., Thompson, S.L., 1993. Past climate and the role of ocean heat transport: model simulations for the Cretaceous. Paleoceanography 8, 785-798.

Berger, A.L., 1978. Long-term variations of caloric insolation resulting from the earth's orbital elements. Quaternary Research 9, 139-167.

Berner, R.A., 1994. GEOCARB II, a revised model of atmospheric CO_2 over Phanerozoic time. American Journal of Science 294(1), 56-91.

Berner, R.A., Kothavala, Z., 2001. GEOCARB III: A revised model of atmospheric CO_2 over Phanerozoic time. American Journal of Science.301, 182-204.

Brenchley, P.J., Newall, G., 1980. A facies analysis of the Upper Ordovician regressive sequences in the Oslo region, Norway - A record of glacio-eustatic change. Palaeogeography Palaeoclimatology Palaeoecology 31, 1-38.

Brenchley, P.J., Marshall, J.D., Carden, G.A.F., Robertson, D.B.R., Long, D.G.F., Meidla, T., Hints, L., Anderson, T.F., 1994. Bathymetric and isotopic evidence for a short-lived Late Ordovician glaciation in a greenhouse period. Geology 22(4), 295-298.

Brenchley, P.J., Carden, G.A.F., Marshall, J.D., 1995. Environmental changes associated with the 'first strike' of the Late Ordovician mass extinction. Modern Geology 20, 69-82.

Carrera, M.G., Rigby, J.K., 1999. Biogeography of Ordovician sponges. Journal of Paleontology 73, 26-37.

Crowley, T.J., Mengel, J.G., Short, D.A., 1987. Gondwanaland's seasonal cycle. Nature 329, 803-807.

Crowley, T.J., Baum, S.K., 1991. Toward reconciliation of Late Ordovician (~440 Ma) glaciation with very high CO_2 levels. Journal of Geophysical Research 96(12), 22,597-22,610.

Crowley, T.J., Baum, S.K., Kim, K.-Y., 1993. General circulation model sensitivity experiments with pole-centered supercontinents. Journal of Geophysical Research 98(5), 8793-8800.

Crowley, T.J., Baum, S.K., 1995. Reconciling Late Ordovician (440 Ma) glaciation with very high (14x) CO_2 levels. Journal of Geophysical Research 100, 1093-1101.

Dalla Salda, L.H., Dalziel, I.W.D., Cingolani, C.A., Varela, R., 1992. Did the Taconic Appalachians continue into southern South America?. Geology. 20, 1059-1062.

Dalziel, I.W.D., Salda, L.H.D., Gahagan, L.M., 1994. Paleozoic Laurentia-Gondwana interaction and the origin of the Appalachian-Andean mountain system. Geological Society of America Bulletin 106, 243-252.

Endal, A.S., Sofia, S., 1981. Rotation in solar-type stars, I, Evolutionary Models for the spin-down of the sun. Astrophysical Journal 243, 625-640.

Fairbridge, R. W., 1968. The Encyclopedia of Geomorphology. Van Nostrand Reinhold, New York.

Fortey, R.A., 1984. Global earlier Ordovician transgressions and regressions and their biological implications. In Bruton, D.L. (Ed.), Aspects of the Ordovician system IV, Paleont. Contrib. Univ. Oslo, Universitetsforlaget, pp. 35-50.

Frakes, L.A., Francis, J.E., 1988. A guide to Phanerozoic cold polar climates from high-latitude ice-rafting in the Late Cretaceous. Nature 333, 547-549.

Frakes, L.A., Francis, J.E., Syktus, J.I., 1992. Climate modes of the Phanerozoic: the history of the earth's climate over the last 600 million years. Cambridge University Press, Cambridge.

Gibbs, M.T., 1996. Glaciation, chemical weathering and the carbon cycle. Ph.D. Thesis, The Pennsylvania State University, USA.

Gibbs, M.T., Barron, E.J., Kump, L.R., 1997. An atmospheric pCO_2 threshold for glaciation in the Late Ordovician. Geology 25(5), 447-450.

Gibbs, M.T., Bice, K.L., Barron, E.J., Kump, L.R., 2000. Glaciation in the early Paleozoic "greenhouse"; the roles of paleogeography and atmospheric CO_2. In Huber, T., MacLeod, K.G., Wing, S.L., (Eds.), Warm climates in Earth history. Cambridge University Press, pp. 386-422.

Hallam, A., 1984. Pre-Quaternary sea-level changes. Annual Review of Earth Planetary Sciences 12, 205-243.

Holland, S.M., Patzkowsky, M.E., 1996. Sequence stratigraphy and long-term paleoceanographic change in the Middle and Upper Ordovician of the Eastern United States. In Witzke, J., Ludvigson, G.A., Day, J., (Eds.), Paleozoic sequence stratigraphy; views from the North American Craton. Geological Society of America Special Paper 306, pp. 117-129.

Holland, S.M., Patzkowsky, M.E., 1997. Distal orogenic effects on peripheral bulge sedimentation: Middle and Upper Ordovician of the Nashville Dome. Journal of Sedimentary Research 67, 250-263.

Kump, L.R., Arthur, M.A., Patzkowsky, M.E., Gibbs, M.T., Pinkus, D.S., Sheehan, P.M., 1999. A weathering hypothesis for glaciation at high atmospheric pCO_2 during the Late Ordovician. Palaeogeography Palaeoclimatology Palaeoecology 152(1-2), 173-187.

Lavoie, D., 1995. Late Ordovician high-energy temperate-water carbonate ramp, southern Quebec, Canada; implications for Late Ordovician oceanography. Sedimentology 42(1), 95-116.

Lavoie, D., Asselin, E., 1998. Upper Ordovician facies in the Lac Saint-Jean outlier, Quebec (eastern Canada); palaeoenvironmental significance for Late Ordovician oceanography. Sedimentology 45(5), 817-832.

Leggett, J.K., McKerrow, W.S., Cooks, L.R.M., Rickards, R.B., 1981. Periodicity in the early Palaeozoic realm. Geological Society of London Journal 138, 167-176.

Lenz, A.C., 1982. Ordovician to Devonian sea-level changes in western and northern Canada. Canadian Journal of Earth Sciences 19, 1919-1932.

Mac Niocaill, C., van der Pluijm, B.A., Van der Voo, R., 1997. Ordovician paleogeography and the evolution of the Iapetus ocean. Geology 25, 159-162.

Marshall, J.D., Brenchley, P.J., Mason, P., Wolff, G.A., Astini, R.A., Hints, L., Meidla, T., 1997. Global carbon isotopic events associated with mass extinction and glaciation in the Late Ordovician. Palaeogeography Palaeoclimatology Palaeoecology 132(1-4), 195-210.

McKerrow, W.S., 1979. Ordovician and Silurian changes in sea-level. Geological Society of London Journal 136, 137-145.

Moores, E.M., 1991. Southwest U.S.-East Antarctica (SWEAT) connection: A hypothesis. Geology 19, 425-428.

Paris, F., Elaouad-Debbaj, Z., Jaglin, J.C., Massa, D., Oulebsir, L., 1995. Chitinozoans and Late Ordovician glacial events on Gondwana. In Cooper, D., Droser, M.L., Finney, S.L., (Eds.), Ordovician Odyssey: Short Papers for the Seventh International Symposium on the Ordovician System, Fullerton, CA, pp.171-176.

Patzkowsky, M.E., Holland, S.M., 1993. Biotic response to a Middle Ordovician paleoceanographic event in eastern North America. Geology 21, 619-622.

Patzkowsky, M.E., Slupik, L.M., Arthur, M.A., Pancost, R.D., Freeman, K.H., 1997. Late Middle Ordovician environmental change and extinction; Harbinger of the Late Ordovician or continuation of Cambrian patterns?. Geology 25(10), 911-914.

Pitman, W.C., III, 1978. The relationship between eustacy and stratigraphic sequences of passive margins. Geological Society of America Bulletin 89, 1389-1403.

Pollard, D., Thompson, S.L., 1995. User's Guide to the GENESIS Global Climate Model Version 2.0. Interdisciplinary Climate Systems Section. Climate and Global Dynamics Division, Boulder, CO.

Pollard, D., Thompson, S.L., 1997. Driving a high-resolution dynamic ice-sheet model with GCM climate: ice-sheet initiation at 116 000 BP. Annals of Glaciology 25, 296-304.

Pollard, D., PMIP Participating Groups, 2000. Comparison of ice-sheet surface mass budgets from Paleoclimate Modeling Intercomparison Project (PMIP) simulations. Global and Planetary Change 24, 79-209.

Pope, M.C., Read, J.F., 1997. High-resolution stratigraphy of the Lexington Limestone (late Middle Ordovician), Kentucky, U.S.A.; a cool-water carbonate-clastic ramp in a tectonically active foreland basin. In James, N.P., Clark, J.A.D., (Eds.), Cool-water carbonates. Special Publications Society of Economic Paleontologists and Mineralogists Special Publication 56, pp. 410-429.

Pope, M.C., Steffen, J.B., 2003. Widespread, prolonged late Middle to Late Ordovician upwelling in North America: A proxy record of glaciation?. Geology 31, 63-66.

Poussart, P.F., Weaver, A.J., Barnes, C.R.,1999. Late Ordovician glaciation under high atmospheric CO_2; a coupled model analysis. Paleoceanography 14(4), 542-558.

Qing, H., Veizer, J., 1994. Oxygen carbon isotopic composition of Ordovician brachiopods; implications for coeval seawater. Geochimica et Cosmochimica Acta 58(20), 4429-4442.

Ritz, C., Fabre, A., Letre'guilly, A., 1997. Sensitivity of a Greenland icesheet model to ice flow and ablation parameters: Consequences for the evolution through the last climatic cycle. Climate Dynamics 13, 11-24.

Ross, J.R.P, Ross, C.A., 1988. Late Paleozoic transgressive-regressive deposition. In Wilgus, C.K., Hastings, B.S., Kendall, C.G.St.C., Posamentier, H.W., Ross, C.A., Van Wagoner, J.C., (Eds.), Sea-level changes: an integrated approach. Special Publications Society of Economic Paleontologists and Mineralogists Special Publication, 42, pp. 227-247.

Ross, J.R.P, Ross, C.A., 1992. Ordovician sea-level fluctuation. In Webby, B.D., Laurie, J.R. (Eds.), Global Perspectives on Ordovician geology (Proceedings of the Sixth International Symposium on the Ordovician System, University of Sydney, Australia, 15-19 July 1991). A. A.Balkema, Rotterdam, pp. 327-335.

Scotese, C.R., 1997. Paleogeographic atlas. University of Texas at Arlington, USA.

Scotese, C.R., McKerrow, W.S., 1990. Revised world maps and introduction. In Scotese, C.R., McKerrow, W.S., (Eds.), Palaeozoic palaeogeography and biogeography. Geological Society of London Memoir 12, pp. 1-21.

Scotese, C.R., McKerrow, W.S., 1991. Ordovician plate tectonic reconstructions. In Barnes, C.R., Williams, S.H., (Eds.), Advances in Ordovician geology. Canadian Geological Survey Paper 90-9, pp. 271-282.

Thompson, S.L., Pollard, D., 1995. A global climate model (GENESIS) with a land-surface-transfer scheme (LSX). Part 1: Present-day climate. Journal of Climate 8, 732-761.

Thompson, S.L., Pollard, D., 1995b. A global climate model (GENESIS) with a land-surface-transfer scheme (LSX). Part 2: CO_2 sensitivity. Journal of Climate 8, 1104-1121.

Thompson, S.L., Pollard, D., 1997. Greenland and Antarctic Mass Balances for Present and Doubled Atmospheric CO_2 from the GENESIS Version-2 Global Climate Model. Journal of Climate 10, 871-900.

van der Pluijm, B.A., van der Voo, R., Torsvik, T.H., 1995. Convergence and subduction at the Ordovician margin of Laurentia. In Hibbard, J.P., van Staal, C.R., Cawood, P.A., (Eds.), Current Perspectives in the Appalachian-Caledonian Orogen. Volume Geological Association of Canada, Special Paper 41, pp. 127-136.

Veizer, J., Ala D., Azmy, K., Bruckschen, P., Buhl, D., Bruhn, F., Carden, G.A.F., Diener, A., Ebneth, S., Godderis, Y., Jasper, T., Korte, C., Pawellek, F., Podlaha, O.G., Strauss, H., 1999. 87Sr/ 86Sr, d13C and d18O evolution of Phanerozoic seawater. Chemical Geology 161, 59-88.

Vail, P.R, Mitchum, R. M. Jr., Thompson, S. III, 1977. Global Cycles of relative changes in sea level. In C.E. Clayton, (ed.), Seismic stratigraphy - applications to hydrocarbon exploration. Tulsa, Oklahoma, American Association of Petroleum Geologists Memoir 26, pp. 83-97.

Wilde, P., 1991, Oceanography in the Ordovician, in Advances in Ordovician geology. In Barnes, C.R., Williams, S.H., (Eds.), Advances in Ordovician geology. Canadian Geological Survey Paper 90-9, 283-298.

Yapp, C.J., Poths, H., 1992. Ancient atmospheric CO_2 pressures inferred from natural goethites, Nature 355(6358), 342-344.

Chapter 3

Obliquity forcing with 8–12 times preindustrial levels of atmospheric pCO_2 during the Late Ordovician glaciation

Abstract

Results from coupled ice-sheet and atmospheric general circulation models show that the waxing and waning of ice sheets during the Late Ordovician were very sensitive to changes in atmospheric pCO_2 and orbital forcing at the obliquity time scale (30–40 k.y.). Without orbital forcing, ice sheets can grow with pCO_2 level as high as 10 times PAL (preindustrial atmospheric level). However, with orbital forcing, ice sheets can grow only with pCO_2 levels of 8 times PAL or lower. These results indicate that the threshold of pCO_2 for the initiation of glaciation is on the lower end of previously published estimates of 8–20 times PAL. The ice-sheet model results further indicate that during exceptionally long periods of low summer insolation and low pCO_2 levels (8–10 times PAL), large ice sheets could have formed that were able to sustain permanent glaciation under subsequently higher pCO_2 values. This finding suggests that in order to end the Late Ordovician glaciation with a rise in pCO_2, atmospheric pCO_2 must have risen to at least 12 times PAL. Ice sheets therefore introduce non-linearities and hysteresis effects to the Ordovician climate system. These non-linearities might have also played a role in the initiation and termination of other glaciations in Earth history.

Introduction

Changes of atmospheric pCO_2 are generally considered as the main climate driver over geologic time (e.g., Frakes et al., 1992; Crowley and Berner, 2001). However, Veizer et al. (2000) suggested that for part of the Phanerozoic, atmospheric CO_2 concentrations were not the principal driver for global climate. These authors used an energy-balance model that incorporated proxy data for the Phanerozoic atmospheric CO_2 concentration. Their model predicted temperatures that are inconsistent with the geologic climate record. One of the mismatches is the Late Ordovician glaciation, which occurred under pCO_2 levels of 14 ± 6 times PAL (preindustrial atmospheric levels) (Berner and Kothavala, 2001; Yapp and Poths, 1992) and lasted less than 1 m.y. (Brenchley et al., 1995, 2003). Several numerical climate model studies found a high sensitivity of the formation of permanent snow cover with respect to pCO_2 values for the Late Ordovician paleogeography (Crowley and Baum, 1991, 1995; Gibbs et al., 1997, 2000; Poussart et al., 1999). These studies suggested that glaciation started with pCO_2 levels up to 10 times PAL.

The Upper Ordovician rock record indicates that Milankovitch cycles controlled ice sheet growth (Sutcliffe et al., 2000) and halite deposition (Williams, 1991) and suggests that orbital forcing had a significant effect on the Late Ordovician climate system. Because obliquity changes the amplitude of the seasonal cycle and alters the equator-to-pole insolation gradient, obliquity cycles can control whether ice sheets that were initiated during the coldest orbit could survive subsequent orbital variations around a warmer mean. Here we extend previous sensitivity studies by performing simulations

involving an ice-sheet model coupled with an atmospheric general circulation model (AGCM) under a range of atmospheric pCO_2 values and warm- and cold-summer orbits that vary over the obliquity time scale (30–40 k.y.). This approach has been successfully used to investigate other pre-Pleistocene glaciations (e.g., Hyde et al., 1999). Our study goes beyond earlier Ordovician climate studies in that it adds a true ice-sheet model; prior work only looked at snow budgets to estimate the onset of glaciation.

We show how orbital forcing at the obliquity time scale affects the growth of ice sheets and their mean sizes, and we investigate the pCO_2 levels required to build and maintain these ice sheets. We also investigate hysteresis effects of CO_2 levels required for deglaciation of these ice sheets.

Methods

We performed AGCM experiments for the Late Ordovician with GENESIS v.2.0 (Thompson and Pollard, 1997) and coupled the output to a three-dimensional ice-sheet model (Pollard and Thompson, 1997). The GENESIS model includes a 2° x 2° land-surface model incorporating physical effects of vegetation, a six-layer soil model, a snow model, a three-layer thermodynamic sea-ice model, and a slab mixed-layer ocean (Thompson and Pollard, 1997). The model has 18 vertical layers and a spectral resolution of ~3.75° x 3.75°. The GENESIS experiments were run for 40 model years until they reached equilibrium. The ice-sheet model has a 1° x 1° resolution and thermodynamics following Ritz et al. (1997). The model includes a 2-km-thick bedrock with vertical heat diffusion. The monthly mean temperature and precipitation values of the averaged past

10 yr of the stored AGCM climate results were used to drive the ice-sheet model through long-term runs of several 10^5 yr duration, with either invariant climate or with prescribed climate cyclicity as described subsequently. The AGCM's atmospheric temperatures were interpolated to the fine-grid ice-sheet topography by using a constant lapse rate of 6.5°C/km. The surface mass balance was calculated with a degree-day method, as in many coupled climate and ice-sheet studies (e.g., Ritz et al., 1997; Pollard and Thompson, 1997). The coupled atmosphere and ice-sheet model compares well with the geologic record of Antarctica (DeConto and Pollard, 2003), gives realistic orbital sensitivity for the Pleistocene ice volumes (Pollard et al., 2000), and its global sensitivity to doubled CO_2, 2.5ºC, is within "consensus" range (Thompson and Pollard, 1997).

We used Late Ordovician paleogeographic reconstructions with a low sea level (Scotese and McKerrow, 1991). Because no topographic maps for the Late Ordovician have been published, the approach of Crowley and Baum (1995) was followed, and a uniform land elevation of 500 m for all land grid points and 250 m for all coastal areas was specified. Crowley and Baum (1995) showed that this topography was sufficient to generate permanent summer snow cover, which is essential for the formation of ice.

Geochemical modeling (Berner and Kothavala, 2001) and geochemical data from Ordovician paleosols (Yapp and Poths, 1992) indicate that Late Ordovician pCO_2 levels were higher than today, ~14 ± 6 times preindustrial pCO_2. We performed our simulations with pCO_2 levels of 8, 9, 10, and 12 times preindustrial (280 ppm) levels.

In addition, we used reduced solar luminosity (95.5% of present day solar constant of 1365 W/m^2), bare soil (intermediate soil color values), and no vegetation.

For each pCO_2 level, two AGCM simulations were performed, with different orbital parameters yielding extreme cold (eccentricity 0.06, obliquity 22., precession 270) and warm (eccentricity 0.06, obliquity 24.5, precession 90) Southern Hemisphere summers. These extreme values of precession, obliquity, and eccentricity are based on their cycles of the past 5 m.y. (Berger, 1978; Berger and Loutre, 1991). By using these saved monthly mean AGCM solutions, two kinds of long-term ice-sheet runs were performed. First, the ice model was run to equilibrium by using invariant cold-summer AGCM climate. Second, the ice model was run by interpolating between the cold-summer and warm-summer climates, assuming a cosine variation of climate in time between the two extremes with periods of 40 k.y. and 30 k.y.. Actual insolation variations are more complex owing to the variations of eccentricity and precession, but the simple sinusoids used here allow a clearer first look at the effects on Ordovician ice volumes. Therefore, these experiments are designed to assess the stability of the ice sheet under changing orbital parameters, with periodicities representative of modern-day and Late Ordovician obliquity cycles. Although the modern-day obliquity cycle has a periodicity of 41 k.y., the Late Ordovician obliquity periods were shorter because of Moon-Earth interactions through time (Berger and Loutre, 1994; Berger et al., 1992). This shorter Late Ordovician periodicity is supported by Fourier spectral analysis of geochemical data of halite deposits for that time period (Williams, 1991).

Results

In runs without orbital forcing, none of the warm-summer orbit simulations resulted in the formation of ice sheets. Ice-sheet growth occurred only in the cold-summer orbit simulations with pCO_2 levels of 10x PAL and lower (Fig. 3.1). In runs with orbital forcing and initiated with no ice, only the simulations with 8x pCO_2 sustained permanent ice sheets (Figs. 3.2 and 3.3). In the simulations with 9x PAL and 10x PAL, the ice sheets were unable to grow large enough to prevent their complete melting during the next warm-summer phase (Figs. 3.2 and 3.3), producing intermittent ice-sheet buildups interrupted by ice-free periods. The increased solar insolation during the warm-summer orbit also prevents the ice sheets from accumulating as much ice as in the ice-sheet simulation without orbital forcing. Although the maximum ice-sheet volume reaches ~168 x 10^6 km^3 in the simulation with pCO_2 levels of 8x PAL with no orbital forcing, the influence of the warm-summer orbit leads to ice-sheet volumes between ~20 and 40 x 10^6 km^3.

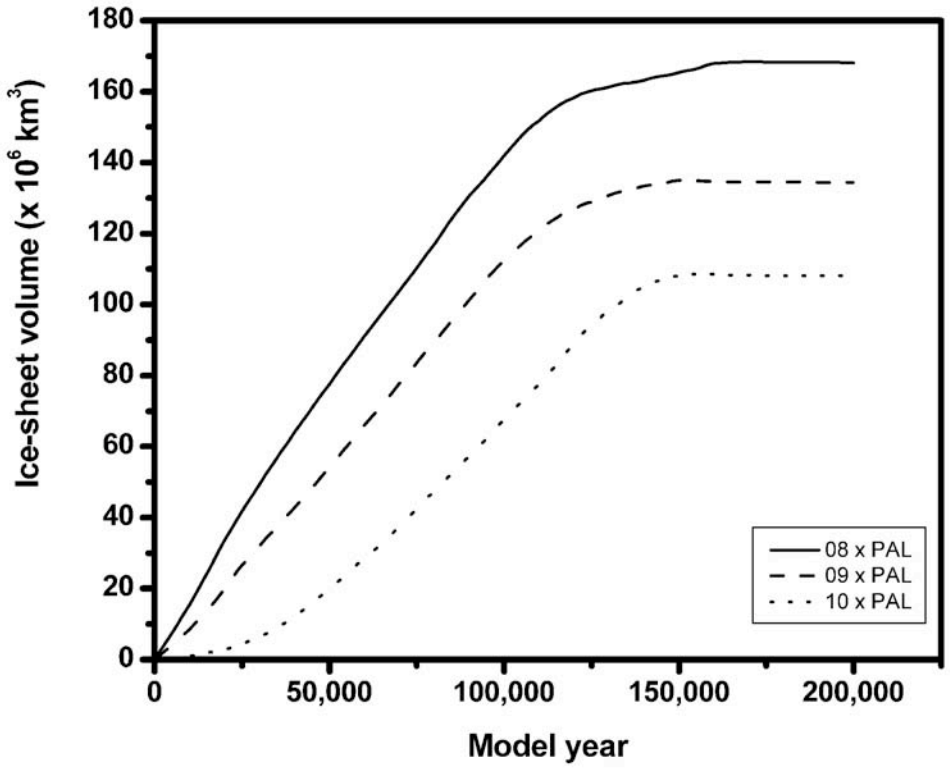

Figure 3.1: Ice-sheet volumes for simulations without orbital forcing.

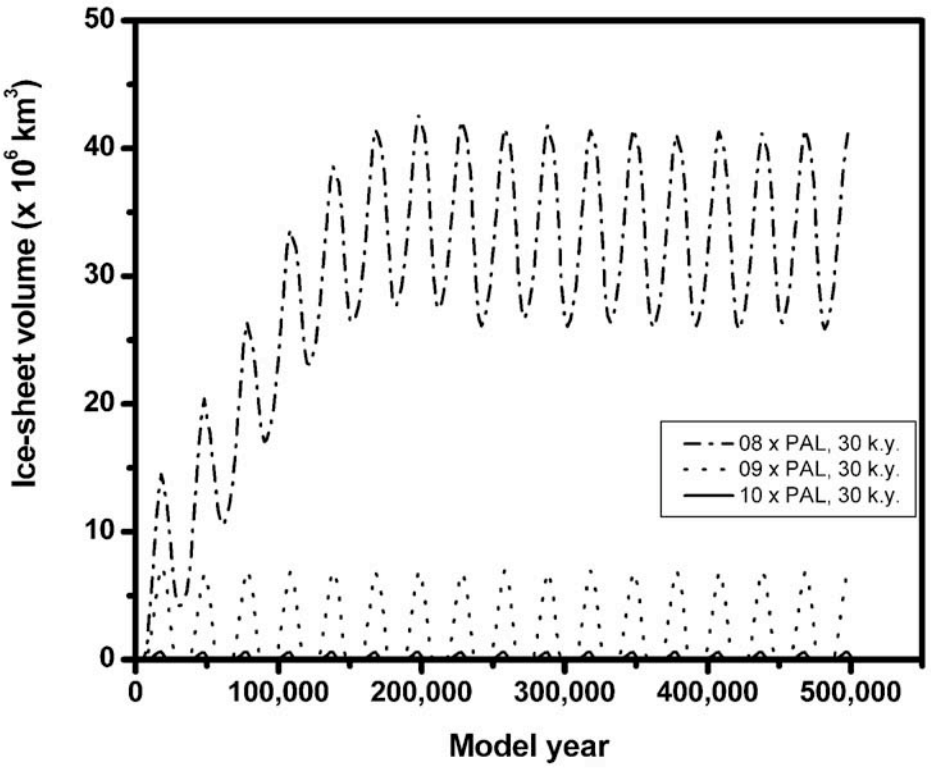

Figure 3.2: Ice-sheet volumes for simulations with orbital-forcing periodicities of 30 k.y..

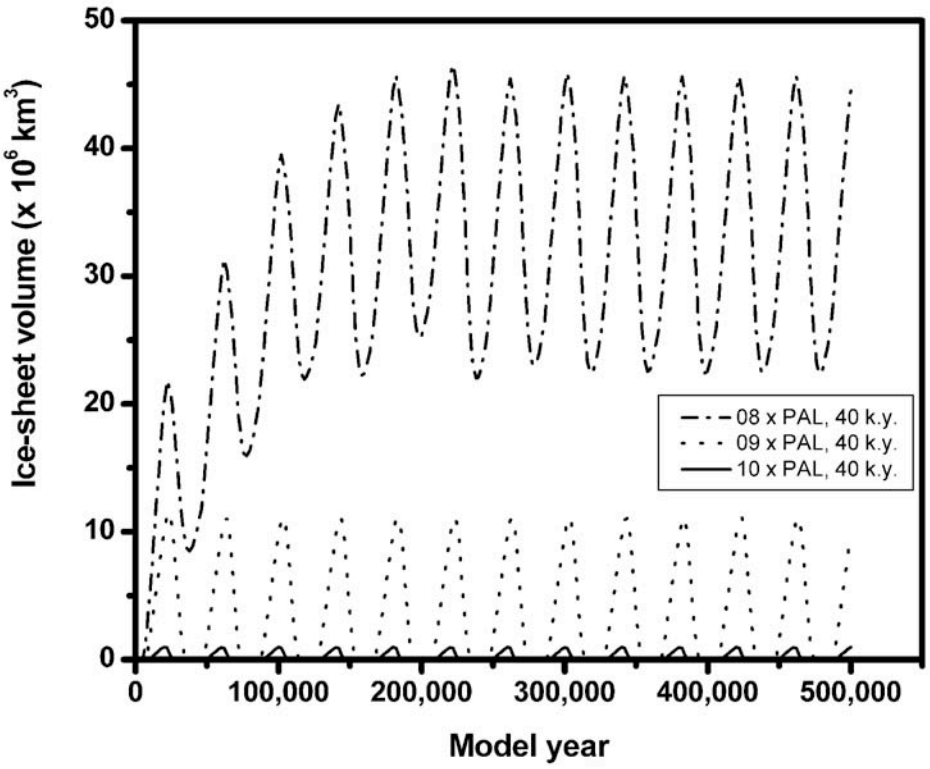

Figure 3.3: Ice-sheet volumes for simulations with orbital-forcing periodicities of 40 k.y..

Ice-sheet sustainability also depends on whether there is an ice sheet present at the start of the simulation. For all simulations, except for the experiment with pCO_2 levels of 10x PAL and a period of 40 k.y., the ice sheet that was formed under no orbital influence (Fig. 3.1) was big enough to be sustained, at a smaller size, during the orbital forcing (Figs. 3.4 and 3.5). In these cases, the ice sheet did not completely melt during the warm-summer orbit; even when pCO_2 was at a level that did not lead to permanent ice sheets when the runs started without ice sheets. Within the second warm-summer cycle, the ice sheets shrink ~40% for those cases (Fig. 3.5).

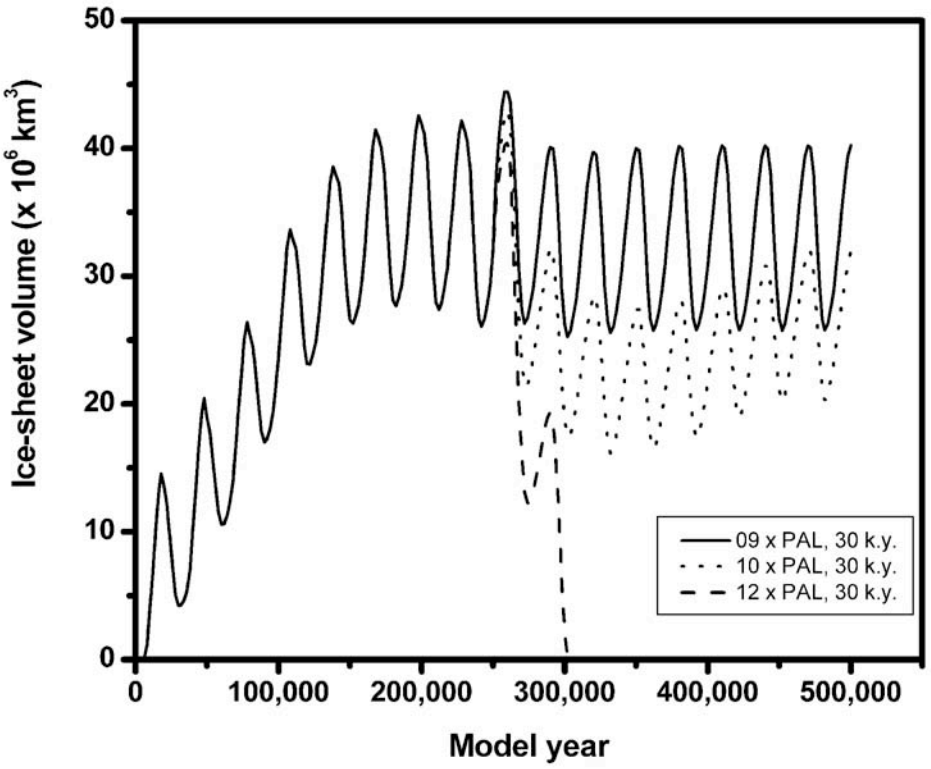

Figure 3.4: Ice-sheet volumes for simulations with orbital-forcing periodicities of 30 k.y. and with preexisting ice-sheet volume for simulation with 8x PAL for the first 250 k.y..

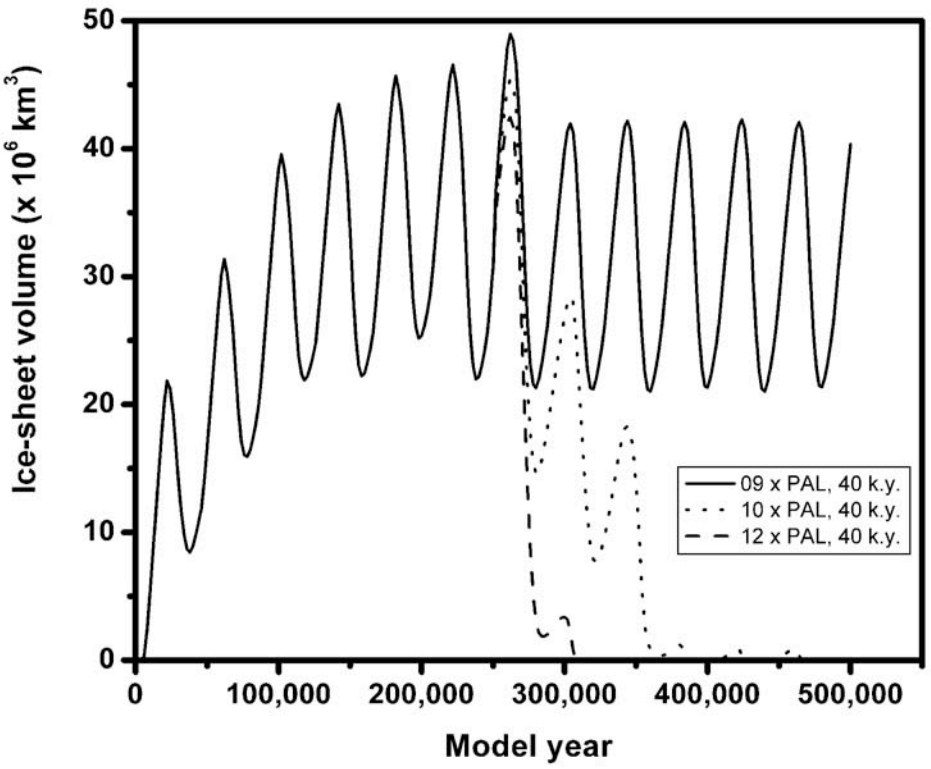

Figure 3.5: Ice-sheet volumes for simulations with orbital-forcing periodicities of 40 k.y. and with preexisting ice-sheet volume for simulation with 8x PAL for the first 250 k.y..

Our simulations indicate that without preexisting ice, permanent ice sheets cannot form with orbital forcing and pCO_2 values of 9x PAL and higher. However, ice sheets can be sustained for pCO_2 levels of 9x PAL (for 30 k.y. and 40 k.y. orbital periodicities) and 10x PAL (only 30 k.y. orbital periodicities) if the runs start with preexisting ice sheets formed during a run of 8x PAL. These observed multiple equilibria of the steady-state ice sheets depend therefore on the size of preexisting ice and the amplitude of the orbital forcing, i.e., insolation. The small ice-sheet instability (SISI) was first described by Weertman (1961) and has since then been described from different ice-sheet models

(e.g., Abe-Ouchi and Blatter, 1993); it is the consequence of the large-scale geometry of the ice-sheet profile and its intersection with the poleward-dipping climatic snowline. Additional simulations are necessary to further define the atmospheric boundary conditions under which the Late Ordovician glaciation was subject to SISI.

Figure 3.6 shows the maximum and minimum extent of the ice sheets with pCO_2 levels of 8x PAL and orbital-forcing periodicities of 30 k.y.. The ice-sheet results show that ice-sheet coverage in the center of Gondwana was sensitive to insolation changes. During the colder periods, ice sheets extended as far toward the equator as 70°S, but melted back during warmer orbits. There are no major differences in ice thickness and distribution between the maximum and minimum extents of the ice sheet for the different orbital periodicities of 30 k.y. and 40 k.y. (not shown).

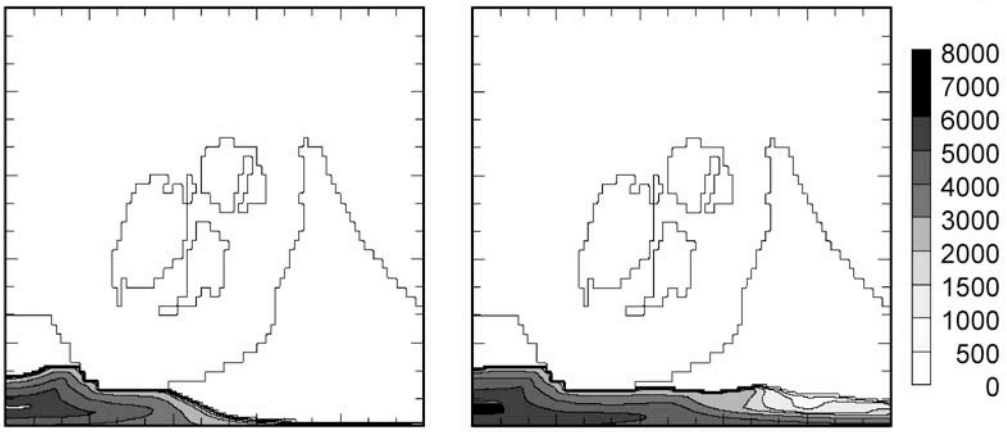

Figure 3.6: Ice-sheet height for simulations with atmospheric pCO_2 levels of 9x PAL with minimal and maximal ice extent for 30 k.y. cyclicity.

Discussion

Several studies investigated the effect of astronomical orbital parameters on the stratigraphic record and ice ages during both the Quaternary and earlier epochs (e.g., de Boer and Smith, 1994; Schwarzacher, 1993). Although precise dating of Ordovician strata is difficult, there is reason to believe that obliquity influenced climate in the same way as it does today and did during the last ice age. This is supported by evidence in the rock record that shows that orbital forcing played a role in the climate system during the Ordovician (Goldhammer et al., 1993; Sutcliffe et al., 2000; Williams, 1991). Our results suggest that Milankovitch cycles at the time scale of the obliquity cycle could have had a strong influence on the waxing and waning of ice sheets during the Late Ordovician glaciation. Under the influence of warm-summer orbits, permanent ice-sheet growth occurred only with pCO_2 levels of 8x PAL or lower. These results constrain the threshold

of atmospheric pCO_2 levels to start glaciation at the lower end of previous estimates (Yapp and Poths, 1992; Berner and Kothavala, 2001). Our results further suggest that adding Milankovitch cyclicity to our simulations prevents the ice sheets from obtaining unreasonably large ice volumes. Without the influence of the warm-summer orbit, the ice volume with 8x PAL reaches ~168 x 106 km3. This volume is about four times larger than the simulated Northern Hemisphere ice-sheet volume over the past 600 k.y. (Li et al., 1998).

Our ice-sheet model results also have important implications for the end of the Late Ordovician glaciation. If ice sheets grew at low pCO_2 (at and below 8x PAL) levels, a rise in pCO_2 to levels higher than 10x PAL would be necessary to melt the ice sheets. Our results therefore support the findings of Kump et al. (1999), who suggested that during the Late Ordovician, pCO_2 levels rose and that the initiation and demise of the Late Ordovician glaciation were due to the interplay of tectonism with carbonate and silicate weathering.

Our results further indicate that climatic changes at the obliquity time scale could have had a significant effect on the waxing and waning of ice sheets during the Late Ordovician. However, the main Milankovitch cycles—those due to precession, obliquity, and eccentricity—combine to produce more complex cycles in the amount of solar energy reaching the outer atmosphere of the Earth. Because AGCMs only simulate a "snapshot" of climate during a Milankovitch cycle, more experiments are needed to fully investigate the sensitivity of the Late Ordovician climate system to stacked Milankovitch cycles. A related limitation of our AGCM plus ice-sheet simulations is that they are run with invariant pCO_2 levels. The combined effects of changes in orbital and pCO_2 forcing

might help explain the short duration of the Late Ordovician glaciation, but more sensitivity studies are necessary to investigate these feedback cycles in more detail.

Conclusions

(1) The ice-sheet model results with orbital forcing indicate that in order to initiate the growth of permanent ice sheets, the atmospheric pCO_2 level must have fallen to 8x PAL or below. This value is at the lower end of estimates of pCO_2 levels for the Late Ordovician based on geochemical modeling (Berner and Kothavala, 2001) and geochemical data from paleosols (Yapp and Poths, 1992). In addition, it is at the lower end of most threshold estimates based on AGCM results (Crowley and Baum, 1991; Crowley and Baum, 1995; Gibbs et al., 1997, 2000; Poussart et al., 1999).

(2) Our simulations indicate that large ice sheets, grown during extreme periods of low pCO_2 (8x PAL or lower), can subsequently be sustained during periods of higher pCO_2 (9–10x PAL) that would otherwise prevent the growth of ice from ice-free starting conditions. Thus, if atmospheric pCO_2 was the main driver of climate during the Late Ordovician, pCO_2 must have risen to >10x PAL to melt the Gondwana ice sheet and end glaciation.

(3) These results are a demonstration of interactions that may be important in other glaciations in Earth history, like the Neoproterozoic snowball Earth (e.g., Hoffman et al., 1998). Ice-sheets and orbital forcing can introduce nonlinearities and bifurcations that significantly alter the response to CO_2 and CO_2 thresholds necessary for the initiation and termination of ice ages.

Acknowledgements

We thank the Penn State Earth and Mineral Science Environment Institute, NASA Astrobiology Institute (NCC2-1057), and National Science Foundation (EAR 00-01918 and EAR 01-06737) for supporting this research.

References Cited

Abe-Ouchi, A., and Blatter, H., 1993, On the initiation of ice sheets: Annals of Glaciology, v. 18, p. 203–207.

Berger, A.L., 1978, Long-term variations of caloric insolation resulting from earth's orbital elements: Quaternary Research, v. 9, p. 139–167.

Berger, W., and Loutre, M.F., 1991, Insolation values for the climate of the last 10 million years: Quaternary Science Reviews, v. 10, p. 297–317.

Berger, W., and Loutre, M.F., 1994, Astronomical forcing through geological time, in de Boer, P.L., and Smith, D.G., eds., Orbital forcing and cyclic sequences: International Association of Sedimentologists Special Publication 19, p. 15–24.

Berger, W., Loutre, M.F., and Laskar, J., 1992, Stability of the astronomical frequencies over the Earth's history for paleoclimate studies: Science, v. 255, p. 560–566.

Berner, R.A., and Kothavala, Z., 2001, Geocarb III: A revised model of atmospheric CO_2 over Phanerozoic time: American Journal of Science, v. 301, p. 182–204.

Brenchley, P.J., Carden, G.A.F., and Marshall, J.D., 1995, Environmental changes associated with the “first strike” of the Late Ordovician mass extinction: Modern Geology, v. 22, p. 69–82.

Brenchley, P.J., Carden, G.A., Hints, L., Kaljo, D., Marshall, J.D., Martma, T., Meidla, T, and Nolvak, J., 2003, High-esolution stable isotopestratigraphy of Upper Ordovician sequences: Constraints on the timing of bioevents and environmental changes associated with mass extinction and glaciation: Geological Society of America Bulletin, v. 115, p. 89-104.

Crowley, T.J., and Baum, S.K., 1991, Toward reconciling Late Ordovician (ca. 440 Ma) glaciation with very high CO_2 levels: Journal of Geophysical Research, v. 96, p. 597–610.

Crowley, T.J., and Baum, S.K., 1995, Reconciling Late Ordovician (440 Ma) glaciation with very high CO_2 levels: Journal of Geophysical Research, v. 100, p. 1093–1101.

Crowley, T.J., and Berner, R.A., 2001, CO_2 and climate change: Science, v. 292, p. 870–872.

de Boer, P.L., and Smith, D.G., 1994, Orbital forcing and cyclic sequences: International Association of Sedimentologists Special Publication 19, 559 p.

DeConto, R.M., and Pollard, D., 2003, Rapid Cenozoic glaciation of Antarctica induced by declining atmospheric CO_2: Nature, v. 421, p. 245-249.

Frakes, L.A., Francis, E., and Syktus, J. I., 1992, Climate modes of the Phanerozoic: the history of the Earth's climate over the past 600 million years: Cambridge, United Kingdom, Cambridge University Press, 274 p.

Gibbs, M.T., Barron, E.J., and Kump, L.R., 1997, An atmospheric pCO_2 threshold for glaciation in the Late Ordovician: Geology, v. 25, p. 447–450.

Gibbs, M.T., Bice, K.L., Barron, E.J., and Kump, L.R., 2000, Glaciation in the early Paleozoic "greenhouse": The roles of paleogeography and atmospheric CO_2, in Huber, B.T., et al., eds., Warm climates in Earth history: Cambridge, Cambridge University Press, p. 386–422.

Goldhammer, R.K., Lehmann, P.J., and Dunn, P.A., 1993, The origin of high-frequency platform carbonate cycles and third-order sequences (Lower Ordovician El Paso Group, West Texas): Constraints from outcrop data and stratigraphic modeling: Journal of Sedimentary Petrology, v. 63, p. 318–359.

Hoffman, P.F., Kaufman, A.J., Halverson, G.P., and Schrag, D.P., 1998, A Neoproterozoic snowball Earth: Science, v. 281, p. 1342–1346.

Hyde, W.T., Crowley, T.J., Tarasov, L., and Peltier, W.R., 1999, The Pangean ice age: Studies with a coupled climate-ice sheet model: Climate Dynamics, v. 15, p. 619–629.

Kump, L.R., Arthur, M., Patzkowsky, M., Gibbs, M., Pinkus, D.S., and Sheehan, P., 1999, A weathering hypothesis for glaciation at high atmospheric pCO_2 during the Late Ordovician: Palaeogeography, Palaeoclimatology, Palaeoecology, v. 152, p. 173–187.

Li, X.S., Berger, A., and Loutre, M.F., 1998, CO_2 and Northern Hemisphere ice volume variations over the middle and late Quaternary: Climate Dynamics, v. 14, p. 537–544.

Pollard, D., Clark, P., Hostetler, S., and Marshall, S., 2000. Driving ice-sheet models using a generic matrix of GCM climates [abs]: Ice Sheets and Sea Level of the Last Glacial Maximum, Environmental Processes of the Ice Age: Land, Ocean Glaciers, EPILOG/IMAGES 2000 meeting, Mt. Hood, Oregon, October 1-5, 2000.

Pollard, D., and Thompson, S.L., 1997, Driving a high-resolution dynamic ice-sheet model with GCM climate: Ice-sheet initiation at 116,000 BP: Annals of Glaciology, v. 25, p. 296–304.

Poussart, P.F., Weaver, A.J., and Barnes, C.R., 1999, Late Ordovician glaciation under high atmospheric CO_2: A coupled model analysis: Paleoceanography, v . 14, p. 542–558.

Ritz, C., Fabre, A., and Letréguilly, A., 1997, Sensitivity of a Greenland icesheet model to ice flow and ablation parameters: Consequences for the evolution through the last climatic cycle: Climate Dynamics, v. 13, p. 11–24.

Schwarzacher, W., 1993, Cyclostratigraphy and Milankovitch Theory: Developmemts in Sedimentology 52, Amsterdam, Elsevier, 225 p.

Scotese, C.R., and McKerrow, W.S., 1991, Ordovician plate tectonic reconstructions, in Barnes, C.R., and Williams, S.H., eds., Advances in Ordovician geology: Geological Survey of Canada Paper 90-9, p. 225–234.

Sutcliffe, O.E., Dowdeswell, J.A., Whittington, R.J., Theron, J.N., and Craig, J., 2000, Calibrating the Late Ordovician glaciation and mass extinction by the eccentricity of Earth's orbit: Geology, v. 28, p. 967–970.

Thompson, S.L., and Pollard, D., 1997, Greenland and Antarctic mass balance for present and double atmospheric CO_2 from the GENESIS version-2 global climate model: Journal of Climate, v. 10, p. 871–900.

Veizer, J., Godderis, Y., and Francois, L.M., 2000, Evidence for decoupling of atmospheric CO_2 and global climate during the Phanerozoic eon: Nature, v. 408, p. 698–701.

Weertman, J., 1961, The Stability of Ice-Age Ice Sheets: Journal of Geophysical Research, v. 66, p. 3783-3792.

Williams, G.E., 1991, Milankovitch-band cyclicity in bedded halite deposits contemporaneous with Late Ordovician–early Silurian glaciation, Canning Basin, Western Australia: Earth and Planetary Science Letters, v. 103, p. 143–155.

Yapp, C.H., and Poths, H., 1992, Ancient atmospheric CO_2 inferred from natural goethites: Nature, v. 355, p. 342–344.

Chapter 4

Response of Late Ordovician paleoceanography to changes in sea level, continental drift, and atmospheric pCO_2: potential causes for long-term cooling and glaciation

Abstract

We performed sensitivity experiments using an ocean general circulation model at two stages of the Late Ordovician (Caradocian, ~454 Ma; Ashgillian, ~446 Ma) under a range of atmospheric pCO_2 values (8-18x PAL; pre-industrial atmospheric level) at high and low sea level.

The model results indicate that the long-term cooling trend during the Late Ordovician can be explained by progressive cooling of the global ocean in response to falling levels of atmospheric pCO_2, sea level change, and paleogeographic change. These results also explain the occurrence of low latitude cool-water carbonates in North America.

In all simulations, a drop in sea level led to a reduction in poleward ocean heat transport. This indicates a possible positive feedback that could have enhanced global cooling in response to sea level drop during the Late Ordovician. Alterations in poleward ocean heat transport linked to changes of atmospheric pCO_2 also indicate that there is a threshold of 10x PAL, above which ocean current change cannot be responsible for glaciation in the Late Ordovician. Continental drift could explain the observed global cooling trend in the Late Ordovician through a combined poleward ocean heat transport

feedback and increased ice-albedo effect if atmospheric pCO_2 was low during the entire Late Ordovician.

The model results further indicate that the response of meridional overturning to changes in paleogeography, atmospheric pCO_2, and sea level is stronger than the response of surface circulation to these perturbations. Because the overturning circulation is so strong, meridional overturning was the dominant mechanism for described changes in heat transport in the Late Ordovician.

Introduction

The glaciation at the end of the Ordovician has attracted attention not only because of its association with a major mass extinction event (Berry and Boucot, 1973; Sheehan, 1973; Sepkoski, 1996), but also because of its short duration (Brenchley et al., 1994; Marshall et al., 1997; Paris et al., 1995; Qing and Veizer, 1994). Ordovician climate is characterized by warm temperatures, high sea level, and atmospheric pCO_2 levels estimated between 8-20 times higher than today (Yapp and Poths, 1992; Berner, 1994; Berner and Kothavala, 2001), leading to an overall greenhouse world during most of the Ordovician. However, near the end of the Ordovician, a major glaciation occurred with a duration of less than 1 million years (Frakes, 1979; Brenchley et al., 1994; Qing and Veizer, 1994; Paris et al., 1995; Marshall et al., 1997). Recent research into its origin has focused mainly on the drawdown of atmospheric pCO_2 (Brenchley et al., 1994, 1995; Kump et al., 1999). Several authors have used energy balance models (Crowley and Baum, 1991) and atmospheric circulation models (Crowley and Baum, 1995; Crowley et

al., 1993; Gibbs, 1996; Gibbs et al., 1997; Gibbs et al., 2000) to investigate the impact of paleogeography and pCO_2 on the Late Ordovician climate system. These model studies have revealed that a Late Ordovician paleogeography makes the formation of permanent snow cover highly sensitive to atmospheric pCO_2 levels. Herrmann et al. (in press) extended the climate modeling approach by using the global atmospheric general circulation model GENESIS v.2.0 to (1) quantify the contribution to global cooling of the movement of Gondwana during the Late Ordovician by directly comparing Caradocian and Ashgillian paleogeographies under a reasonable range of pCO_2 values, (2) assess the effect of the reduced land area at high sea level, which was the condition prior to glaciation, and (3) evaluate the influence of reduced poleward ocean heat transport on global climate. They also coupled a 3-dimensional ice sheet model to the global climate model to investigate the necessary boundary conditions for glaciation (Herrmann et al., 2003). They showed that the paleogeographic evolution coupled with an ice-albedo feedback and/or a drop in atmospheric pCO_2 can only be regarded as pre-conditioning factors for the Late Ordovician glaciation. With a high sea level and a normal heat transport (i.e, a value that replicates the modern climate) ice sheets do not form, even with atmospheric pCO_2 levels as low as 8x PAL. If atmospheric pCO_2 did not drop below the estimates given by Berner (1994) and Yapp and Poths (1992), then either sea level must be lowered from its generally high Late Ordovician levels, or poleward ocean heat transport must be reduced to cause glaciation (Herrmann et al., in press). These results indicate that the ocean played a critical role in the Late Ordovician climate system, but the nature of that role remains uncertain. GENESIS treats the ocean as a non-dynamic slab with a thickness of 50 m. In slab ocean idealization, there are no currents and

poleward ocean heat transport is parameterized by diffusion with a prescribed value. Because of the absence of a dynamical ocean in this atmospheric general circulation model, no potential climate feedbacks of the global ocean with respect to changes in pCO_2, paleogeography, and sea level can be investigated with GENESIS simulations.

Here we use an ocean general circulation model to investigate the response of paleoceanography to changes in sea level, continental drift, and atmospheric pCO_2 during the Late Ordovician. Understanding changes in surface circulation, poleward ocean heat transport, and thermal structure of the ocean is important in order to explain the observed long-term cooling trend of the Late Ordovician (Frakes et al., 1992; Pope and Steffen, 2003) that resulted in the Late Ordovician glaciation. Reduced poleward ocean heat transport, for example, leads to lower temperatures in the high latitudes and can contribute to the initiation of ice sheet growth. In present-day oceans, ocean heat transport is facilitated by both meridional overturning and horizontal gyre circulation. Vertical overturning is the dominant mechanism of poleward ocean heat transport in the North Atlantic (Hall and Bryden, 1982) while in the North Pacific, where no deep-water is formed, heat transport by subtropical gyres is more important (Bryden et al., 1991).

In an important previous study, Poussart et al. (1999) used a coupled atmosphere-ocean-sea ice model to investigate the role of the ocean on the climate system during the last stage of the Ordovician (Ashgillian). Their computed surface circulation patterns were similar to the conceptual model of Wilde (1991). They found that the Late Ordovician paleogeographic configuration resulted in an increase of southward ocean heat transport of up to ~42% compared to present-day. Poussart et al. (1999) also found a sensitivity of the meridional overturning, and thus poleward ocean heat transport, to

changes in the ice-snow albedo parameter. With a higher ice-snow albedo parameter, the ice/snow concentration over sea and land changes, which leads to an equatorward shift of the location of deep-water formation. Additionally, the overturning strengthens below 2000 m. Poussart et al. (1999) showed that the poleward ocean heat transport was sensitive to the Late Ordovician paleogeography and snow/ice cover.

We extend this previous study by directly comparing ocean model simulations using Caradocian and Ashgillian paleogeographies under a reasonable range of pCO_2 values. In addition, we quantify the effect on paleoceanographic conditions of different sea level stands during the Late Ordovician. We also evaluate the importance of potential feedbacks of poleward ocean heat transport with respect to these changes and assess the importance of ocean heat transport changes and ocean temperatures for the long-term cooling and the onset of the Late Ordovician glaciation.

Our results show that the long-term cooling trend can be explained by progressive cooling of the global ocean in response to lower levels of atmospheric pCO_2, coupled with sea level and paleogeographic changes. In our experiments, surface circulation is most sensitive to sea level change. Furthermore, we show that meridional overturning was the main mechanism of poleward ocean heat transport during these time periods. The largest reduction in southward ocean heat transport occurs in Ashgillian simulations with low sea level and low pCO_2 levels (8x PAL).

Methods

Output from an atmospheric general circulation model (AGCM; GENESIS v.2.0) Herrmann et al. (in press) provided the forcing boundary conditions and initial conditions for the Geophysical Fluid Dynamics Laboratory modular ocean model MOM v.2.2 (Pacanowski, 1996). A variety of sea surface boundary conditions, including the annual mean wind stress, evaporation, and precipitation over a range of pCO_2 values (8x, 10x, 12x, 15x, and 18x PAL), and high and low sea levels (Table 4.1) were computed from ten separate GENESIS simulations. The OGCM equations were integrated for 2000 years using Gent-Williams isopycnal mixing. To speed up calculations, we employed a five-fold acceleration in the deep ocean (i.e., the deep ocean currents were effectively simulated for 10000 years). In this uncoupled modeling strategy, there are no feedbacks between the oceanic and atmospheric general circulation models. However, similar uncoupled model studies of the present-day ocean are consistent with observations and this approach has been used in other paleoceanographic studies (e.g., Poulsen et al., 1999, 2001).

Table 4.1: Surface boundary conditions for the OGCM. For a detailed discussion of the atmospheric boundary conditions see Herrmann et al. (in press).

Experiment	Paleogeography	Sea Level	Atmospheric pCO_2	Atmospheric General Circulation Model Boundary Conditions used in all simulations
1	Caradocian	High	2240 (ppm)	Land-Sea distribution: Paleogeography of Scotese and McKerrow (1991) Orbital Parameters: • "Cold-Summer Orbit": • eccentricity: 0.06 • obliquity: 22. • precession: 270. perihelion to N.H. vernal equinox Solar luminosity: 4.5% reduction of present day Vegetation and soil type: No vegetation with intermediate soil color values Other trace gas concentrations: Methane (0.65 ppm); N_2O (0.275 ppm); CFCs (0ppm)
2	Caradocian	High	2800 (ppm)	
3	Caradocian	High	3360 (ppm)	
4	Caradocian	High	4200 (ppm)	
5	Caradocian	High	5040 (ppm)	
6	Caradocian	Low	2240 (ppm)	
7	Caradocian	Low	4200 (ppm)	
8	Ashgillian	High	2240 (ppm)	
9	Ashgillian	High	2800 (ppm)	
10	Ashgillian	High	3360 (ppm)	
11	Ashgillian	High	4200 (ppm)	
12	Ashgillian	High	5040 (ppm)	
13	Ashgillian	Low	2240 (ppm)	
14	Ashgillian	Low	4200 (ppm)	

The OGCM has a latitudinal and longitudinal resolution of 4˚ and 16 unevenly spaced vertical layers (see Fig. 4.1). This resolution has been shown to be sufficient for solving many paleoceanographic problems (e.g., Haupt and Seidov, 2001). The Late Ordovician paleogeographic reconstructions (Fig. 4.1), including continental shelf areas and sea floor spreading centers, are based on Scotese and McKerrow (1990, 1991) and Scotese (1997). The paleobathymetry in the deep ocean was reconstructed with an age-depth relationship of cooling sea floor (Sclater et al., 1971; Seibold and Berger, 1996). The depth of the spreading ridge was set at 2616 m, which is the average depth for modern spreading ridges (Sclater et al., 1971). The subsidence of the sea floor was calculated using the distance from the spreading ridge and a spreading rate of 5 cm/year, which is comparable to modern-day spreading rates in the Atlantic Ocean (Le Pichon, 1968). Estimated Ordovician drifting rates are 6-8 cm/year for Baltica, Siberia, and Gondwana (Scotese and McKerrow, 1991) and 10 cm/year for Baltica and Avalonia

(Harper et al., 1996; van de Pluijm et al., 1995). Given uncertainties with estimating paleospreading rates based on paleomagnetism in the Ordovician, our assumed spreading rate is of the same magnitude, but might lead to somewhat deeper ocean basins. During the Middle and Late Ordovician, wide areas of the continental blocks were flooded and estimates for the sea level highstands range between 175 m and 600 m (Vail et al., 1977; Hallam, 1984; Algeo and Seslavinsky, 1995a, 1995b). In order to represent this high sea level, the continental shelf depth was set to 400 m for the high sea level simulations. Low sea level simulations have no shelf areas. We performed our simulations with this wide range in sea levels in order to investigate the oceanic response to these extreme boundary conditions. Results from an experiment using a shelf depth of 150 m (not shown) show only minor changes compared to the low sea level (exposed shelf) experiment. Thus, we focus our discussion on the extreme values of high and low sea level.

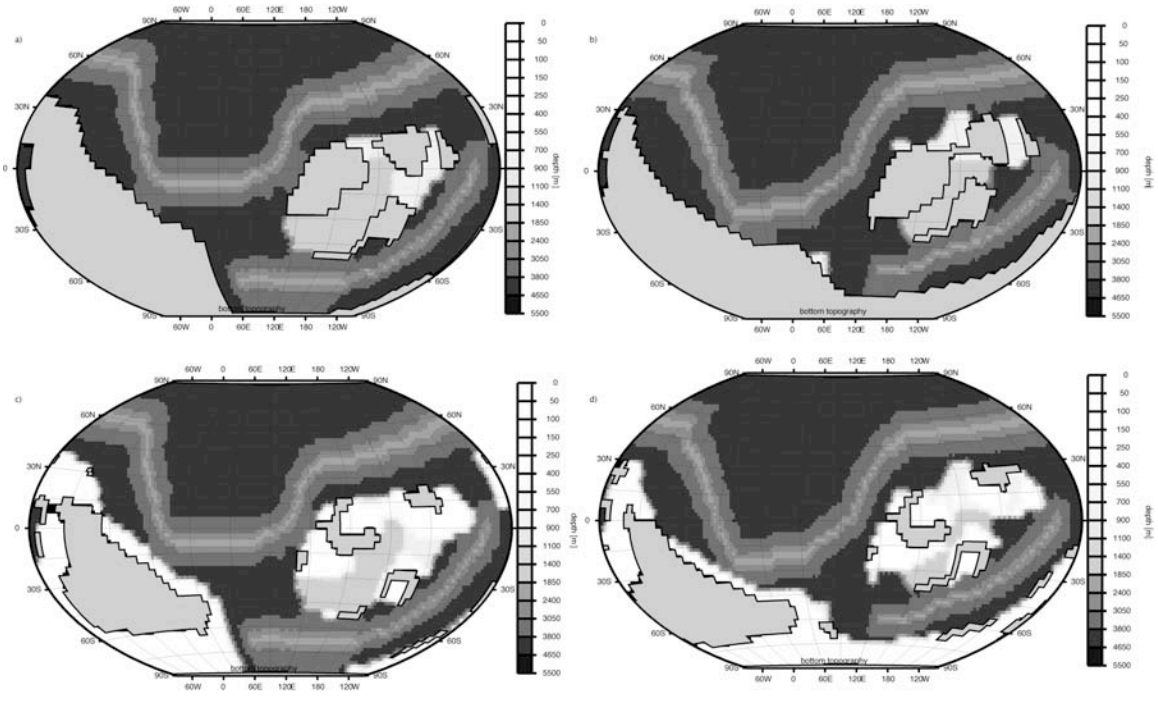

Figure 4.1: Paleogeography and bathymetry used for the ocean general circulation model (OGCM). a) Caradocian with low sea level, b) Ashgillian with low sea level, c) Caradocian with high sea level, d) Ashgillian with high sea level. The scale on the right side of each figure shows the 16 vertical levels used in the OGCM.

Results

Atmospheric forcing

Higher atmospheric pCO_2 levels cause higher annual mean surface temperatures (Fig. 4.2). Atmospheric general circulation, and therefore sea surface climatology, is sensitive to changes in atmospheric pCO_2, paleogeography, and sea level (Fig. 4.3). For atmospheric pCO_2 levels of 12x PAL and higher, paleogeography also affects the annual global mean temperatures. With these high pCO_2 values, experiments with an Ashgillian

paleogeography lead to lower annual mean temperatures than experiments with Caradocian paleogeography (Fig. 4.2). This difference can be explained with the increased cooling effect of the southern part of Gondwana that moved towards the South Pole (Fig. 4.3a and 4.3b). This cooling is largely caused by a change in albedo, which is associated with the changed land-sea distribution in the higher southern latitudes. However, for pCO_2 levels lower than 12x PAL, the increased sea-ice formation in the southern and northern higher latitudes generally does not lead to significant differences in annual global mean temperatures (Fig. 4.2). Changes in pCO_2 level also affect the equator-to-pole temperature gradients (Fig. 4.3a and 4.3b). The zonally averaged annual near surface atmospheric temperature gradient increases from approximately 29°C to 43°C with a drop in pCO_2 from 18x PAL to 8x PAL in the Caradocian experiments (Fig. 4.3a). Similarly, this temperature gradient increases from approximately 30°C to 44°C due to a drop in pCO_2 in the Ashgillian experiments. The net moisture flux (precipitation minus evaporation) in tropical regions is also sensitive to changes in paleogeography and atmospheric pCO_2 level (Fig. 4.3c and 4.3d). Due to the intensified hydrologic cycle under high pCO_2 levels, the net moisture flux increases with increased pCO_2 values. Ashgillian experiments have higher net moisture flux in the tropics than Caradocian experiments with the same atmospheric pCO_2 values. Late Ordovician zonally averaged eastward wind stresses are not very sensitive to changes in paleogeography or to changes in atmospheric pCO_2 (Fig. 4.3e and 4.3f).

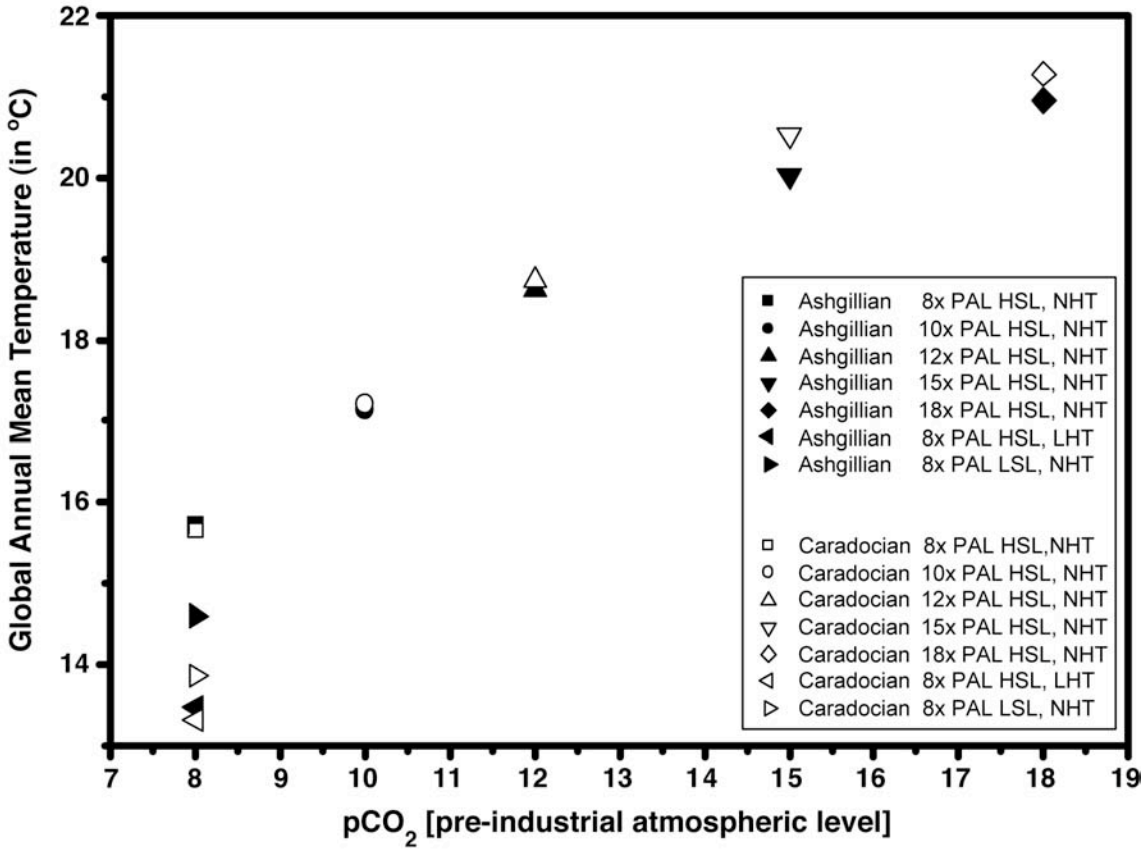

Figure 4.2: Relationship between atmospheric pCO_2, mean annual temperature, paleogeography, and prescribed poleward ocean heat transport of the atmospheric general circulation model results of Herrmann et al. (in press). A more detailed description of the boundary conditions can be found in Herrmann et al. (in press). PAL is pre-industrial level of atmospheric pCO_2, HSL is high sea level, LSL is low sea level, NHT is normal heat transport, and LHT is low heat transport.

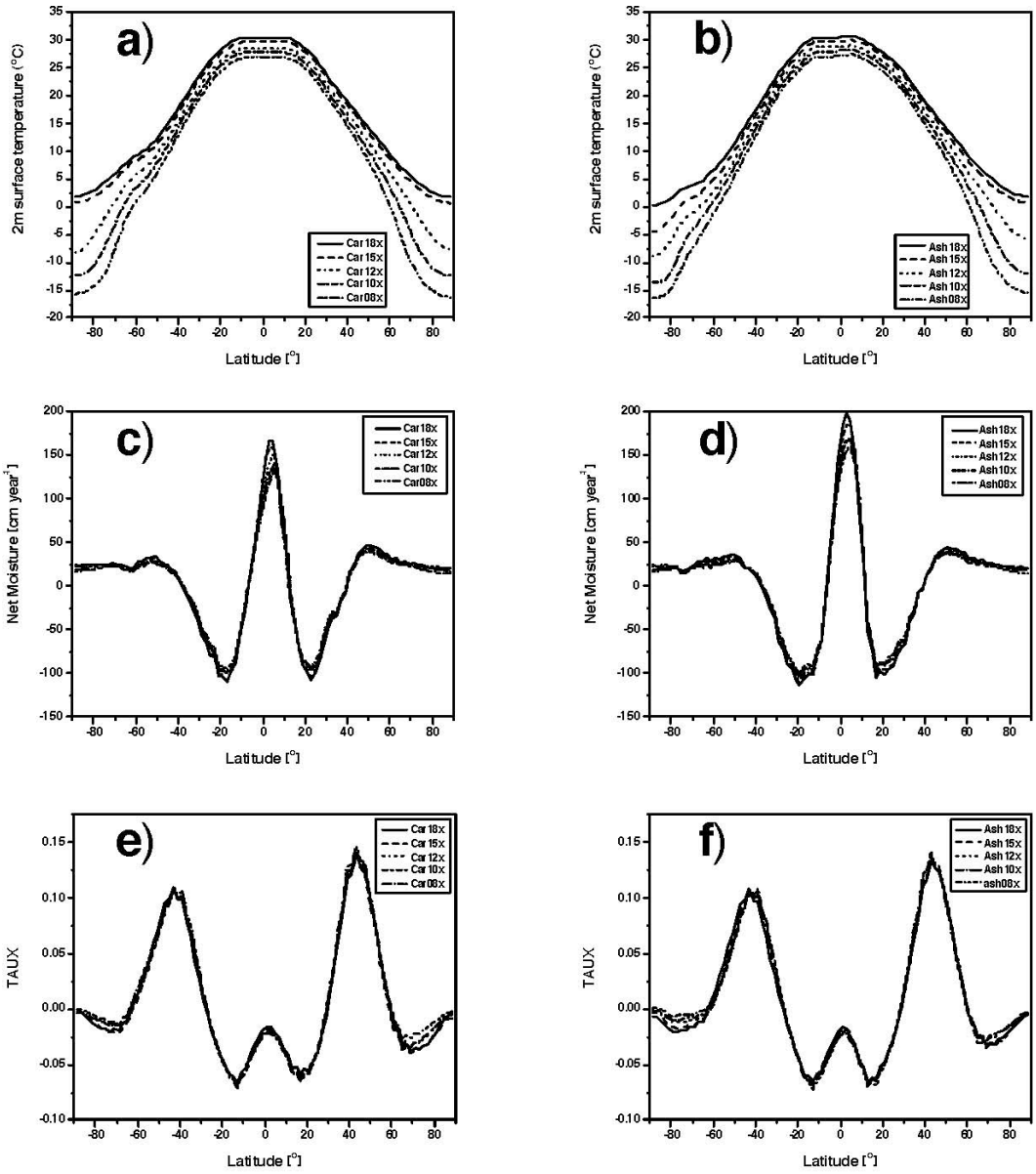

Figure 4.3: Global zonally averaged, mean annual 2m air temperature (°C) for a) Caradocian, and b) Ashgillian experiments; net moisture flux (precipitation minus evaporation) (cm/year) for c) Cardocian, and d) Ashgillian experiments; zonal windstress (N/m^2) for e) Cardocian, and f) Ashgillian experiments.

Ocean surface circulation

Poussart et al. (1999) have published OGCM simulations with similar surface circulation patterns to the conceptual model of Wilde (1991). They found four major ocean gyre systems: 1) the north Panthalassic convergence, 2) the south Panthalassic convergence, 3) the south Paleo-Tethys convergence, and 4) north Paleo-Tethys convergence. Because of the absence of large land masses in the Northern Hemisphere, the ocean circulation is predominantly zonal there. In addition to this so-called circumpolar current system (Panthalassic Circumpolar Current), Poussart et al. (1999) identified the Iapetus Current (connecting the south Panthalassic and the south Paleo-Tethys gyres), the North and South Equatorial Currents, and the Antarctica Current (western boundary current along Gondwana traveling south towards the South Pole).

Our OGCM results agree with this general circulation scheme (Fig. 4.4 and 4.5). In addition, a Southern Gondwana Current (SGC) is present in the simulations with a high sea level. This current flows from the western side of Gondwana to the eastern side of Gondwana (Fig. 4.4a).

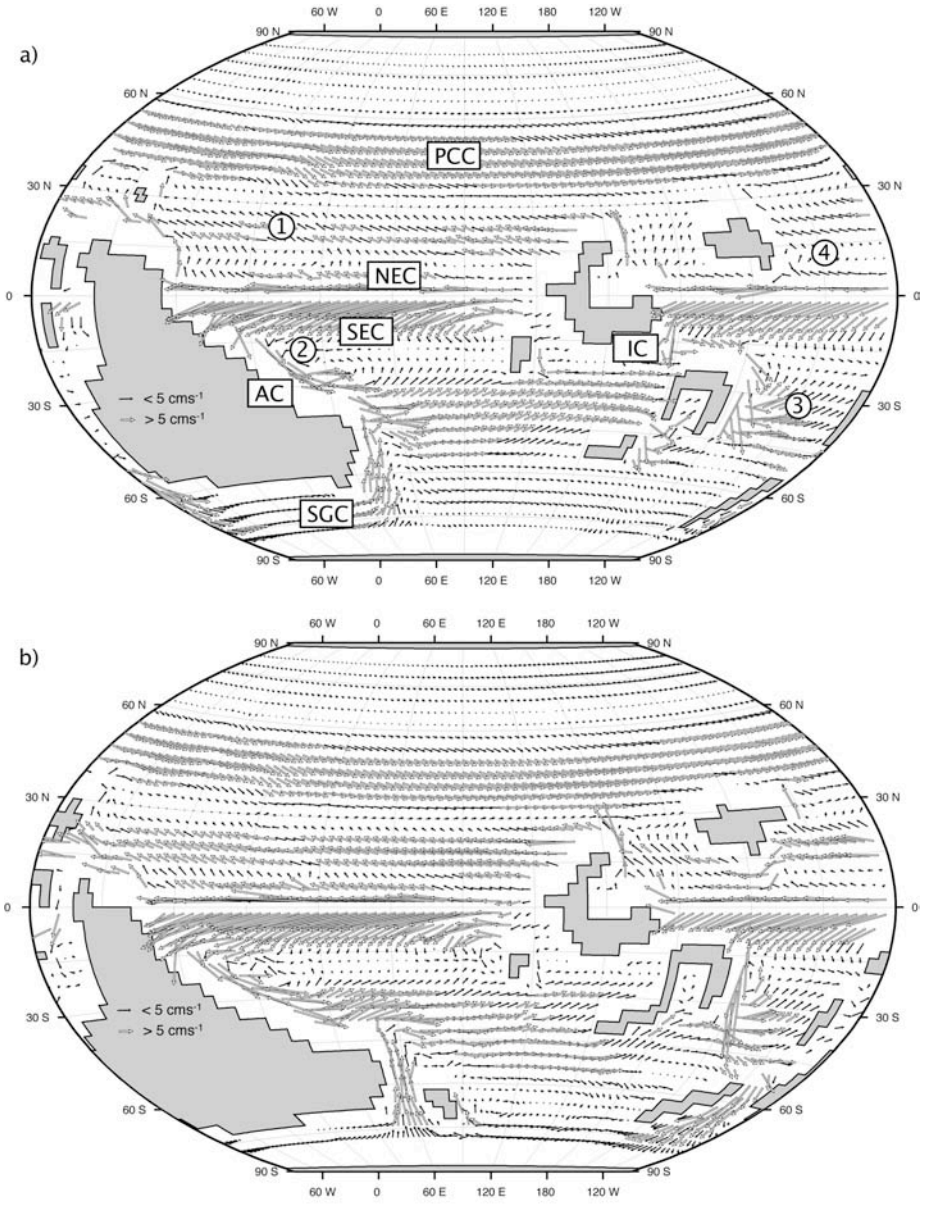

Figure 4.4: Surface currents for experiments with high sea level and atmospheric pCO_2 levels of 15x PAL for a) Caradocian and b) Ashgillian paleogeography. Numbers represent gyre systems: 1 – North Panthalassic Convergence, 2 – South Panthalassic Convergence, 3 – South Paleo-Tethys Convergence, and 4 – North Paleo-Tethys Convergence. Letters represent surface currents: SGC – Southern Gondwana Current, PCC – Panthalassic Circumpolar Current, IC – Iapetus Current, NEC and SEC – North and South Equatorial Currents, and AC – Antarctica Current.

Changes in paleogeography during the two time intervals have only a minor effect on the surface circulation pattern. Southward movement of Gondwana in the Ashgillian caused a reduction in the SGC. Consequently, the strength of the eastward flowing south Panthalassic convergence decreases in strength. The northward movement of Baltica in the Ashgillian narrowed the Iapetus ocean width, which in turn, narrowed and slowed down the Iapetus Current (Fig. 4.4).

Changes in atmospheric pCO_2 have almost no effect on the global ocean circulation pattern. The only noticeable change is found in the merging zone of the Antarctica current and the SGC in the Ashgillian. At lower levels of atmospheric pCO_2, the convergence zone is stronger due to an increased strength of the SGC.

Sea level change is the most important factor for the Late Ordovician ocean circulation. At low sea level stands, the SGC system disappears. Due to the further restriction of the Iapetus ocean with the exposed shelf areas, the Iapetus current became narrower. However, as it narrowed, the intensity of the current increased (Fig. 4.5).

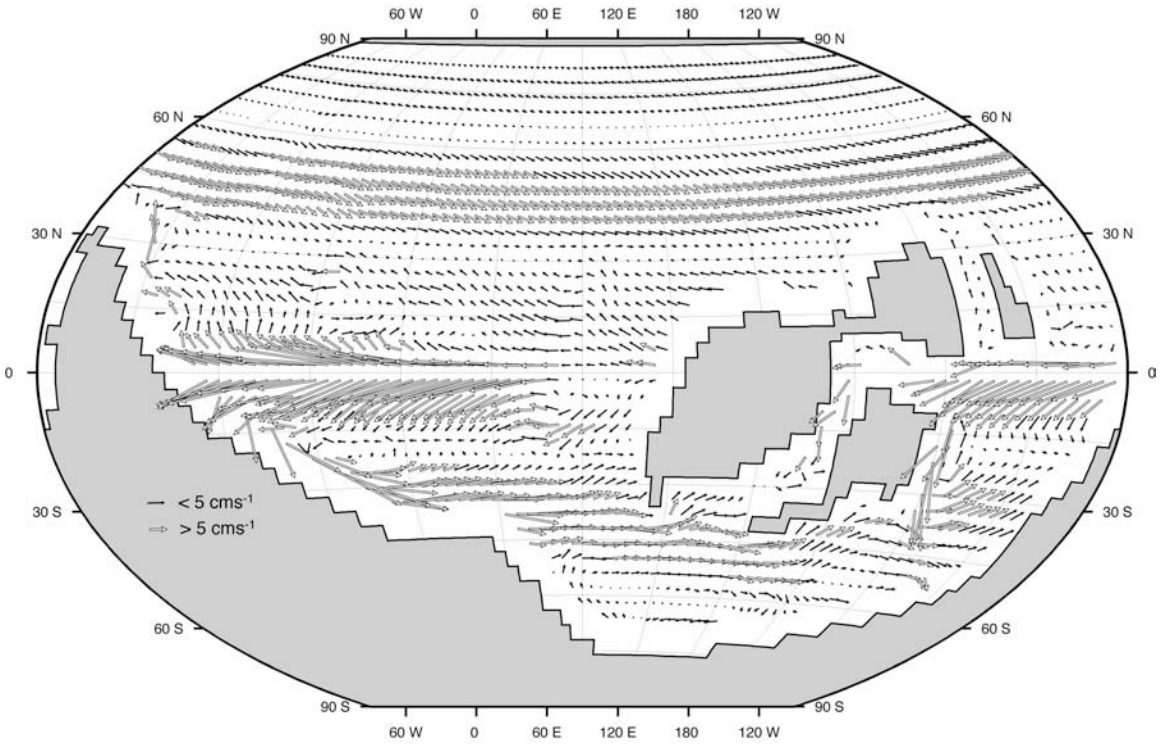

Figure 4.5: Surface currents for Ashgillian experiments with low sea level and atmospheric pCO_2 levels of 15x PAL.

Global Ocean Temperature

The average mean ocean temperature of the sea surface (Fig. 4.6) and deep water (Table 4.2) is very sensitive to changes in atmospheric pCO_2, paleogeography, and sea level.

Table 4.2: Late Ordovician ocean model results. The name of each experiment refers to Table 4.1. Shown are the average temperature of the ocean (T_{avg}), average temperature for ocean depth of 0-150 m ($T_{0\text{-}150}$), 150-400 m ($T_{150\text{-}400}$), and below 600 m (T_{600}).

Experiment	T_{avg}	$T_{0\text{-}150}$	$T_{150\text{-}400}$	T_{600}
1	2.08	15.42	12.77	0.48
2	1.88	16.7	13.26	0.13
3	4.04	18.24	14.86	2.38
4	8.07	20.03	16.83	6.7
5	8.07	20.03	16.83	6.7
6	0.73	13.24	10.12	-0.49
7	2.15	17.09	13.13	0.71
8	1.65	14.85	11.55	0.12
9	2.01	15.83	12.48	0.39
10	2.38	16.87	13.38	0.68
11	4.23	18.17	14.78	2.6
12	5.76	19.04	15.79	4.21
13	1.24	15.65	11.6	-0.09
14	2.22	18.7	14.36	0.68

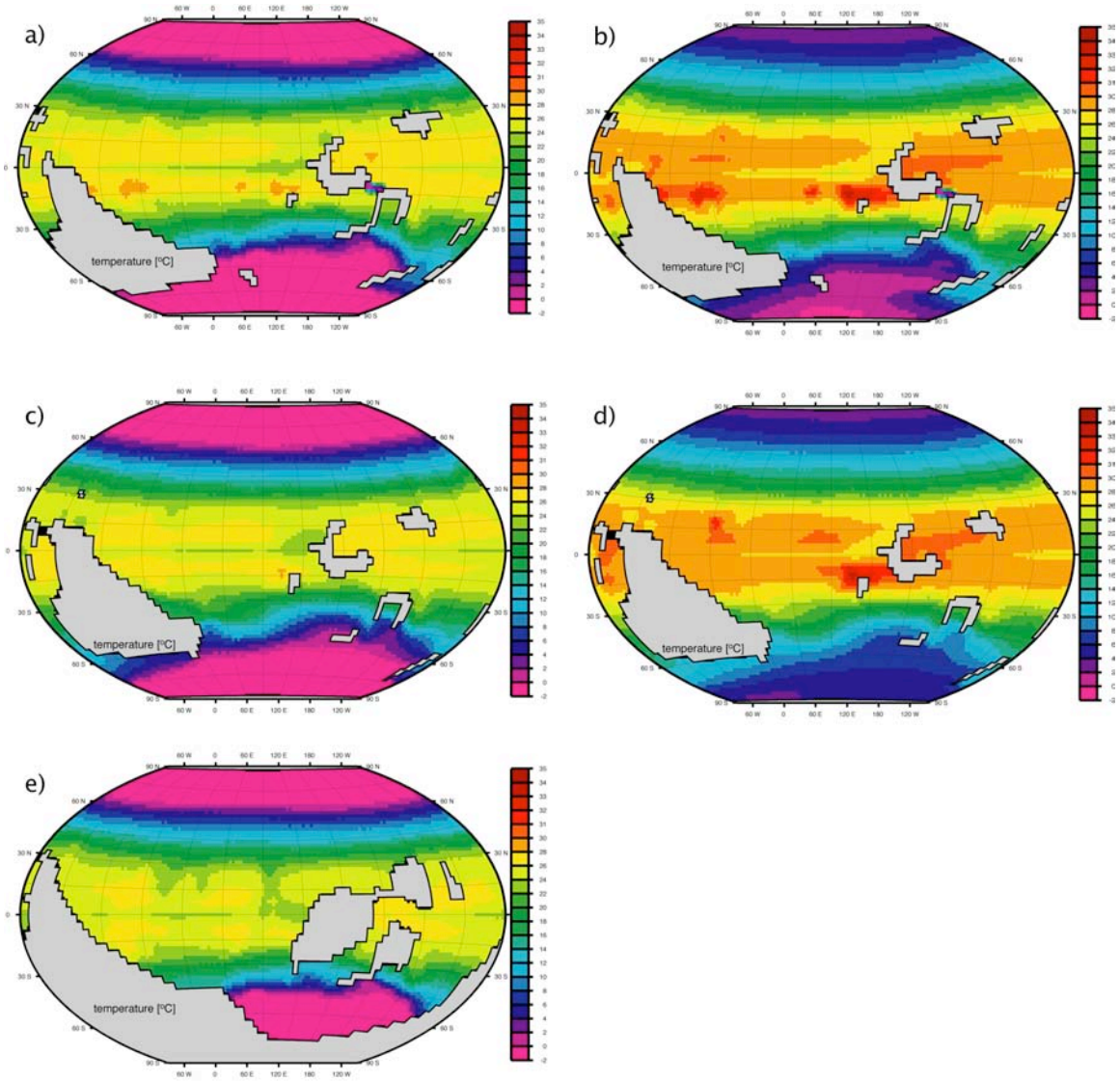

Figure 4.6: Annual mean sea surface temperature distribution for simulations with high sea level, Ashgillian paleogeography, and pCO_2 levels of a) 8x, and b) 15x PAL; high sea level, Caradocian paleogeography, and pCO_2 levels of c) 8x, and d) 15x PAL; low sea level, Ashgillian paleogeography, and pCO_2 levels of e) 8x.

For the Caradocian simulations with high sea level and atmospheric pCO_2 levels of 18x PAL and 15x PAL, the surface ocean water stays above 0ºC in the higher latitudes and equatorial surface waters are above 30ºC. In the simulations with atmospheric pCO_2 levels with 12x PAL and lower, the equatorial surface waters cool below 30ºC, and the

water masses with 0ºC to -2ºC expands towards the equator from the higher latitudes. The average ocean temperature for the Caradocian high sea-level simulations also drops from about 8.1ºC with atmospheric pCO_2 levels of 18x PAL to about 2.1ºC for the 8x PAL simulation.

Ashgillian simulations give colder ocean temperatures than Caradocian simulations with identical atmospheric pCO_2 levels. In contrast to the Caradocian simulations, Ashgillian simulations with high sea level and atmospheric pCO_2 levels of 15x PAL have surface water temperatures in the higher latitudes below 0ºC. With falling atmospheric pCO_2 levels, cold water expands toward the equator and the equatorial surface waters cool below 30ºC. The average ocean temperature for the Ashgillian high sea-level simulations also drops from about 5.8ºC with atmospheric pCO_2 levels of 18x PAL to about 1.7ºC for the 8x PAL simulation. Ashgillian simulations with lower sea-level yield colder temperatures than those with high sea-level. A drop from atmospheric pCO_2 levels of 15x to 8x leads to a colder temperatures in the higher Northern latitudes and colder equatorial waters. However, the surface water temperature distribution in the higher southern latitudes does not change significantly.

Meridional overturning

The paleogeographic configuration with no land masses in the Northern Hemisphere leads to an hemispherically asymmetric meridional overturning in the Late Ordovician (Fig. 4.7). All deepwater is formed in the southern hemisphere. Without

deepwater formation in the Northern Hemisphere, southern bottom water penetrates far to the north and is the only deepwater mass in the Late Ordovician oceans.

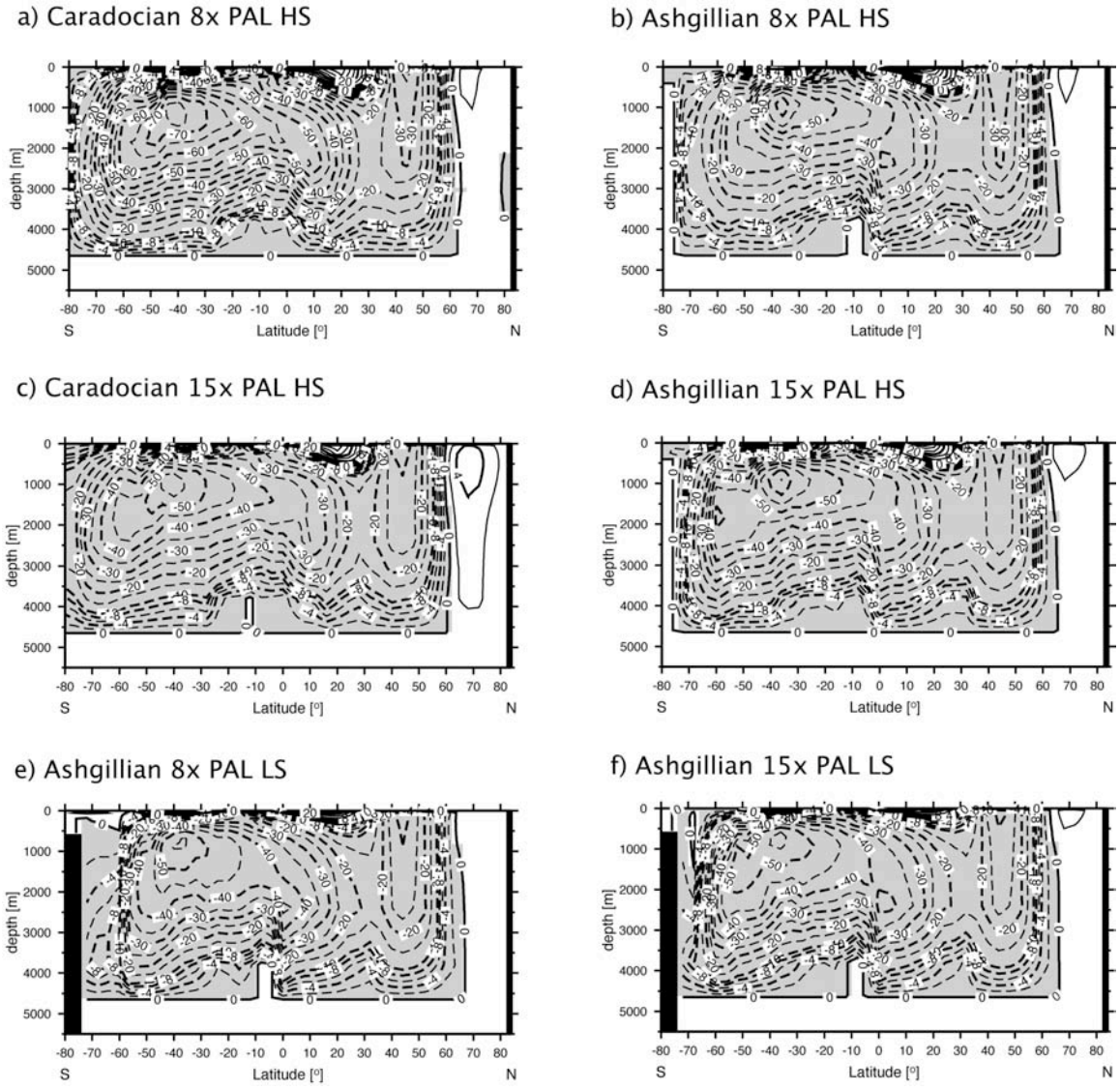

Figure 4.7: Latitude-depth plots of meridional overturning streamlines. PAL – pre-industrial atmospheric level of pCO_2; HS – high sea level; LS – low sea level. Mass transport values are in units of 10^6 m^3s^{-1}. Negative values have a counter-clockwise rotation.

The strength of the overturning depends on changes in paleogeography, atmospheric pCO_2, and sea level. The strongest overturning occurs with a Caradocian paleogeography and atmospheric pCO_2 values of 8x PAL (Fig. 4.7a). With an atmospheric pCO_2 level of 15x PAL and a Caradocian paleogeography, the meridional overturning becomes stronger in the Northern Hemisphere and weaker in the Southern Hemisphere. Compared to the Caradocian simulations with a high sea level, the Ashgillian simulations have a weaker overturning and the location of the deep water formation has shifted equatorward. While changes in atmospheric pCO_2 affect the strength of the meridional overturning in the Caradocian, changes in atmospheric pCO_2 have almost no effect on the overturning in the Ashgillian simulations. The model results suggest that a sea level drop in the Ashgillian could lead to an equatorward shift of deepwater formation and weakening of meridional circulation.

Ocean heat transport

Atmospheric pCO_2

During the Caradocian, a decrease in atmospheric pCO_2 leads to an increase in southward ocean heat transport (Fig. 4.8). The strongest southward ocean heat transport occurs at atmospheric pCO_2 levels of 8x PAL. A drop from 18x PAL to 8x PAL leads to an increase in southward ocean heat transport by about 57%.

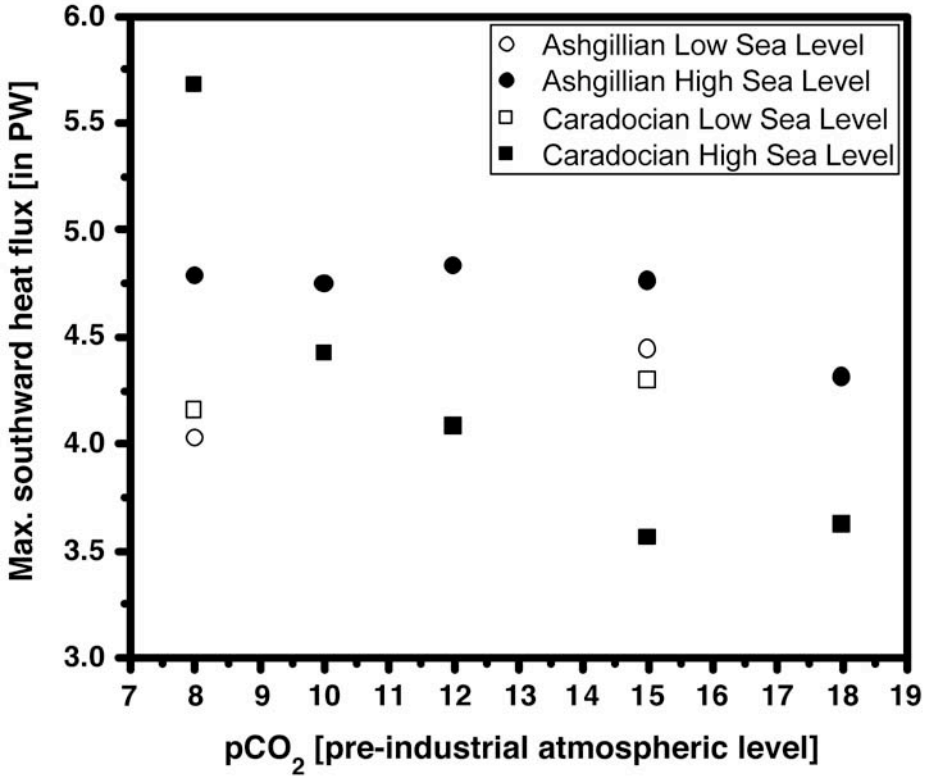

Figure 4.8: Southward ocean heat transport (in PW; 1PW=10^{15}W) for simulations with high and low sea level, Caradocian and Ashgillian paleogeographies, and different pCO_2 levels. Note that the magnitude of southward heat flux is correlated with the intensity of meridional overturning (Fig. 4.7). Due to the presence of a single overturning cell in the southern hemisphere (Fig. 4.7) that drives heat transport, only the maximum southward heat transport is plotted.

During the Ashgillian, there is almost no change in southward ocean heat transport in the simulations with atmospheric pCO_2 levels between 15 x and 8x PAL (Fig. 4.8). A decrease in atmospheric pCO_2 level from 18x PAL to 15x PAL causes an increase in southward ocean heat transport of by about 10%. However, when atmospheric pCO_2 level falls below 15x PAL, there is no further increase in poleward ocean heat transport.

These differences in sensitivity of the ocean heat transport to changes in pCO_2 show that the response of the system is non-linear. Poleward heat transport depends on

the overall intensity of overturning. The highest heat transport in Figure 4.8 for example corresponds with the highest overturning in Figure 4.7.

Paleogeography

With atmospheric pCO_2 values above 10x PAL, the Ashgillian paleogeography causes a 10-20% increase in ocean heat transport in the Southern Hemisphere compared to the Caradocian paleogeography. At 10x PAL, the Caradocian and Ashgillian southward ocean heat transports are almost the same, while at 8x PAL the Ashgillian heat transport is about 25% weaker in the Southern Hemisphere than the Caradocian (Fig. 4.8).

Sea Level

The low sea level experiments with atmospheric pCO_2 values of 8x PAL show a lower southward ocean heat transport than the simulation with a high sea level (Fig. 4.8). In the Caradocian, southward ocean heat transport is about 35% lower in the experiments with a lower sea level than in the runs with higher sea level; in the Ashgillian such reduction is smaller and only about 20%. In the Caradocian simulation with atmospheric pCO_2 values of 15x PAL, sea level drop causes an increase in southward ocean heat transport.

Discussion

Late Ordovician paleogeography was characterized by (1) an equatorial belt of land and shallow seas, (2) no land masses close to the Ordovician North Pole, and (3) an extensive land mass at the Ordovician South Pole (Scotese and McKerrow, 1990; Scotese and McKerrow, 1991; Scotese, 1997) (Fig. 4.2). Wilde (1991) speculated that due to very different paleogeographic positions of the continents during the Ordovician, the oceanic circulation patterns were not comparable to those of today since the location of the climate belts might have differed from their modern position. He suggested that due to equatorial barriers the deep circulation of the Northern and Southern Ocean were independent. Due to the lack of meridional barriers, the Northern Hemisphere would have been dominated by zonal (east-west) surface currents. Furthermore, he suggested that the oceans in the Southern Hemisphere had similar surface current patterns like today's oceans due to continental barriers in the Southern Hemisphere. Poussart et al. (1999) published OGCM results for the last stage of the Late Ordovician (Ashgillian) that showed similar modeled surface circulation patterns to the conceptual model of Wilde (1991). Our OGCM results agree with the general circulation schemes of Wilde (1991) and Poussart et al. (1999).

Paleogeographic changes

The paleogeographic evolution during the Late Ordovician includes: (1) northward movement of Baltica and Siberia, and (2) a southward movement of Gondwana. Herrmann et al., (in press) examined the hypothesis of earlier AGCM studies

that continental drift contributed to global cooling during the Late Ordovician (Crowley and Baum, 1991; Crowley and Baum, 1995; Crowley et al., 1993; Gibbs et al., 2000). Herrmann et al. (in press) found no temperature differences between the Caradocian and Ashgillian paleogeography with atmospheric pCO_2 values below 12x PAL. However, they did find that above atmospheric pCO_2 values of 12x PAL, the Ashgillian paleogeography led to lower global annual mean temperatures. This result suggests that only during times of high pCO_2 (above 12x PAL) and high sea level was continental drift an important factor that pre-conditioned the global climate system for glaciation. In this study, for atmospheric pCO_2 values above 10x PAL, the Ashgillian paleogeography is characterized by an increased southward ocean heat transport that would have counteracted the cooling effect of increased land-sea ratio in the high latitudes of the Southern Hemisphere. However, for pCO_2 values below 10x PAL, the simulations with an Ashgillian paleogeography have lower southward heat transport values than the Caradocian simulations.

Sea-level changes

Herrmann et al. (in press) suggested sea level changes had a strong influence on the build-up of ice sheets. Ice sheets could form with a low sea level, ocean heat transport at its present-day intensity, and an atmospheric pCO_2 level of 8x PAL (Fig. 4.2). Our results emphasize that a sea level change has the potential to initiate glaciation or to enhance glaciation by a positive feedback. At 8x and 15x PAL, low sea level simulations have a weaker southward ocean heat transport regardless of land-sea distributions. A drop

in sea level in the Ashgillian at low atmospheric pCO_2 levels could establish a positive feedback. This feedback could initiate and/or amplify glaciation by reducing the southward ocean heat transport due to a reduction of meridional overturning.

The onset of glaciation using this mechanism depends on the timing of the sea level drop. Many Late Ordovician sea level curves suggest that the sea level drop was confined to the Ashgillian stage (Brenchley and Newall, 1980; Leggett et al., 1981; Lenz, 1982). However, other authors believe that sea level began to drop before the Ashgillian stage (McKerrow, 1979; Fortey, 1984; Ross and Ross, 1988, 1992). Provided the sea level dropped before the Ashgillian when pCO_2 was low, due to factors other than glacio-eustatic sea level changes (e.g. changes in spreading rates; Pitman, 1978), this sea level drop could have led to breaching a threshold for the initiation of ice sheets. The glaciation can be initiated by the amplified cumulative effects of reduced poleward ocean heat transport and increased surface albedo. Alternatively, if sea level drop prior to the Ashgillian stage is caused by the initial build up of ice in certain areas (e.g., mountain glaciers) this could have caused a positive feedback driving the climate system toward glaciation.

Atmospheric pCO_2

Our results show that the progressive cooling of the ocean during the Late Ordovician can be attributed to changes in atmospheric pCO_2, paleogeography, and sea level. Model results indicate a strong influence of atmospheric pCO_2 on surface and deep water temperatures. This is consistent with the interpretation that global cooling during

the Late Ordovician could have been the result of a drawdown of pCO_2 due to the deposition of organic matter (Brenchley et al., 1994, 1995) or by increased silicate weathering (Kump et al., 1999). The drawdown of pCO_2 as a potential cause for the global cooling and the onset of the Late Ordovician glaciation is further supported by several atmospheric general circulation model studies that have found a high sensitivity of the formation of permanent snow cover and ice sheets with respect to atmospheric pCO_2 values for the Late Ordovician paleogeography (Crowley et al., 1993; Crowley and Baum, 1995; Gibbs, 1996; Gibbs et al., 1997; Gibbs et al., 2000; Herrmann et al., in press). Herrmann et al. (in press, 2003) coupled a 3-dimensional ice sheet model to their AGCM to determine the threshold for initiation of glaciation. They showed that it is impossible to initiate ice sheets in southern Gondwana with pCO_2 values as low as 8x PAL and a high sea level. Only if both poleward ocean heat transport (prescribed in the AGCM) weakens and/or sea level drops can ice sheets form at atmospheric pCO_2 levels of 8x PAL. Therefore, Herrmann et al. (in press) argue that a drop in pCO_2 serves only as a preconditioning factor. Our OGCM results support the idea that a drop in atmospheric pCO_2 levels alone was not sufficient to breach the threshold of glaciation given the estimates of Berner (1994) and Yapp and Poths (1992) of atmospheric levels of 14±6x PAL. In the Ashgillian, there is almost no change in poleward ocean heat transport with atmospheric pCO_2 levels between 15x and 8x PAL keeping the poles relatively warmer despite the lower atmospheric pCO_2 levels.

Regional change reflects global cooling

An understanding of global oceanic circulation patterns and its response to perturbations of the global climate system is necessary to explain both global and regional paleoceanographic events during this time period. The spatial and temporal distribution of glacial marine and continental deposits for instance, indicate that the beginning of the glaciation was in the Middle Ordovician (Frakes et al., 1992) and therefore points towards progressive cooling of the atmosphere during the Late Ordovician. In the Early Chatfieldian of North America, sedimentological and faunal evidence indicates a transition from warm-water to cool-water conditions in the Early Late Ordovician (Brookfield, 1988; Brookfield and Brett, 1988; Patzkowsky and Holland, 1993; Lavoie, 1995; Holland and Patzkowsky, 1996; Pope and Read, 1997; Lavoie and Asselin, 1998; Lavoie et al., 1998). This transition from warm-water to cool-water carbonates is problematic since paleogeographic reconstructions and paleoclimatic indicators place North America in tropical to subtropical latitudes during this period (Scotese and McKerrow, 1990, 1991; Scotese, 1997). Global interpretations for this transition suggest that the lithologic and oceanographic changes of North America are the result of the onset of icehouse conditions which eventually led to a glaciation in the Latest Ordovician (Lavoie, 1995; Pope and Read, 1997; Lavoie and Asselin, 1998). The presence of wide-spread upwelling conditions along the southern margin of Laurentia in the Middle Ordovician support the interpretation that the initiation of the glaciation occurred during this time period and reached its maximum in the Hirnantian (Pope and Steffen, 2003). Kolata et al. (2001) describe an oceanic passage through which cold

oceanic waters could reach the epeiric sea of Laurentia. Regardless of the passage way onto the craton, in order for cold water to reach the center of the continent, the surrounding open ocean must cool down. Our model results indicate that the open ocean waters along the southeastern coast of Laurentia cooled down in response to lower atmospheric pCO_2 levels. The temperature drops from about 24°-26°C to about 18°-20°C in response to a drop in pCO_2 from 18x to 8x. This colder water could have penetrated the epeiric sea of Laurentia. The cooling trend of the Late Ordovician ocean in response to the onset of the glaciation is supported by sedimentological evidence from deep-sea sediments (Armstrong and Coe, 1997).

Conclusions

One of the biggest mass extinctions of the Phanerozoic occurred in the Late Ordovician. In the absence of evidence for extraterrestrial causes for this mass extinction, the major glaciation at the end of the Ordovician has been suggested as the cause. Previous AGCM studies focused on a drawdown of atmospheric pCO_2 to levels as low as 8x PAL as the single cause for the initiation and growth of ice sheets. Our results suggest that the story is more complicated and support the findings of Herrmann et al. (in press) who argue that a drop in pCO_2 level to as low as 8x PAL was not sufficient to initiate a major glaciation. We suggest that other environmental changes, most importantly a drop in sea level and/or continental drift, were necessary conditions for glaciation. Southward movement of Gondwana and a dropping sea-level would have caused a reduction in southward ocean heat transport creating a positive feedback that may have led to the

initiation and/or amplification of Gondwana glaciation. Moreover, the general observed cooling trend during the Late Ordovician in North America (eg., Brookfield, 1988; Brookfield and Brett, 1988; Patzkowsky and Holland, 1993; Lavoie, 1995; Holland and Patzkowsky, 1996; Pope and Read, 1997; Lavoie and Asselin, 1998; Lavoie et al., 1998) can be explained by these global mechanisms.

Acknowledgments

We thank the Penn State Earth and Mineral Sciences Environmental Institute, the Penn State Astrobiology Research Center, and NSF (EAR-0106737 and ATM 00-00454). Acknowledgment is also made to the donors of the American Chemical Society Petroleum Research Fund for partial support of this research (ACS Petroleum Research Fund PRF #36812-AC8). We also express our appreciation to the editors, one anonymous reviewer, and Dr. C. Poulsen for their critical reviews of the manuscript.

References Cited

Algeo, T.J., Seslavinsky, K.B., 1995a. The Paleozoic world: Continental flooding, hypsometry, and sea level. American Journal of Science 295, 787-822.

Algeo, T.J., Seslavinsky, K.B., 1995b. Reconstructing epeirogenic and eustatic trends from paleo-continental flooding data. In: Haq, B.U. (Ed.), Sequence stratigraphy and depositional response to eustatic, tectonic and climate forcing. Kluwer Academic Press, Dordrecht, Netherlands, pp. 209-246.

Armstrong, H.A., Coe, A.L., 1997. Deep-sea sediments record the geophysiology of the Late Ordovician glaciation. Journal of the Geological Society of London 154, 929-934.

Berner, R.A., 1994. GEOCARB II: A revised model of atmospheric CO_2 over Phanerozoic time. American Journal of Science 294, 56-91.

Berner, R.A., Kothavala, Z., 2001. GEOCARB III: A revised model of atmospheric CO_2 over Phanerozoic time. American Journal of Science 301, 182-204.

Berry, W.B.N., Boucot, A.J., 1973. Glacio-eustatic control of Late Ordovician-Early Silurian platform sedimentation and faunal changes. Geological Society of America Bulletin 84, 275-284.

Brenchley, P.J., Newall, G., 1980. A facies analysis of the Upper Ordovician regressive sequences in the Oslo region, Norway - A record of glacio-eustatic change. Palaeogeography, Palaeoclimatology, Palaeoecology 31, 1-38.

Brenchley, P.J., Marshall, J.D., Carden, G.A.F., Robertson, D.B.R., Long, D.G.F., Meidla, T., Hints, L., Anderson, T.F., 1994. Bathymetric and isotopic evidence for a short-lived Late Ordovician glaciation in a greenhouse period. Geology 22, 295-298.

Brenchley, P.J., Carden, G.A.F., Marshall, J.D., 1995. Environmental changes associated with the 'first strike' of the Late Ordovician mass extinction. Modern Geology 20, 69-82.

Brookfield, M.E., 1988. A mid-Ordovician temperate carbonate shelf - the Black River and Trenton Limestone Groups of southern Ontario, Canada. Sedimentary Geology 60, 137-153.

Brookfield, M.E., Brett, C.E., 1988. Paleoenvironments of the Mid-Ordovician (Upper Caradocian) Trenton limestones of southern Ontario, Canada: Storm sedimentation on a shoal-basin shelf model. Sedimentary Geology 57, 75-105.

Bryden, H.L., Roemmich, D., Church, J., 1991. Ocean heat transport across 24°N in the Pacific. Deep Sea Research 38, 297-324.

Crowley, T.J., Baum, S.K., 1991. Towards reconciling Late Ordovician (~440 Ma) glaciation with very high CO2 levels. Journal of Geophysical Research 96, 597-610.

Crowley, T.J., Baum, S.K., 1995. Reconciling Late Ordovician (440 Ma) glaciation with very high CO2 levels. Journal of Geophysical Research 100, 1093-1101.

Crowley, T.J., Baum, S.K., Kim, K.-Y., 1993. General circulation model sensitivity studies experiments with pole-centered supercontinents. Journal of Geophysical Research 98, 8793-8800.

Fortey, R.A., 1984. Global earlier Ordovician transgressions and regressions and their biological implications. In: Bruton, D.L. (Ed.), Aspects of the Ordovician System. Palaeontological Contributions from the University of Oslo. Universitetsforlaget, pp. 23-35.

Frakes, L.A., 1979. Climates throughout geologic time. Elsevier, Amsterdam. 310 pp.

Frakes, L.A., Francis, J.E., Syktus, J.I., 1992. Climate Modes of the Phanerozoic: the history of the earth's climate over the past 600 million years. Cambridge University Press, Cambridge. 274 pp.

Gibbs, M.T., 1996. Glaciation, chemical weathering, and the carbon cycle. Ph.D. Thesis, The Pennsylvania State University, University Park, 211 pp.

Gibbs, M.T., Barron, E.J., Kump, L.R., 1997. An atmospheric pCO_2 threshold for glaciation in the Late Ordovician. Geology 25, 447-450.

Gibbs, M.T., Bice, K.L., Barron, E.J., Kump, L.R., 2000. Glaciation in the Early Paleozoic "greenhouse": the roles of paleogeography and atmospheric CO_2. In: Huber, B.T., MacLeod K.G., Wing, S.L. (Eds.), Warm climates in Earth history, Cambridge University Press, Cambridge, pp. 386-422.

Hall, M.M., Bryden, H.L., 1982. Direct estimates and mechanisms of ocean heat transport. Deep Sea Research 29, 339-359.

Hallam, A., 1984. Pre-Quaternary sea-level changes. Annual Review of Earth Planetary Sciences 12, 205-243.

Harper, D.A.T., Mac Niocaill, C., Williams, S.H., 1996. The palaeogeography of early Ordovician Iapetus terranes: an integration of faunal and palaeomagnetic constraints. Palaeogeography, Palaeoclimatology, Palaeoecology 121, 297-312.

Haupt, B.J., Seidov, D., 2001. Warm deep-water ocean conveyor during Cretaceous time. Geology 29, 295-298.

Herrmann, A.D., Patzkowsky, M.E., Pollard, D., 2003. Obliquity forcing of with 8-12 times pre-industrial levels of atmospheric pCO_2 during the Late Ordovician, Geology 31, 485-488.

Herrmann, A.D., Patzkowsky, M.E. and Pollard, D., in press. The impact of paleogeography, pCO_2, poleward ocean heat transport and sea level change on global cooling during the Late Ordovician: A climate model analysis.

Holland, S.M., Patzkowsky, M.E., 1996. Sequence stratigraphy and long-term paleoceanographic change in the Middle and Upper Ordovician of the eastern United

States. In: Witzke, B.J., Ludvigson G.A., Day, J. (Eds.), Paleozoic Sequence Stratigraphy: Views from the North American craton. Geological Society of America Special Paper 306, Boulder, Colorado, pp. 117-129.

Kolata, D.R., Huff, W.D., Bergström, S.M, 2001. The Ordovician Sebree trough: an oceanic passage to the Midcontinent United States. Geological Society of America Bulletin 113, 1067-1078.

Kump, L.R., Arthur, M., Patzkowsky, M., Gibbs, M., Pinkus, D.S., Sheehan, P., 1999. A weathering hypothesis for glaciation at high atmospheric pCO_2 during the Late Ordovician. Palaeogeography, Palaeoclimatology, Palaeoecology 152, 173-187.

Lavoie, D., 1995. A Late Ordovician high-energy temperate-water carbonate ramp, southern Quebec, Canada: implications for Late Ordovician oceanography. Sedimentology 42, 95-116.

Lavoie, D., Asselin, E., 1998. Upper Ordovician facies in the Lac Saint-Jean outlier, Québec (eastern Canada): palaeoenvironmental significance for Late Ordovician oceanography. Sedimentology 45, 817-832.

Lavoie, D., Ndzangou, O.S. and Bourque, P.-A., 1998. The Black River - Trenton transition near Quebec City: a case for an Ordovician global change? Geological Association of Canada-Mineralogical Association of Canada Annual Meeting, Field Trip A8 Guidebook, Québec, 1-58 pp.

Leggett, J.K., McKerrow, W.S., Cooks, L.R.M., Rickards, R.B., 1981. Periodicity in the early Palaeozoic realm. Geological Society of London Journal 138, 167-176.

Canada. Canadian Journal of Earth Sciences 19, 1919-1932.

Le Pichon, X., 1968. Sea-floor spreading and continental drift. Journal of Geophysical Research 73, 3661-3697.

Marshall, J.D., Brenchley, P.J., Mason, P., Wolff, G.A., Astini, R.A., Hints, L., Meidla, T., 1997. Global carbon isotopic events associated with mass extinction and glaciation in the late Ordovician. Palaeogeography, Palaeoclimatology, Palaeoecology 132, 195-210.

McKerrow, W.S., 1979. Ordovician and Silurian changes in sea-level. Geological Society of London Journal 136, 137-145.

Pacanowski, R.C. (Editor), 1996. MOM 2. Documentation, User's Guide and Reference Manual. GFDL Ocean Technical Report, No. 3.2, Princeton, N.J.

Paris, F., Elaouad-Debbaj, Z., Jaglin, J.C., Massa, D., Oulebsir, L., 1995. Chitinozoans and Late Ordovician glacial events on Gondwana. In: Cooper, D., Droser, M.L., Finney, S.L. (Eds.), Ordovician Odyssey: Short Papers for the Seventh International Symposium on the Ordovician System, Fullerton, CA, pp. 171-176.

Patzkowsky, M.E., Holland, S.M., 1993. Biotic response to a Middle Ordovician paleoceanographic event in eastern North America. Geology 21, 619-622.

Pitman, W.C., III, 1978. The relationship between eustacy and stratigraphic sequences of passive margins. Geological Society of America Bulletin 89, 1389-1403.

Pope, M.C., Read, J.F., 1997. High-resolution stratigraphy of the Lexington limestone (Late Middle Ordovician), Kentucky, U.S.A.: A cool-water carbonate-clastic ramp in a tectonically active foreland basin. In: Noel, P., Clarke, J.A.D. (Eds.), Cool-water carbonates. Society of Economic Paleontologists and Mineralogists Special Publication, pp. 410-429.

Pope, M.C., Steffen, J.B., 2003. Widespread, prolonged late Middle to Late Ordovician upwelling in North America: A proxy record of glaciation?. Geology 31, 63-66.

Poulsen, C.J., Barron, E.J., Peterson, W.H., Wilson, P.A., 1999. A reinterpretation of mid-Cretaceous shallow marine temperatures through model-data comparison. Paleoceanography 14, 542-558.

Poulsen, C.J., Barron, E.J., Arthur, M.A., Peterson, W.H., 2001. Response of the mid-Cretaceous global oceanic circulation to tectonic and CO_2 forcings. Paleoceanography 16, 576-592.

Poussart, P.F., Weaver, A.J., Barnes, C.R., 1999. Late Ordovician glaciation under high atmospheric CO_2: A coupled model analysis. Paleoceanography 14, 542-558.

Qing, H., Veizer, J., 1994. Oxygen carbon isotopic composition of Ordovician brachiopods; implications for coeval seawater. Geochimica et Cosmochimica Acta 58, 4429-4442.

Ross, J.R., Ross, C.A., 1992. Ordovician sea-level fluctuations. In: Webby, B.D., Laurie, J.R. (Eds.), Global perspectives of Ordovician geology, Balkema, Rotterdam, pp. 327-335.

Ross, J.R., Ross, C.A., 1988. Late Paleozoic transgressive-regressive deposition. In: Wilgus, C.K., Hastings, B., Kendall, C.G.St.C., Posamentier, H., Ross, C., Van Wagoner, J.C. (Eds.), Sea-level changes: an integrated approach. Society of Economic Paleontologists and Mineralogists Special Publication 42, pp. 227-247.

Sclater, J.G., Anderson, R.N., Bell, M.L., 1971. Elevation of ridges and evolution of the Central Eastern Pacific. Journal of Geophysical Research 76, 7888-7915.

Scotese, C.R., 1997. Paleogeographic Atlas. University of Texas at Arlington, Arlington, Texas, 1-38 pp.

Scotese, C.R., McKerrow, W.S., 1990. Revised world maps and introduction. In: McKerrow, W.S., Scotese, C.R. (Eds.), Palaeozoic palaeogeography and biogeography, London, Geological Society Memoir No. 12, pp. 1-21.

Scotese, C.R., McKerrow, W.S., 1991. Ordovician plate tectonic reconstructions. In: Barnes, C.R., Williams, S.H. (Eds.), Advances in Ordovician geology. Geological Survey of Canada Paper 90-9, pp. 225-234.

Seibold, E., Berger, W.H., 1996. The sea floor; an introduction to marine geology. Springer Verlag, Berlin, 356 pp.

Sepkoski, J.J., Jr., 1996. Patterns of Phanerozoic extinction: a perspective from global data bases. In: Walliser, O.H. (Ed.), Global Events and Event Stratigraphy in the Phanerozoic. Springer Verlag, Berlin, pp. 35-51.

Sheehan, P.M., 1973. The relation of Late Ordovician glaciation to the Ordovician-Silurian changeover in North American brachiopod faunas. Lethaia 6, 147-154.

Vail, P., Mitchum, R., Thompson, S., 1977. Seismic stratigraphy and global changes of sea level, part 4: global cycles of relative changes of sea level. In Payton, C. (Ed.) Seismic Stratigraphy - Applications to Hydrocarbon Exploration, American Association of Petroleum Geologists Memoir 26, 83-97.

van de Pluijm, B.A., van der Voo, R. and Torsvik, T.H., 1995. Convergence and subduction at the Ordovician margin of Laurentia. In: Hibbard, J.P., van Staal, C.R.,

Cawood, P.A. (Eds.), Current perspectives in the Appalachian-Caledonian orogen, Geological Association Canada Special Paper 41, pp. 127-136.

Wilde, P., 1991. Oceanography in the Ordovician. In: Barnes, C.R., Williams, S.H. (Eds.), Advances in Ordovician geology. Geological Survey of Canada Paper 90-9, pp. 225-234.

Yapp, C.H., Poths, H., 1992. Ancient atmospheric CO_2 inferred from natural geothites. Nature 355, 342-344.

Chapter 5

Middle Ordovician (Caradoc) global paleobiogeography: evaluation of ocean general circulation model results

Abstract

Multivariate analyses of 42 localities of the Caradoc containing a total of 490 genera from around the globe indicate the presence of latitudinal and longitudinal gradients in taxonomic composition. Articulate brachiopods and trilobites dominate most localities with minor representation by corals, sponges, bivalves, gastropods, and cephalopods.

Cluster analysis of the 42 localities identified five major clusters that correspond to distinct paleocontinent regions: Laurentia, Baltica, and three Gondwanan regions, namely China, Australia, and South Central Europe. The Chinese cluster is distinct from other tropical regions indicating strong longitudinal differentiation in taxonomic composition among regions in the tropics. Latitudinal differentiation among regions is best shown by the relationships among Laurentia (tropical), Baltica (intermediate latitudes), and South Central Europe (high latitudes). This relationship is supported by detrended correspondence analysis showing the localities from these regions arrayed along an axis from low to high latitudes.

The spatial distribution of Caradocian marine organisms is consistent with climatic and oceanographic gradients inferred from coupled ocean-climate models. These models indicate that the ocean-climate system was dominated by strong latitudinal

temperature gradients and vigorous horizontal and vertical ocean circulation in the Caradoc. The paleobiogeographic data thus provide an important corroboration of the global ocean-climate models and lead to a more robust inference of the early Late Ordovician global ecosystem.

Introduction

The diversity of marine organisms underwent dramatic changes during the Ordovician, as this was a time of extensive diversification and radiation of marine life. However, the Ordovician period ended with a major mass extinction (Sepkoski, 1996). In terms of severity, it is the second most devastating extinction to marine life in Earth history with about 26% of the families, 49% of all genera, and up to 85% of species becoming extinct (Jablonski, 1991; Sepkoski, 1996).

Soon after the description of evidence in north Africa for glaciation at high latitudes during the Late Ordovician (Beuf et al., 1971; Dangeard and Doré, 1971), the extinction event was attributed to environmental changes associated with this glaciation (e.g., Berry and Boucot, 1973; Sheehan, 1973). Since evidence for extraterrestrial causes is lacking (Orth et al., 1986; Robertson et al., 1991; Wang et al., 1992; Wilde et al., 1986), the interpretation that the glaciation caused the mass extinction is generally accepted. The Late Ordovician mass extinction event is therefore unique in that it is possibly the only mass extinction event of the biggest five mass extinctions that was caused by environmental perturbation intrinsic to Earth's climate system.

These perturbations led to the glaciation at the end of the Ordovician and ended the warm greenhouse condition that persisted through the Ordovician (Fischer, 1984). The greenhouse conditions were presumably characterized by sluggish circulation. For example, based on the widespread distribution of early Paleozoic black shales and their smaller geographic extent through the later Paleozoic, Berry and Wilde (1978) suggested that the deep ocean was progressively ventilated with atmospheric oxygen. Railsback et al. (1990) also concluded that the overall warm climate of the Ordovician prior to the glaciation presumably led to warm, saline, and anoxic deep oceans with sluggish surface circulation of the global ocean. The initiation of increased thermohaline circulation at the beginning of the glaciation caused the overturn of this anoxic and nutrient-rich deep water and produced increased primary productivity due to enhanced upwelling (Brenchley et al., 1995). This increased productivity has been proposed as one of the mechanisms for the Late Ordovician mass extinction as it interrupted the long established oligotrophic ecosystems. Understanding the thermal structure of the global ocean prior to the glaciation is therefore important to test this hypothesis concerning the cause for this mass extinction.

Numerical models of the Earths ocean circulation provide a tool to investigate hypotheses of ocean circulation within reasonable boundary conditions. For example, global ocean circulation model (OGCM) results for the Late Ordovician indicate that a strong temperature gradient from the poles to the equator existed at pCO_2 levels as high as 18x pre-industrial atmospheric levels (PAL) (Herrmann et al., in press; Poussart et al., 1999). These models further indicate that the deep ocean was characterized by vigorous meridional overturning rather than by sluggish circulation proposed by earlier workers.

Thus, these numerical models support the interpretation that steep thermal gradients and perhaps extensive ice-sheets already existed in the Caradoc (e.g., Frakes et al., 1992; Pope and Steffen, 2003), despite the relatively high atmospheric pCO_2 values of up to 14±6 x pre-industrial atmospheric levels (e.g., Berner, 1994; Berner and Kothavala, 2001; Yapp and Poths, 1992).

Global paleobiogeographic patterns have the potential to constrain ocean model results, as faunal diversity patterns of modern marine invertebrates correlate with sea surface temperatures (e.g., Jablonski et al., 2000; Roy et al., 1998). However, few studies have attempted to make a comparison between numerical model results and biogeographic pattern for the geologic past and the validation of numerical models of global paleoceanographic ocean circulation or numerical climate simulations is seldom accomplished. One notable exception compared vegetation patterns with atmospheric general circulation model results (Rees et al., 2002).

It is the purpose of this paper to use multivariate analyses to define global biogeographic regions for the Middle Ordovician (Caradoc) and compare these results to the OGCM results of Herrmann et al. (in press). Fortey and Mellish (1992) showed that different kinds of fossils can show different patterns of paleobiogeographical distribution in the Ordovician. Therefore, a multi-taxon approach should lead to a more robust result than the study of a single taxon. Thus, the paleobiogeographic analysis is based on presence/absence data, compiled from the Paleobiology Database (PBDB), of 490 genera from different higher taxonomic groups (Anthozoa, Porifera, Bivalvia, Gastropoda, Brachiopoda, Trilobita, and Cephalopoda) at 42 different locations. Cluster analysis was performed on the data to identify biogeographic units. Detrended correspondence

analysis (DCA) was performed to explore the relations between taxonomic and environmental gradients. Strong latitudinal and longitudinal gradients are indicated by the multivariate analysis and these compare well with the suggested climatic gradients as hindcast by the ocean circulation model and with previously published paleobiogeographic studies of the Ordovician.

Analytical Methods and Data

The PBDB (http://www.paleodb.org) contains collection based occurrence data for marine and terrestrial animals and plants of any geological age culled from the paleontologic literature. The geographic scale of collections can range from a small outcrop containing a single fossil to a basin wide description; similarly, the stratigraphic scale in the PBDB can span rock units ranging from beds to formations. I sampled the PBDB for the global occurrences of Anthozoa, Brachiopoda, Bivalvia, Gastropoda, Cephalopoda, and Trilobita in the Caradoc. The downloaded data set was checked for taxonomic consistency using standard paleontologic references and synonymous occurrences were corrected. In addition, occurrences that were not resolved to the genus level were removed from the data set. The resulting original dataset comprised 11,069 occurrences of 738 genera at 49 locations. This data set contained multiple occurrences of the same genus at the same location and I therefore lumped all the occurrences of the same genus at one locality together. Localities in this paper are defined as present day geopolitical entities of roughly the same size, i.e. states and provinces of large countries (e.g., United States and China) and countries of smaller size (e.g., Portugal, Spain, etc).

After lumping the occurrences together, I compiled a single data matrix for the Caradoc, noting the presence and absence for each genus at every location.

I then culled the data in several ways to study the faunal distribution. First, I removed genera from the data matrix that only occurred at one location. While genera that are restricted to a particular area are useful in studying the overall diversity, genera that only occur at one locality are not useful for faunal comparisons among different areas (e.g., Anstey et al., 2003; Fortey and Cocks, 2003). This is because genera that occur only at one location do not provide enough evidence for linkage among areas based on shared taxa. In addition, low diversity assemblages tend to form outliers in multivariate analyses. Therefore, localities with less than 15 occurring genera were removed from the dataset. This resulted in a data set of 490 genera occurring at 42 locations.

Biogeographic datasets are best analyzed with multivariate statistical techniques due to their multidimensional nature (Raup and Crick, 1979; Shi, 1993). I used the statistical program PC-ORD (McCune and Mefford, 1999) to carry out a multivariate statistical study on the dataset utilizing a combination of ordination and cluster analysis. Cluster analysis aims to find grouping in localities that share similarities in faunal composition and tends to form discrete groupings even in the presence of an underlying environmental gradient. Thirty-nine similarity coefficients have been used in biogeography to measure the similarity of the composition of two samples (Shi, 1993). I used the Jaccard coefficient: JC = C/(A+B+C), where C is the number of taxa in common, A and B represents the number of taxa exclusive to assemblage A or B. The Jaccard coefficient is a commonly used similarity coefficient and well suited for binary

data (i.e. presence/absence data), since it has been shown that it is very consistent and unlikely to be affected by sampling biases or inefficiencies (e.g., Cheetham and Hazel, 1969; Krebs, 1999; Shi, 1993). The dendrograms were created using the unweighted pair-group method that used the arithmetic average as the clustering algorithm.

In order to explore further the relationships among localities, I also performed detrended correspondence analysis (DCA), which is commonly used in modern ecological studies (Gauch, 1982). DCA corrects for the arch effect and the compression of the ends of the gradients of correspondence analysis by detrending and rescaling the axis. Detrending removes the arch effect by dividing the first axis into segments and then by centering the second axis on zero (Gauch, 1982). Rescaling shifts the positions of samples along ordination axes to make the beta diversity constant. This is necessary so that given distances in ordination space along the axis have the same meaning in different parts of the ordination diagram. In DCA, these units are expressed in so-called 'standard deviations of species turnover'. Therefore, very long gradient lengths in the ordination indicate that very few species (or genera in this study) are shared between opposite ends of the gradient and thus high beta diversity. DCA is therefore designed specifically to look at taxonomic change along environmental gradients and has been shown to be useful in distinguishing biogeographic units (Tuckey, 1990). The suggested default values of PC-ORD for rescaling threshold and number of segments for the axis were used and rare species were down-weighted.

For this study, the paleogeographic reconstructions of Scotese (1997) and Scotese and McKerrow (1990, 1991) were chosen (Fig. 5.1), although I evaluate other hypotheses with the paleobiogeographic data below. These reconstructions provide consistency with

most published oceanographic and climate models for the Ordovician (e.g., Carrera and Rigby, 1999; Gibbs et al., 1997; Poussart et al., 1999; Wilde, 1991). The results of the multivariate analysis are compared to sea surface temperature data and ocean circulation results of Herrmann et al. (in press) (Fig. 5.2 and 5.8).

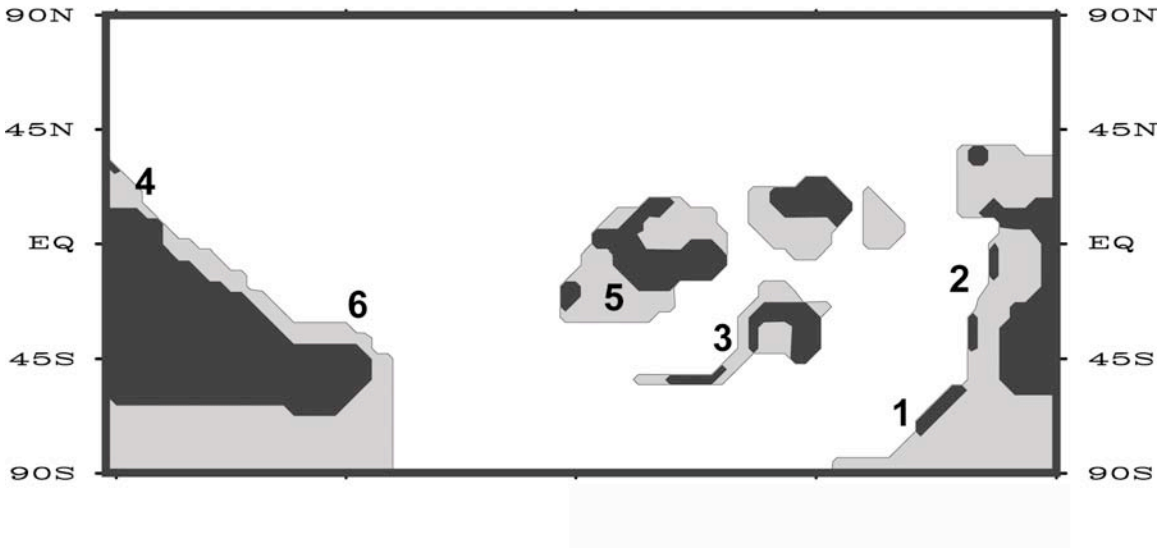

Figure 5.1: Paleogeography of the Caradoc (after Scotese and McKerrow, 1990, 1991). Light grey areas are flooded shelf areas, solid black areas are permanently exposed land areas. Approximate location of biogeographic provinces discussed in this paper: 1) South Central Europe (France, Spain, Morocco, Portugal, Czech Republic), 2) China, 3) Baltica and Avalonia (United Kingdom, Sweden, Norway), 4) Australia, 5) North America (localities from United States and Canada), and 6) South America (Argentina, Bolivia, Venezuela).

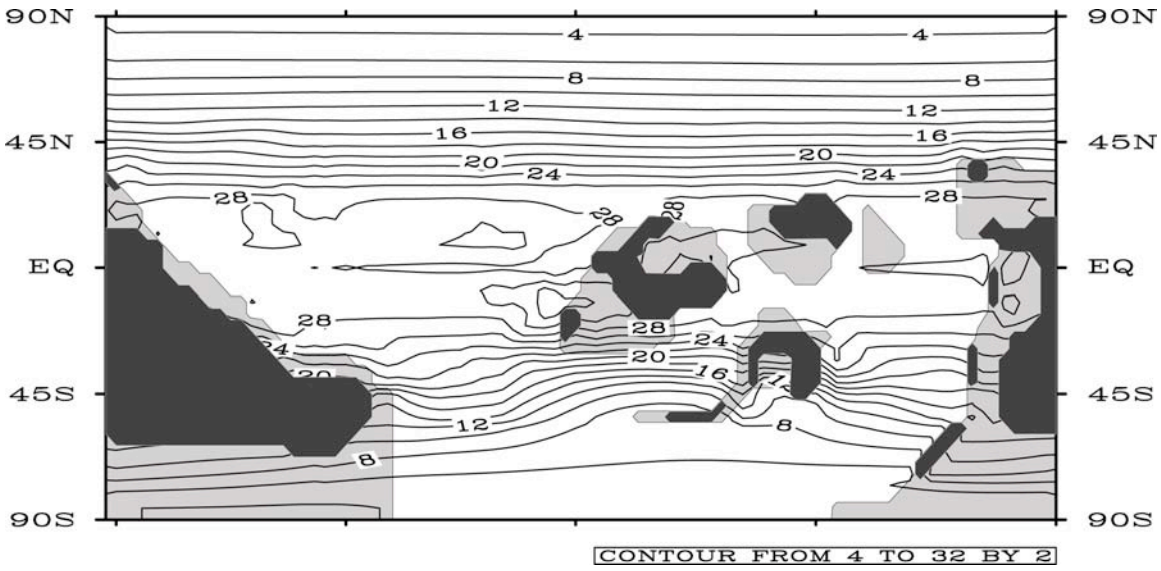

Figure 5.2: Sea surface temperatures of the Caradoc (after Herrmann et al., in press). Light grey areas are flooded shelf areas, solid black areas are permanently exposed land areas. Temperature contour intervals in degrees Celsius. Contour interval 2 degrees, labeling interval 4 degrees. Simulation was performed with pCO_2 level of 15 x pre-industrial atmospheric levels (PAL) of 280 ppm. Note that 15 x PAL is within the proposed range of atmospheric pCO_2 during the Late Ordovician (Berner, 1994; Berner and Kothavala, 2001; Yapp and Poths, 1992).

Results

Cluster analysis of the 42 locations produced five major clusters (Fig. 5.3). These clusters correspond closely to paleocontinents during the Ordovician (Fig. 5.1). Laurentia and Baltica cluster the tightest, then South Central Europe, followed by China. All locations from modern-day North America cluster together in a Laurentian cluster and the Baltic cluster is comprised of Norway, Sweden and United Kingdom. All Chinese locations cluster tightly together. Similarly, all locations from south central Europe (France, Portugal, Spain, Morocco, Czech Republic) cluster distinctively together.

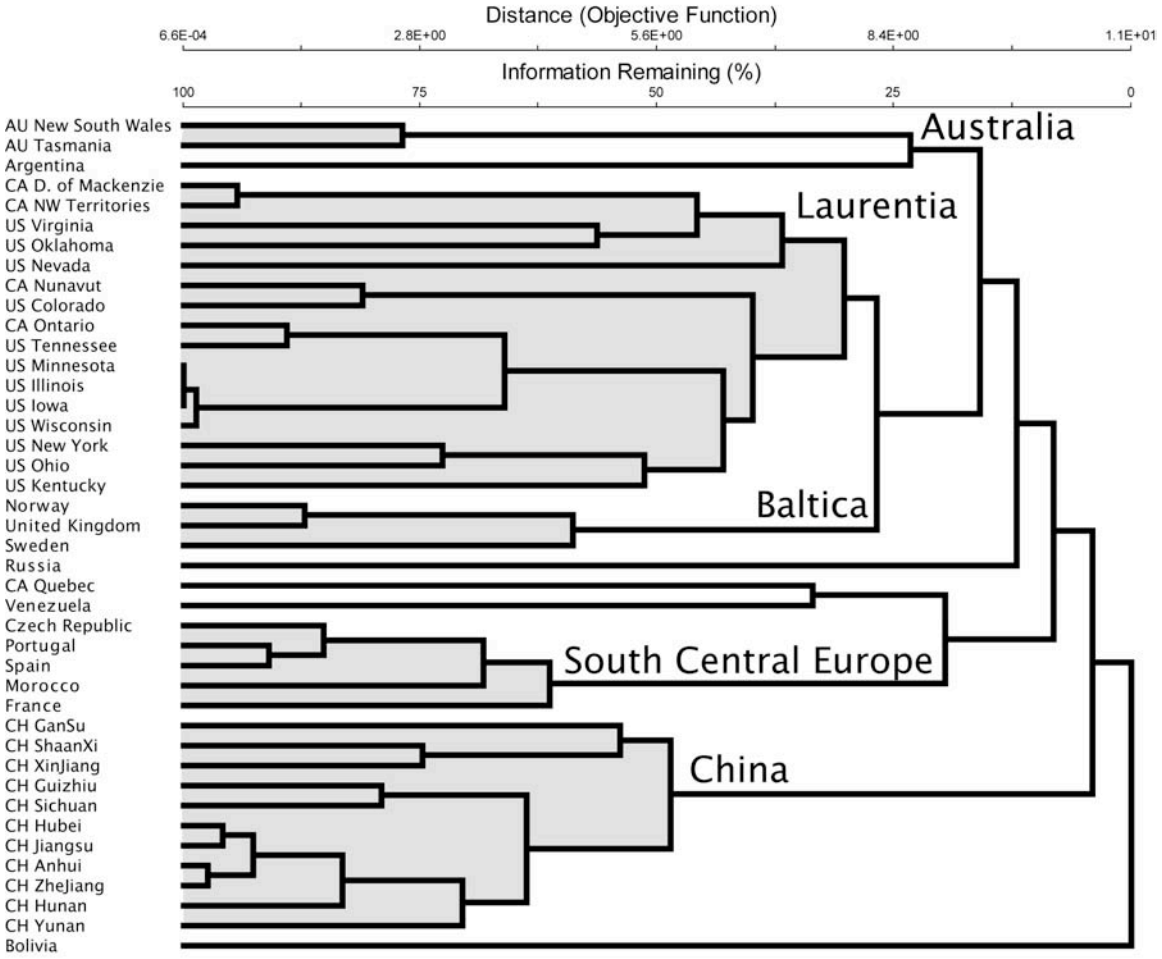

Figure 5.3: Cluster analysis results of all 42 locations. CA – Canada, US – United States, AU – Australia, CH – China.

The plot of DCA axis 1 versus DCA axis 2 supports the above five groups (Fig. 5.4). Low scores on the first axis but high scores on the second axis characterize the localities from Canada and the United States. These localities separated from the Chinese localities, which are depicted by high second axis scores, but relatively high scores on the first axis. Australian localities plot between the Chinese cluster and Laurentian cluster. Baltic localities plot in the middle of the DCA scatter plot due to their medium scores on

both the first and the second axis. The southern central European localities are very distinct due to their high second axis scores and medium to low first axis scores.

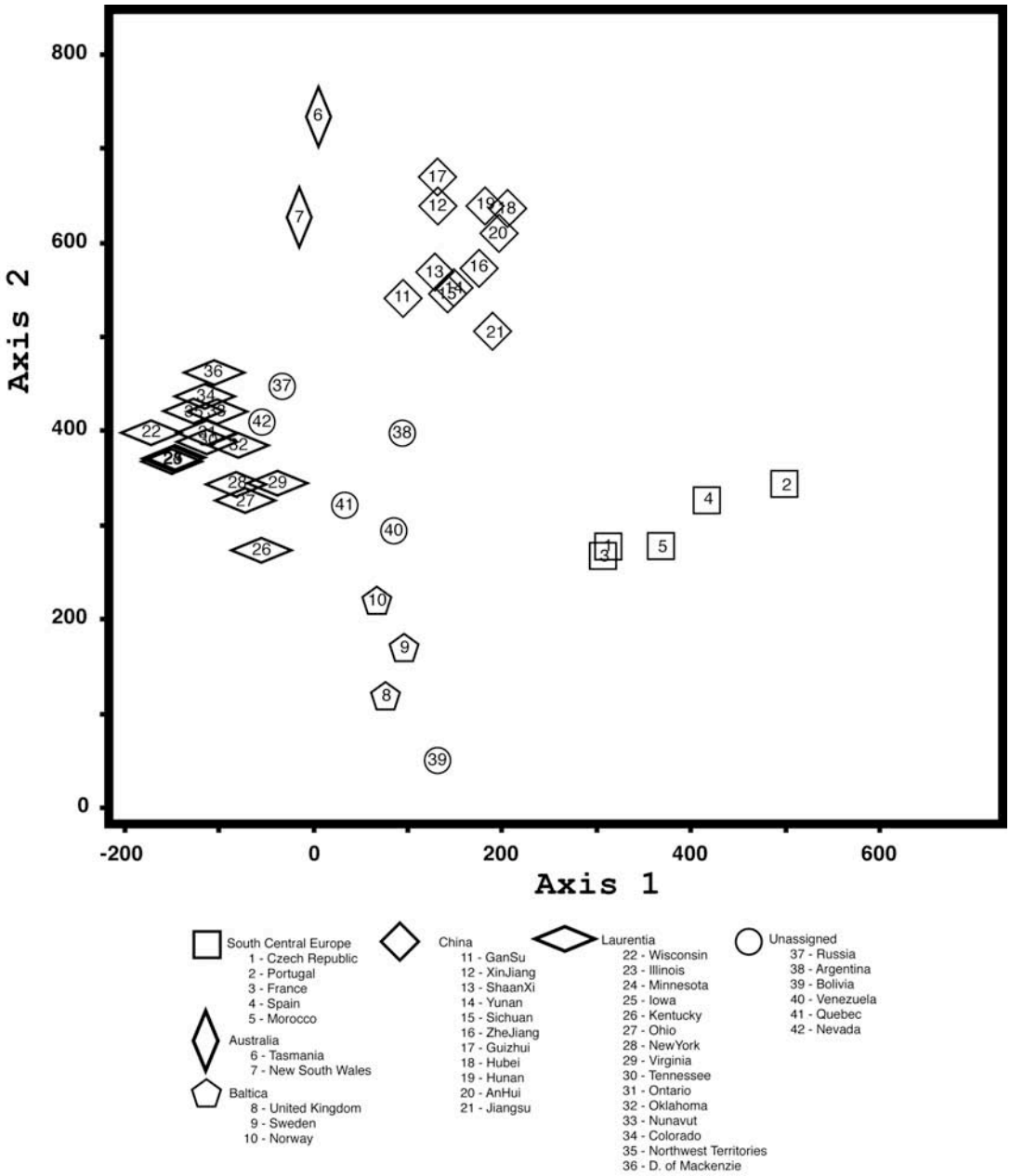

Figure 5.4: Ordination results from detrended correspondence analysis of all 42 locations and 490 genera. 'Unassigned' localities refer to localities that did not cluster with other groups in the cluster analysis.

In order to look at potential latitudinal gradients in greater detail, I also investigated the locations of the Iapetus region separately (Laurentia, Baltica, and South Central Europe). These areas are generally considered to be in close proximity but at different latitudes (Fig. 5.1). This multivariate analysis also suggests the presence of latitudinal gradients (Fig. 5.5). High latitude areas (South Central Europe) are separated from equatorial Laurentia by the subtropical Baltic areas.

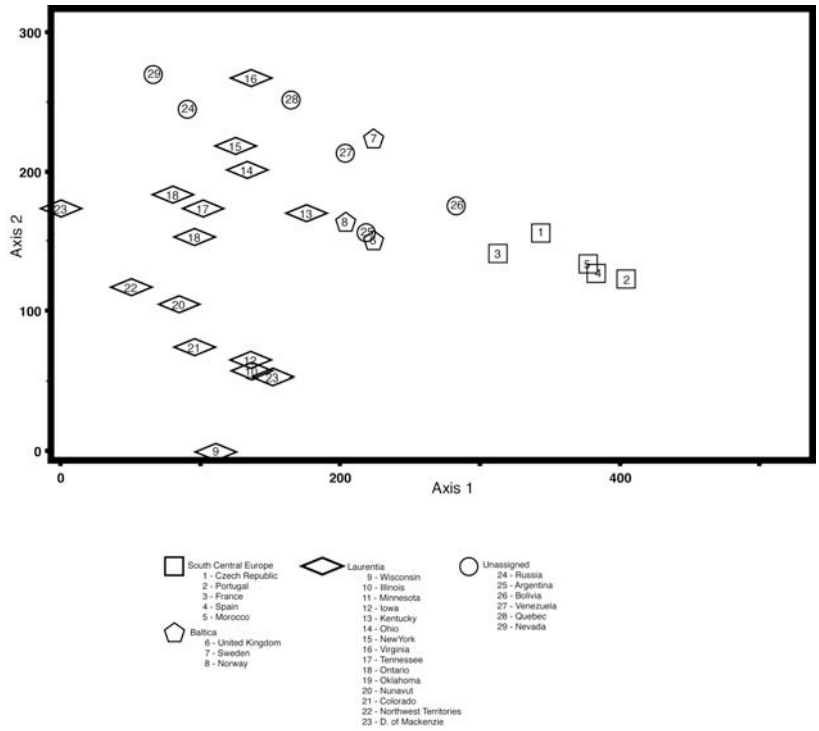

Figure 5.5: Detrended correspondence analysis of the Iapetus region. 'Unassigned' localities refer to localities that did not cluster with other groups in the cluster analysis.

Global Paleogeographical Implications

Geography exerts a strong influence on climate and therefore a good understanding of the location of the continents is important for paleoclimatologic studies

(Parrish, 1998). In order to constrain independently paleogeographic reconstructions for the Ordovician that are based on geophysical, lithological, and paleomagnetic models, different methods have been devised, including oceanic circulation models (e.g., Christiansen and Stouge, 1999) and paleobiogeographic distribution patterns (e.g., Fortey and Cocks, 2003, and references therein). Despite decades of intensive research, the interpretations of Ordovician paleogeography have proved controversial. Most paleogeographic reconstructions favor the model that the Taconic orogeny was caused by the equatorward movement of Baltica and Avalonia, which led to the closing of the Iapetus ocean (e.g., Cocks, 2000; Mac Niocaill and Smethurst, 1994; Mac Niocaill et al., 1997; Scotese and McKerrow, 1990; Scotese and McKerrow, 1991; van der Pluijm et al., 1995). However, an alternative hypothesis has been proposed that the Taconic orogeny was caused by the collision between North America and South America (e.g., Dalla Salda et al., 1992; Dalziel et al., 1994). Although this model, which is largely based on the SWEAT hypothesis (*sensu* Moores, 1991), is possible given the fact that paleomagnetic data provide no longitudinal constraints for the location of continents, it has been rejected based on paleontological and geological reasons (Mac Niocaill et al., 1997; van der Pluijm et al., 1995).

The present multivariate analysis also does not support the continent-continent collision of Gondwana and Laurentia, which would link the Taconic Orogeny in North America with the Famatinian Orogeny in South America (Dalziel et al., 1994). Argentina and Australia, which were both part of Gondwana, cluster together. In addition, Venezuela clusters more closely with the south central European localities, which are generally regarded as high latitude locations along the Gondwana margin (Fig. 5.1).

These Gondwana related localities are distinctly different from the Laurentian localities. This indicates that Gondwana was separated from Laurentia, probably by an ocean (i.e., Phoibic Ocean of Golanka (2002)). In addition, the DCA analysis (Fig. 5.4) also indicates, based on similar first axis scores, a greater affinity of South American localities with Baltica than with Laurentia. This makes the reconstruction of Dalziel et al. (1994) more unlikely as one would expect a closer clustering of South America to Laurentia than to Baltica. The use of the paleogeographic reconstructions of Scotese (1997) and Scotese and McKerrow (1990, 1991) are therefore justified for the paleoclimate and paleoceanographic models discussed below.

Paleobiogeography and corroboration of ocean general circulation results

Paleobiogeographic patterns of organisms are controlled by physical and biological factors. In particular, these factors include geographic barriers (e.g., continents or ocean basins), atmospheric and oceanic circulation patterns, temperature, latitude, mode of life of adult and/or larval stages of a certain organism (i.e., pelagic vs. benthic), and the specific life form of the organism (e.g., Cook and Taylor, 1975; Fortey and Mellish, 1992; Taylor, 1977). Today, most taxonomic groups display a steep latitudinal diversity gradient where high latitude and temperate areas typically have fewer species than tropical areas (e.g., Chown and Gaston, 2000; Crame et al., 2000; Fischer, 1960; Huston, 1994). Most of these conclusions are based on studies of terrestrial organisms. However, Roy et al. (1998) studied marine diversity trends in modern gastropods and showed that gastropod diversity in the western Atlantic and eastern Pacific Oceans

correlate significantly with average sea surface temperature. These authors speculate that diversity is linked to sea surface temperature through some aspect of productivity. Similarly, Jablonski et al. (2000) showed that the diversity trends in bivalves also correlate strongly with mean sea-surface temperatures. Therefore, numerical models of Ordovician ocean circulation can potentially be used to explore hypotheses underlying physical gradients in paleobiogeographic studies that indicate the presence of latitudinal faunal gradients, assuming that Ordovician diversity patterns were also affected by global climate trends. Alternatively, continental dispersal could explain endemism and paleobiogeographic separation during this time period. However, the narrowing and closing of several large ocean basins (e.g., Iapetus Ocean) and the presence of potential migration in form of oceanic islands (e.g., in the Iapetus ocean; Harper et al. (1996)) or landbarriers (e.g., between Baltica and Southern Europe; Young (1990)) in the Late Ordovician suggest that continental dispersal cannot account alone for faunal separation and endemism in the Caradoc.

The model results of Herrmann et al. (in press) indicate that the long-term cooling trend during the Late Ordovician can be explained by progressive cooling of the global ocean in response to falling levels of atmospheric pCO_2, sea level change, and paleogeographic change. Figure 5.2 shows the Caradoc sea surface temperatures for the simulation with atmospheric pCO_2 levels of 15 x pre-industrial. Despite the high pCO_2 values, the sea surface temperatures exhibit a steep thermal latitudinal gradient from equator to poles. The paleobiogeographic units of South Central Europe are confined to high latitudes where sea surface temperatures remain around 12°C. Baltic paleobiogeographic units correlate with intermediate sea surface temperatures of ~20°C,

while paleobiogeographic units comprising the paleocontinents of Laurentia and China are associated with sea surface temperatures above 20°C. The gradient along axis 1 in the DCA (Fig. 5.5) can therefore be interpreted to correspond to temperature, but probably also reflect other important variables (e.g., ocean circulation, productivity) that change with latitude.

Comparison with previously published paleobiogeographic studies of taxa used in the present study

Anthozoans

Figure 5.6a shows the detrended correspondence analysis of the anthozoans. The lack of genera from the locations at higher latitudes indicate that these areas were out of the tropical habitat zone for these organisms. Webby (1992) studied the global biogeography of corals and stromatoporoids during the Ordovician. He demonstrated the presence of an "American-Siberian" assemblage that was characterized by warm, equatorial waters and a restricted "Euroasiatic" assemblage that was characterized by cooler water that was supplied by currents from the southern higher latitudes. Carrera and Rigby (1999) studied the global distribution of sponges, which are often associated with Middle to Late Ordovician reefs and showed that the increased faunal endemism of sponges in the Late Ordovician and the general distribution patterns of sponges are related to continental convergence and latitudinal climate gradients. Earlier, Webby (1984) studied Ordovician reefs, of which corals and stromatoporoids were a major part during this time period, and their relationship to climate. He concluded that during this

time period the tropical and subtropical belts contacted and expanded several times. The reefs during the Ordovician had a restricted distribution within tropical and subtropical carbonate depositional belts, which indicate a temperature gradient existed from the pole to the equator (Webby, 1984). In a later paper, Webby (2002) extended and expanded his earlier database on Ordovician reefs and investigated the Ordovician reef development in more detail. In this study, he showed that in the Early Ordovician, microbial reefs were distributed in warm, shallow tropical waters in the low latitudes. He speculated that during this time the ocean circulation was sluggish and saline, anoxic deep waters existed. He attributed this to higher-than-normal temperatures that might have promoted the growth of microbial communities at the expense of metazoans. With a rise in oxygenation of the shallow water near the middle-Late Ordovician boundary, sessile, respiring metazoans significantly contributed in the colonization of new reef habitats. The majority of the Ordovician reefs inhabited the warmer, wind-mixed, well-lit surface waters of lower latitudes, with only a few reefs described from possible cooler-water, high-latitude locations. The concentration of corals in the lower latitudes and the lack of coral occurrences in higher latitudes in the present database (Fig. 5.6a) are in good agreement with the interpretation of Webby (2002).

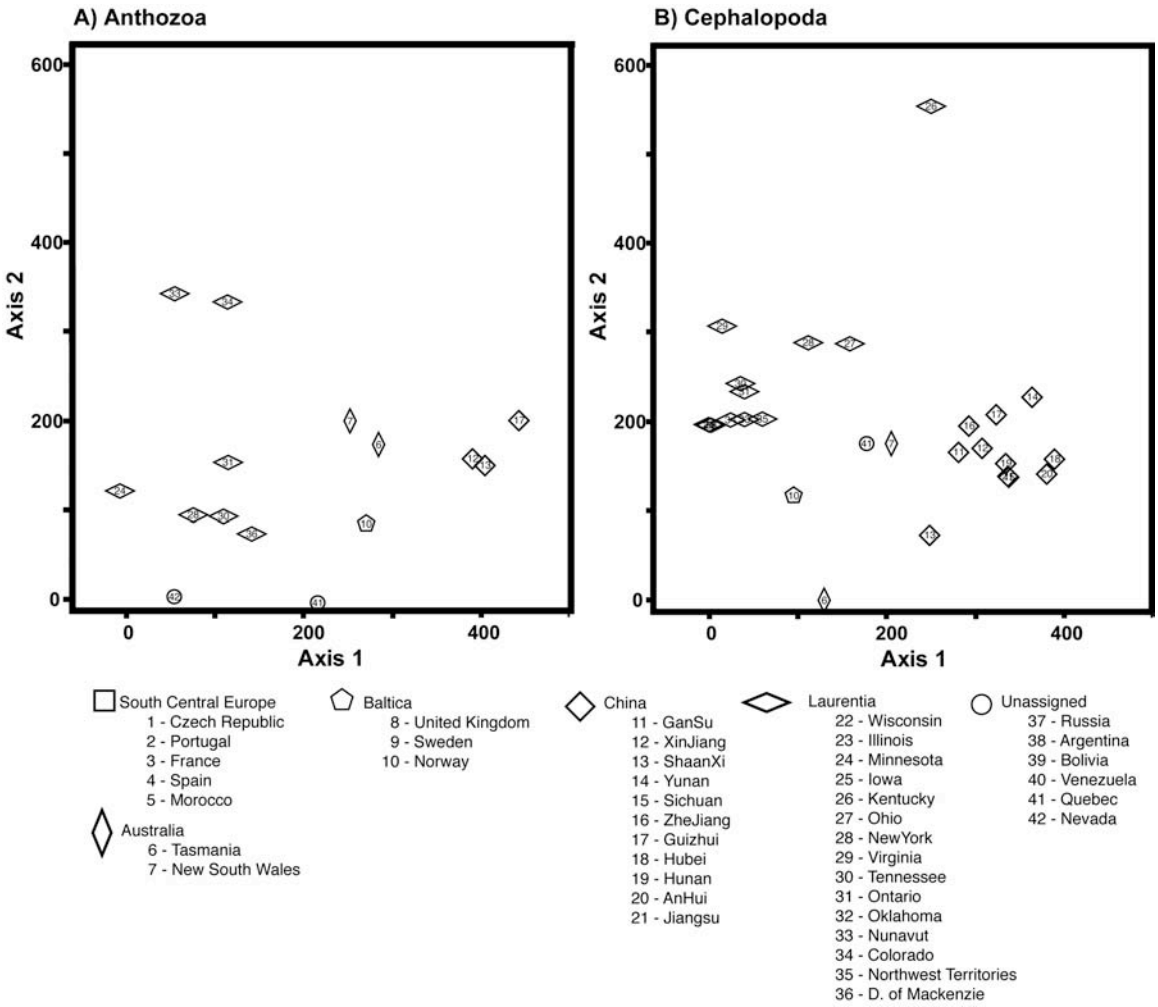

Figure 5.6: Detrended correspondence analysis of global occurrences of a) anthozoans, and b) cephalopods. 'Unassigned' localities refer to localities that did not cluster with other groups in the cluster analysis.

Cephalopoda

Similar to the distribution of corals, cephalopods are also concentrated in tropical regions (Fig. 5.6b). Despite early criticism of their paleobiogeographic usefulness due to post-mortem drift of cephalopod cones (Fell, 1968), Crick (1980; 1990) showed that the

distribution of Arenigian nautiloids was not significantly altered by post-mortem drift. Crick (1980) showed that the nautiloid paleobiogeography was determined by 1) the distance across deep ocean floor and along expanses of continuous shelf, 2) emergent portions of landmasses, and 3) differences in neritic and oceanic environments. His statistical analysis defined four faunal provinces: an Asian province, a Gondwanan province, a Baltic province, and a Laurentian province. Crick (1980) interpreted the Baltic province to be a cold-temperate, high-latitude fauna. In a later paper, Crick (1990) studied the biogeography of nautiloid cephalopods from the Cambrian to the Devonian. Crick (1990) proposed that the width and depth of oceanic basins constituted important physical barriers for the dispersal of cephalopod genera and he demonstrated that the paleobiogeography of the Caradoc of this group was characterized by low endemism among the different paleocontinents. Crick (1990) also showed that nautiloid cephalopod evolution was repeatedly marked by a crisis that was followed by an expansion of surviving taxa into mostly subtropical and equatorial shallow seas. The high diversity of cephalopod genera in lower latitudes and the lower number of genera in higher latitudes as reported by Crick (1990: his table 2) support his earlier interpretation of a climatic gradient towards the poles not only of the Arenig but also for the Caradoc. The lack of high-latitude cephalopods can be attributed to their preference for subtropical to equatorial shallow seas (Crick, 1980; 1990). The gradient along the first DCA axis (Fig. 5.6b), separating locations from China and Laurentia, can be interpreted in terms of the vast equatorial deep sea areas separating the two continental plates (Crick, 1980; 1990) (Fig. 5.1).

Bivalvia

The paleobiogeography of bivalves during the Ordovician has been interpreted in terms of increasing temperature from higher latitudes towards the equator (Cope, 2002). The Early Ordovician radiation of bivalves happened in shallow water siliciclastic shelves of Gondwana at all latitudes (Babin, 1995; Cope, 2002). Before the Mid-Ordovician, bivalves were mainly confined to Gondwana since the wide ocean area inhibited larval dispersal. However, the occurrence of a few genera in both high and median latitudes led Cope (2002) to the conclusion that in the Early Ordovician the temperature gradient was not particularly strong. Nevertheless, during the Late Ordovician high latitude faunas became more impoverished and dominated by a few bivalve lineages with low levels of endemism, indicating to Cope (2002) that the latitudinal temperature gradients became more pronounced. Cope's biogeographic interpretation that there was a strong latitudinal temperature gradient in the Caradoc is consistent with the results of this study (Fig. 5.5 and 5.7a). However, in addition to the latitudinal thermal gradients, siliciclastic substrates were also important. Miller (1997) for example suggested that bivalves depended on the increase of siliciclastic influx from the Taconic orogeny to increase in diversity in Laurentia.

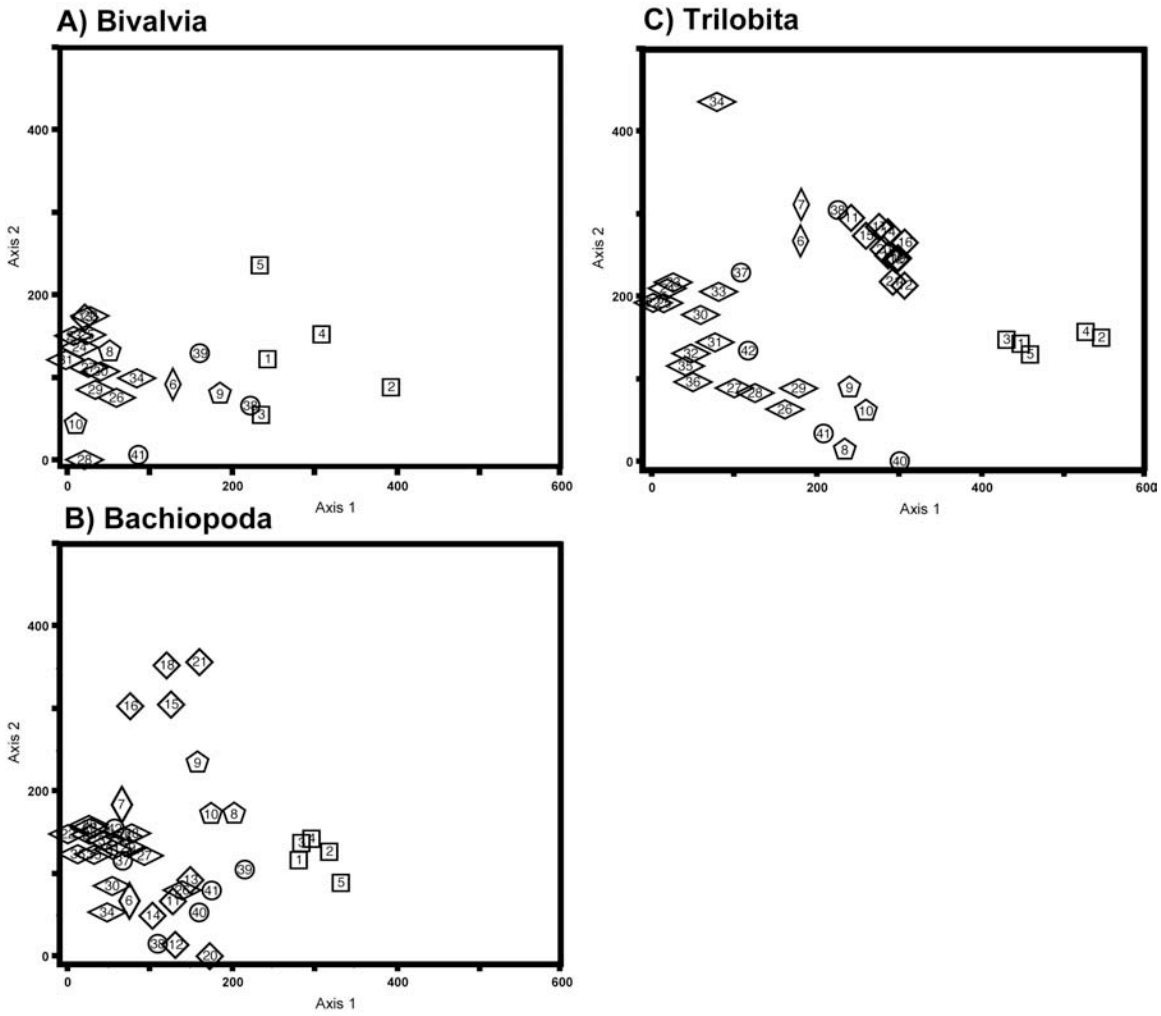

Figure 5.7: Detrended correspondence analysis of global occurrences of a) bivalves, b) brachiopods, and c) trilobites. 'Unassigned' localities refer to localities that did not cluster with other groups in the cluster analysis. Locality names same as figure 5.6.

Brachiopoda and Trilobita

In general, the Ordovician brachiopod and trilobite genera show similar paleobiogeographic distribution patterns (Fig. 5.7b and 5.7c) and yield the same paleogeographic answer (Fortey and Cocks, 2003). In an early paper, Williams (1973)

studied the paleobiogeography of brachiopods and their relation to Ordovician paleogeography and showed the presence of five distinct provinces that had pronounced endemism of brachiopod faunas until the Ashgillian, when the number of faunal provinces declined to three and the geographic extent of the brachiopod genera increased. Later studies with larger datasets found similar patterns (Sheehan and Coorough, 1990). The paleobiogeography of brachiopods has been interpreted in terms of climatic zonation during the Ordovician. The so-called Celtic and Toquima-Table Head faunas for example have been interpreted to be cool middle to high peri-Gondwanan latitude and low latitude warm water faunal assemblages (Neuman and Harper, 1992). DCA results presented here (Fig. 5.7b) show a separation of locations from the high latitudes and equatorial locations, with Baltic locations in intermediate position along axis 1, supporting a latitudinal zonation of brachiopods.

Trilobites show a similar pattern in that the high latitude Southern European locations are distinctly separated along the first axis from the Chinese and Laurentian locations (Fig. 5.7c). This supports early descriptions of trilobite distribution patterns (Whittington, 1966, 1973; Whittington and Hughes, 1973), which are also generally interpreted in terms of latitudinal temperature gradients. In these studies, four to five paleobiogeographic provinces were erected for the trilobites, with the boundaries mostly paralleling paleolatitudinal belts. In a study of the effect of different life modes on Ordovician trilobite extinction, Chatterton and Speyer (1989) showed that trilobite forms with extended planktotrophic larval stages were mostly confined to tropical regions, with a sharp decrease in diversity towards the polar regions.

Comparison with previously published paleobiogeographic studies of other taxa

Conodonts

After euconodont faunas replaced protoconodont-paraconodont faunas in the Early Ordovician, conodont paleobiogeography was characterized by distinct provincialism throughout most of the Ordovician (Bergström, 1990). Provincialism did not decrease towards the Late Ordovician as in other taxonomic groups, rather there is a strong separation of the "Mediterranean province" of South Central Europe in the higher latitudes and "Baltic" and Mid-continent provinces" of the lower latitudes. Bergström (1990) suggested that the dispersal of low latitude faunal elements to high latitudes, which often coincided with warm-water carbonate sedimentation in the high latitude areas, indicate that water temperature was a very important controlling factor in the observed provincialism. The disappearance of the Atlantic fauna in the Late Ordovician was attributed by Bergström (1990) to the spread of cold water conditions in response to the glaciation. Armstrong and Owen (2002) studied diversity changes of euconodonts in the Iapetus Ocean from the Late Ordovician to the Silurian. These authors suggest that the change in diversity on Avalonia was caused by Avalonia drifting from its earlier colder, high latitude location into low latitude, warmer tropical waters. The extinction of taxa adapted to cold water conditions, caused by northward drift into warmed tropical waters, strongly indicates the existence of extreme latitudinal temperature gradients during the Late Ordovician.

Graptolites

It has been proposed that the life habitat of graptolites was comparable to modern zooplankton that live in upwelling zones close to the shelf break in the vicinity of the oxygen minimum zone (Berry et al., 1987; Finney and Berry, 1997) and that their planktic habitat makes them less useful for biogeographic studies because they can potentially cross oceanographic barriers that would impede the migration of benthic organisms (Finney and Xu, 1990; Fortey and Mellish, 1992). However, it has been suggested that the distribution of graptolites was controlled by climate and the pronounced provincialism of graptolites in the Early Ordovician has been interpreted in terms of gradients of surface ocean water temperatures (e.g., Skevington, 1974; Skevington, 1976). Berry and Wilde (1990) described the global graptolite biogeography for the Ordovician and showed that from the Tremadoc to Ashgill, faunal patterns support the interpretation of the existence of a cold-water and a tropical-water faunal region. These authors demonstrate that these faunal regions are consistent with the paleogeographic reconstructions of Scotese and McKerrow (1990). Finney and Xu (1990) also studied the Ordovician paleobiogeography of graptolites and concluded that the distribution of graptolites was mainly determined by surface ocean conditions rather than proximity of continents (i.e., paleogeography). Their study showed that in the Ordovician a thermal gradient existed between the equator and poles. Provincialism was at its greatest before the Caradoc and with the onset of glaciation, graptolites became more cosmopolitan and provincialism declined, but the occurrence of graptolites was also constrained to the tropics due to steepened thermal gradients (Finney and Xu, 1990). In a

more general study, Rickards et al. (1990) also reiterated the importance of water mass properties on the distribution of graptolites, showing the existence of tropical and cooler water high latitude faunal provinces for the Ordovician and Silurian.

Acritarchs

Acritarchs are good indicators of latitudinal belts (Fortey and Cocks, 2003). Servais et al. (2003) compiled 30 years worth of studies on Ordovician acritarchs and presented their global distribution during the Ordovician. These authors also infer that Ordovician acritarchs provide information about the paleolatitude of paleocontinents due to their ecological affinity to surface water temperature. Therefore, acritarch occurrences in the Ordovician can be used to differentiate warm and cold water faunas (Li and Servais, 2002; Servais et al., 2003). While the Middle Ordovician record of organic-walled phytoplankton is scarce, the Arenigian record shows the differentiation into a higher latitude assemblage and low latitude warm water assemblages, similar to the record of trilobites during this time period (Servais et al., 2003). Vannier et al. (2003) studied caryocaridid zooplankton during the Ordovician and mapped their paleobiogeography. In contrast to acritarch plankton, these authors found that the caryocaridid zooplankton had a cosmopolitan character and occurred along the continental margins of several continental blocks; latitude not being a primary control on their dispersal.

Bryozoans

The global biogeography of bryozoans has been investigated by Anstey et al. (2003) and Tuckey (1990). Tuckey (1990) was the first to propose a global paleobiogeography for Ordovician bryozoans. He showed that the Caradoc was characterized by four global bryozoan provinces: a Siberian, a Mediterranean, a Baltic, and a North American province and proposed that the biogeographic distribution of bryozoans during the Ordovician was the result of continental convergence and latitudinal climatic gradients. In a later paper, Anstey et al. (2003) used a larger dataset and examined the patterns of bryozoan endemism from the Ordovician to the Silurian. These authors proposed that the third axis of their detrended correspondance analysis represented a climatic gradient over time and space, especially in the Ordovician (and not so much, if at all, for the Silurian). However, their analysis did not include locations from high-latitude South Central Europe. Nevertheless, they showed the presence of latitudinal gradients in the Northern Iapetus region, with Northern North America being in the tropical belt, Southern North America in the arid belt, and most of Baltica a potential warm temperate belt.

Algae

Poncet and Roux (1990) studied the paleobiogeography of calcareous algae in the Ordovician. These authors proposed that the cosmopolitan character of the algal faunas in the Early Ordovician indicated the absence of climatic gradients during that time period. However, in the Middle and Late Ordovician, the paleogeographic distribution of algae

indicated the establishment of climatic zonation. While distribution of algae in the tropical regions are cosmopolitan and no paleogeographic provinces can be established, the absence of algae from high latitude Southern Europe and Gondwana indicate climatic gradients that eliminated algae from high latitudes (Poncet and Roux, 1990). The fact that calcareous algae follow the distribution of mud-mounds and algal reefs further supports the interpretation that these organisms are useful as climatic markers (Poncet and Roux, 1990).

Ocean circulation results and proposed paleobiogeography

Biogeographic distribution patterns can be explained by both vicariance and/or dispersal (e.g., Craw et al., 1999; Lieberman, 2000 and references therein). Dispersal and latitudinal gradients of taxonomic groups can be affected by surface ocean circulation patterns and therefore paleocirculation is often inferred from biogeography. While migration patterns can only be discerned by comparing estimated first appearances of taxa on different continents through time, ocean circulation results can rule out potential migration pathways and oceanic barriers. Despite decades of intensive research, disagreement exists about the surface ocean circulation during the Ordovician. Several conceptual global ocean circulation models have been proposed for the Late Ordovician based on the biogeographic distribution of taxa (e.g., Bergström, 1990; Carrera and Rigby, 1999; Cocks and Fortey, 1990; Finney and Xu, 1990; Poncet and Roux, 1990; Rickards et al., 1990; Webby, 1992). These studies sometimes led to contradicting interpretations with regards to surface ocean circulation. For instance, Finney and Chen

(1990) interpret a strong current that flowed from the higher southern latitudes into the Iapetus ocean, while Webby (1992) and Carrera and Rigby (1999) show currents flowing from the equator southward in the Iapetus ocean.

Figure 5.8 shows the surface ocean circulation results of Herrmann et al. (in press) for the Caradoc. These results are consistent with the surface currents simulated by Poussart et al. (1999) for the Ashgill and surface circulation patterns of the conceptual oceanographic model of Wilde (1991). These general circulation patterns also compare well with the suggested surface ocean currents that are based on paleobiogeographic studies. Most of these studies predict zonal circulation in the Northern hemisphere and strong zonal westward flow in the equatorial zone connecting Laurentia with Australia (e.g., Bergström, 1990; Carrera and Rigby, 1999; Webby, 1984, 2002). In addition, there is a gyre system that connects the Baltic and Laurentian region with the Chinese tectonic plates. Cocks and Fortey (1990) proposed a similar gyre system to explain the separation of trilobite faunas into distinct eastern and western provinces during the Caradoc and Ashgill. This interpretation supports the longitudinal gradient that separates Laurentian, Baltic, and Chinese locations (Fig. 5.4). Baltica is located between China and Laurentia and has limited faunal exchange with both China and Laurentia via the two gyre systems. Based on the distribution of corals and stromatoporoids, Webby (1982) also postulated the presence of a counter clockwise gyre affecting the euroasiatic region.

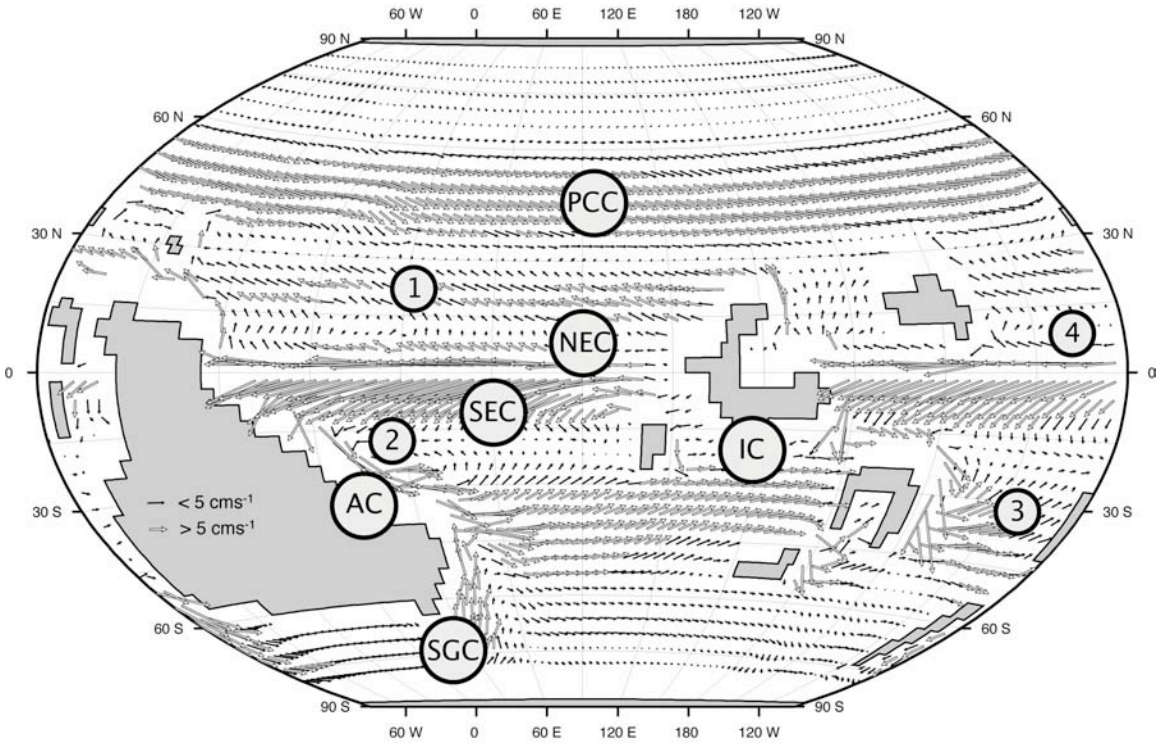

Figure 5.8: Surface ocean circulation pattern of Herrmann et al. (in press) for experiment with high sea level and atmospheric pCO_2 levels of 15x PAL for the Caradoc. Numbers represent gyre systems: 1 – North Panthalassic Convergence, 2 – South Panthalassic Convergence, 3 – South Paleo-Tethys Convergence, and 4 – North Paleo-Tethys Convergence. Letters represent surface currents: SGC – Southern Gondwana Current, PCC – Panthalassic Circumpolar Current, IC – Iapetus Current, NEC and SEC – North and South Equatorial Currents, and AC – Antarctica Current.

Poncet and Roux (1990) proposed that both the proximity of Baltica and North America and the surface ocean currents that originated in North America provided migration pathways between these areas. They suggested that timing of the first appearance of several calcareous algae species indicate oceanic pathways from North America to North European localities via currents flowing to the East. The surface circulation pattern (Fig. 5.8) supports this interpretation as ocean currents flow from North America eastward towards Baltica. These migration currents would have led to

faunal similarities between the two areas, in that taxa from North America could have reach Baltica. The tight clustering of these areas in the cluster analysis (Fig. 3) and the gradient analysis (Fig. 5.5) can therefore be interpreted in terms of the existence of these oceanic migration pathways.

Implications for mass extinction scenarios

Several models have been proposed over the years in order to explain the Late Ordovician mass extinction event. One of these proposed models suggests that the initiation of glaciation resulted in the development of a vigorous thermohaline circulation, which disrupted the warm, saline bottom waters and led to the upwelling of potentially toxic, anoxic bottom waters (e.g., Berry et al., 1995; Brenchley et al., 1995). However, the OGCM results of Herrmann et al. (in press) and Poussart et al. (1999) indicate that very strong meridional overturning existed even under pCO_2 levels of 18x PAL. In these numerical models deep water is formed in the higher southern latitudes and penetrates far into the northern Hemisphere due to the lack of extensive equatorial land barriers and the strongly asymmetric distribution of continents. The paleobiogeographic data also indicate that there was a strong latitudinal thermal gradient in the Caradoc (Fig. 5.5). Therefore, the paleobiogeographic data supports the presence of cold-water masses, and thus potential deep-water formation, in the higher southern latitudes as early as the Caradoc. However, the "overturning ocean" extinction model requires the existence of a stagnant deep ocean over a long time period. The numerical model results therefore indicate that anoxic, warm, saline bottom waters probably were

not involved in the extinction event. Alternatively it has been suggested that the effects of glacio-estatic sea level change and sea surface temperature drop both contributed to the mass extinction event (e.g., Berry and Boucot, 1973; Chen and Rong, 1991; Finney et al., 1998; Stanley, 1984; Wyatt, 1993, 1995). The oxygen isotope excursion that is associated with the Late Ordovician mass extinction event has been interpreted in terms of a 75 m sea level fall and a ~11°C fall of sea level temperature. The combined effects of sea level drop and global cooling could therefore account for the mass extinction event, without the proposed importance of anoxic bottom waters.

Conclusions

Global temperature gradients in the Caradoc

The Caradocian paleobiogeographic units of this study, which were established using quantitative multivariate techniques and a very large database of fossil occurrences of several invertebrate higher taxa, compare favorably to previously established paleobiogeographic provinces of studies that looked at mostly single taxa studies. Most of these studies attributed the paleobiogeographic patterns to temperature gradients. The good correlation between the interpreted latitudinal gradients in faunal composition and the OGCM results support the hypothesis that the observed paleobiogeographic patterns are related to thermal gradients that already existed in the Caradoc, prior to the onset of the Hirnantian glaciation.

Open ocean characteristics of the Caradoc

The existence of upwelling zones in tropical regions that are characterized by cold, nutrient rich waters (Armstrong and Owen, 2002; Pope and Steffen, 2003) indicate the presence of deeper cold water masses in the open oceans during the Late Ordovician. Pope and Steffen (2003) for example described the widespread deposition of phosphatic and cherty carbonates along the southern and western margin of Laurentia. These authors suggested that vigorous thermohaline circulation therefore existed as early as the late Middle Ordovician in response to a prolonged glaciation that lasted 10—14 Ma. This sedimentological evidence supports the climate and ocean model results that also indicate strong meridional overturning in the Late Ordovician as early as the Caradoc.

However, this is in contrast with geochemical data from the Taconic foredeep that indicate the presence of deep saline water masses, interpreted to be a global signal (Railsback et al., 1990). Rather than reflecting a global signal, these data from the Taconic foredeep might suggest only a regionally significant outflow of saline waters from the extensive epicontinental shelf of Laurentia, similar to modern-day outflow of warm saline waters from the Mediterranean Sea into the Atlantic Ocean (e.g., Johnson, 1997) or from the Persian Gulf into the Indian Ocean (e.g., Pratt et al., 1999). More intensive geochemical studies are therefore required to further extend the existing database of water mass properties in the Ordovician. A better understanding of the water mass structure is necessary to fully understand the oceanographic changes that led to the observed faunal diversity dynamics during the Ordovician.

Ocean circulation results

The longitudinal gradient in faunal composition can be explained by a set of gyre systems between Baltica and China and Baltica and Laurentia, supporting the earlier interpretation of Cocks and Fortey (1990).

References cited

Anstey, R.L., Pachut, J.F., and Tuckey, M.E., 2003, Patterns of bryozoan endemism through the Ordovician–Silurian transition: Paleobiology, v. 29, p. 305–328.

Armstrong, H.A., and Owen, A.W., 2002, Euconodont diversity changes in a cooling and closing Iapetus Ocean, in Crame, J.A., and Owen, A.W., eds., Palaeobiogeography and Biodiversity Change: the Ordovician and Mesozoic-Cenozoic Radiations, Volume 194, Geological Society of London Special Publication, p. 85-98.

Babin, C., 1995, The initial Ordovician mollusc radiations on the western Gondwana shelves, in Cooper, J.D., Droser, M.L., and Finney, S.C., eds., Ordovician Odyssey: Short Papers for the Seventh International Symposium on the Ordovician system, SEPM Pacific Section, Fullerton California, p. 491-498.

Bergström, S.M., 1990, Relations between conodont provincialism and the changing palaeogeography during the early Palaeozoic., in McKerrow, W.S., and Scotese, C.R., eds., Palaeozoic palaeogeography and biogeography: Oxford, United Kingdom, p. 105-121.

Berner, R.A., 1994, GEOCARB II: A revised model of atmospheric CO_2 over Phanerozoic time: American Journal of Science, v. 294, p. 56-91.

Berner, R.A., and Kothavala, Z., 2001, GEOCARB III: A revised model of atmospheric CO_2 over Phanerozoic time: American Journal of Science, v. 301, p. 182-204.

Berry, W.B.N., and Boucot, A.J., 1973, Glacio-eustatic control of Late Ordovician-Early Silurian platform sedimentation and faunal changes: Geological Society of America Bulletin, v. 84, p. 275-284.

Berry, W.B.N., Quinby-Hunt, M.S., and Wilde, P., 1995, Impact of Late Ordovician glaciation and deglaciation on marine life, in Commission on Geosciences, E.a.R., ed., Effects of past global change on marine life: Washington, The national academies press, p. 34-46.

Berry, W.B.N., and Wilde, P., 1978, Progressive ventilation of the oceans - an explanation for the distribution of the Lower Paleozoic black shales: American Journal of Science, v. 278, p. 257-275.

—, 1990, Graptolite biogeography; implications for palaeogeography and palaeoceanography, in McKerrow, W.S., and Scotese, C.R., eds., Palaeozoic palaeogeography and biogeography: Oxford, United Kingdom, p. 97-104.

Berry, W.B.N., Wilde, P., and Quinby-Hunt, M.S., 1987, The oceanic non-sulfidic oxygen minimum zone: a habitat for graptolites?: Bulletin of the Geological Society of Denmark, v. 35, p. 103-114.

Beuf, S., Biju-Duval, B., de Charpal, O., Rognon, P., Gariel, O., and Bennacef, A., 1971, Les Grès du Paléozoique Inférieur au Sahara: Paris, Technip.

Brenchley, P.J., Carden, G.A.F., and Marshall, J.D., 1995, Environmental changes associated with the 'first strike' of the Late Ordovician mass extinction: Modern Geology, v. 22, p. 69-82.

Carrera, M.G., and Rigby, J.K., 1999, Biogeography of Ordovician sponges: Journal of Paleontology, v. 73, p. 26-37.

Chatterton, B.D.E., and Speyer, S.E., 1989, Larval ecology, life history strategies, and patterns of extinction and survivorship among Ordovician trilobites: Paleobiology, v. 15, p. 118-132.

Cheetham, A.H., and Hazel, J.E., 1969, Binary (presence-absence) similarity coefficients: Journal of Paleontology, v. 43, p. 1130-1136.

Chen, X., and Rong, J.-y., 1991, Concepts and analysis of mass extinction with the Late Ordovician event as an example: Historical Biology, v. 5, p. 107-122.

Chown, S.L., and Gaston, K.J., 2000, Areas, cradles and museums: the latitudinal gradient in species richness: Trends in Ecology and Evolution, v. 15, p. 311-315.

Christiansen, J.L., and Stouge, S., 1999, Oceanic circulation as an element in palaeogeographical reconstructions: the Arenig (early Ordovician) as an example: Terra Nova, v. 11, p. 73-78.

Cocks, L.R.M., 2000, The Early Palaeozoic geography of Europe: Journal of the Geological Society of London, v. 157, p. 1-10.

Cocks, L.R.M., and Fortey, R.A., 1990, Biogeography of Ordovician and Silurian faunas, in McKerrow, W.S., and Scotese, C.R., eds., Palaeozoic palaeogeography and biogeography: Oxford, United Kingdom, p. 97-104.

Cook, H.E., and Taylor, M.E., 1975, Early Paleozoic continental magin sedimentation, trilobite biofacies, and the thermocline, western United States: Geology, v. 3, p. 559-562.

Cope, J.C.W., 2002, Diversification and biogeography of bivalves during the Ordovician Period, in Crame, J.A., and Owen, A.W., eds., Palaeobiogeography and Biodiversity Change: the Ordovician and Mesozoic-Cenozoic Radiations, Volume 194, Geological Society of London Special Publication, p. 25-52.

Crame, J.A., Culver, S.J., and Rawson, P.F., 2000, Biotic Response to Global Change: The Last 145 Million Years: Cambridge, Cambridge University Press.

Craw, R.C., Grehan, J.R., and Heads, M.J., 1999, Panbiogeography: Tracking the History of Life: Oxford, Oxford University Press, 240 p.

Crick, R.E., 1980, Integration of paleobiogeography and paleogeography: evidence from Arenigian nautiloid biogeography: Journal of Paleontology, v. 54, p. 1218-1236.

—, 1990, Cambro-Devonian biogeography of nautiloid cephalopods, in McKerrow, W.S., and Scotese, C.R., eds., Palaeozoic palaeogeography and biogeography: Oxford, United Kingdom, p. 147-161.

Dalla Salda, L.H., Dalziel, I.W.D., Cingolani, C.A., and Varela, R., 1992, Did the Taconic Appalachians continue into southern South America?: Geology, v. 20, p. 1059-1062.

Dalziel, I.W.D., Salda, L.H.D., and L.M. Gahagan, 1994, Paleozoic Laurentia-Gondwana interaction and the origin of the Appalachian-Andean mountain system: Geological Society of America Bulletin, v. 106, p. 243-252.

Dangeard, L., and Doré, F., 1971, Facies glaciaires de l'Ordovicien supérieur en Normandie: Coll Ordovicien Silurien Brest Mém Bur Rech Géol Min, v. 73, p. 119-128.

Fell, H.B., 1968, The biogeography and paleoecology of the Ordovician seas, in Drake, E.T., ed., Evolution and Environment - A symposium: New Haven, Yale University Press, p. 139-162.

Finney, S.C., and Berry, W.B.N., 1997, New perspectives on graptolite distributions and their use as indicators of platform margin dynamics: Geology, v. 25, p. 919-922.

Finney, S.C., Berry, W.B.N., Cooper, J.D., Ripperdan, R.L., Sweet, W.C., Jacobsen, S.B., Soufiane, A., Achab, A., and Noble, P.J., 1998, Late Ordovician mass extinction: A new perspective from stratigraphic sections in central Nevada: Geology, v. 27, p. 215-218.

Finney, S.C., and Xu, C., 1990, The relationship of Ordovician graptolite provincialism to palaeogeography, in McKerrow, W.S., and Scotese, C.R., eds., Palaeozoic palaeogeography and biogeography: Oxford, United Kingdom, p. 123-128.

Fischer, A.G., 1960, Latitudinal variations in organic diversity: Evolution, v. 14, p. 64-81.

—, 1984, The two Phanerozoic supercycles, in Berggren, W.A., and Van Couvering, J.A., eds., Catastrophes and Earth History: Princeton, Princeton University Press, p. 129-150.

Fortey, R.A., and Cocks, L.R.M., 2003, Palaeontological evidence bearing on global Ordovician-Silurian continental reconstructions: Earth-Science Reviews, v. 61, p. 245-307.

Fortey, R.A., and Mellish, C.J.T., 1992, Are some fossils better than others for inferring palaeogeography? The Early Ordovician of the North Atlantic region as an example: Terra Nova, v. 4, p. 210-216.

Frakes, L.A., Francis, J.E., and Syktus, J.I., 1992, Climate modes of the Phanerozoic: Cambridge, Cambridge University Press, 274 p.

Gauch, H.J.G., 1982, Multivariate Analysis in Community Ecology: Cambridge, Cambridge University Press, 314 p.

Gibbs, M., Barron, E.J., and Kump, L.R., 1997, An atmospheric pCO_2 threshold for glaciation in the Late Ordovician: Geology, v. 25, p. 447-450.

Golonka, J., 2002, Plate-tectonic maps of the Phanerozoic, in Kiessling, W., Flügel, E., and Golonka, J., eds., Phanerozoic Reef Patterns, Volume SEPM Special Publication Numer 72, p. 21-75.

Harper, D.A.T., Mac Niocaill, C., and Williams, S.H., 1996, The palaeogeography of early Ordovician Iapetus terranes: an integration of faunal and palaeomagnetic constraints: Palaeogeography, Palaeoclimatology, Palaeoecology, v. 121, p. 297-312.

Herrmann, A.D., Haupt, B.J., Patzkowsky, M.E., Slingerland, R.L., and Seidov, D., in press, Response of Late Ordovician paleoceanography to changes in sea level, continental drift, and atmospheric pCO_2: potential causes for long-term cooling and glaciation: Paleoecology Paleoclimatology Paleogeography.

Huston, M.A., 1994, Biological Diversity: Cambridge, Cambridge University Press, 701 p.

Jablonski, D., 1991, Extinctions: a paleontological perspective: Science, v. 253, p. 754-757.

Jablonski, D., Roy, K., and Valentine, J.W., 2000, Analysing the latitudinal diversity gradient in marine bivalves, in Harper, E.M., Taylor, J.D., and Crame, J.A., eds., The evolutionary biology of bivalves, Volume 177: London, Geological Society of London Special Publications, p. 361-365.

Johnson, R.G., 1997, Climate control requires a dam at the Strait of Gibraltar: Eos Transactions AGU, v. 78, p. 280-281.

Krebs, C.J., 1999, Ecological methodology, Benjamin/Cummings, 581 p.

Li, J., and Servais, T., 2002, Ordovician acritarchs of China and their utility for global palaeobiogeography: Bulletin de la Société Géologique de France, v. 173, p. 399-406.

Lieberman, B.S., 2000, Paleobiogeography: New York, Kluwer Academic, 208 p.

Mac Niocaill, C., and Smethurst, M.A., 1994, Palaeozoic palaeogeography of Laurentia and its margins: a reassessment of palaeomagnetic data: Geophysical Journal International, v. 116, p. 715-725.

Mac Niocaill, C., van der Pluijm, B.A., and Van der Voo, R., 1997, Ordovician paleogeography and the evolution of the Iapetus ocean: Geology, v. 25, p. 159-162.

McCune, B., and Mefford, M.J., 1999, PC-ORD: multivariate analysis of ecological data version 4: Gleneden Beach, OR, MjM Software Design, 237 p.

Miller, A.I., 1997, Comparative diversification dynamics among palaeocontinents during the Ordovician radiation: GeoBios, v. 20, p. 397-406.

Moores, E.M., 1991, Southwest U.S.-East Antarctica (SWEAT) connection: A hypothesis: Geology, v. 19, p. 425-428.

Neuman, R.B., and Harper, D.A.T., 1992, Paleogeographic significance of Arenig-Llanvirn Toquima-Table Head and Celtic brachiopod assemblages, in Webby, B.D., and Laurie, J.R., eds., Global Perspectives in Ordovician Geology: Rotterdam, Balkema, p. 241-254.

Orth, C.J., Gilmore, J.S., Quitana, L.R., and Sheehan, P.M., 1986, The terminal Ordovician extinction: Geochemical analysis of the Ordovician/Silurian boundary, Anticosti Island, Quebec: Geology, v. 14, p. 433-436.

Parrish, J.T., 1998, Interpreting Pre-Quaternary Climate from the Geologic Record, Columbia University Press, 338 p.

Poncet, J., and Roux, A., 1990, Palaeobiogeography of Ordovician calcareous algae: Palaeogeography, Palaeoclimatology, Palaeoecology, v. 81, p. 1-10.

Pope, M.C., and Steffen, J.B., 2003, Widespread, prolonged late Middle to Late Ordovician upwelling in North America: A proxy record of glaciation?: Geology, v. 31, p. 63-66.

Poussart, P.R., Weaver, A.J., and Barnes, C.R., 1999, Late Ordovician glaciation under high atmospheric CO_2: a coupled model analysis: Paleoceanography, v. 14, p. 542-558.

Pratt, L.J., Johns, W., Murray, S.P., and Katsumata, K., 1999, Hydraulic interpretation of direct measurements in the Bab el Mandab Strait: Journal of Physical Oceanography, v. 29, p. 2769-2784.

Railsback, L.B., Ackerly, S.C., Anderson, T.F., and Cisne, J.L., 1990, Palaeontological and isotope evidence for warm saline deep waters in Ordovician oceans: Nature, v. 343, p. 156-159.

Raup, D.M., and Crick, R.E., 1979, Measurement of faunal similarity in paleontology: Journal of Paleontology, v. 53, p. 1213-1227.

Rees, P.M., Ziegler, A.M., Gibbs, M.T., Kutzbach, J.E., Behling, P.J., and Rowley, D.B., 2002, Permian Phytogeographic patterns and climate data/model comparisons: Journal of Geology, v. 110, p. 1-31.

Rickards, B., Rigby, S., and Harris, J.H., 1990, Graptoloid biogeography: recent progress, future hopes, in McKerrow, W.S., and Scotese, C.R., eds., Palaeozoic palaeogeography and biogeography: Oxford, United Kingdom, p. 139-145.

Robertson, D.B.R., Brenchley, P.J., and Owen, A.W., 1991, Ecological disruption close to the Ordovician-Silurian boundary: Historical Biology, v. 5, p. 131-144.

Roy, K., Jablonski, D., Valentine, J.W., and Rosenberg, G., 1998, Marine latitudinal diversity gradients: Tests of causal hypotheses: Prococeedings National Acadademy of Sciences, v. 95, p. 3699-3702.

Scotese, C.R., 1997, Paleogeographic atlas: Arlington, Texas, University of Texas at Arlington, 1-38 p.

Scotese, C.R., and McKerrow, W.S., 1990, Revised world maps and introduction, in McKerrow, W.S., and Scotese, C.R., eds., Palaeozoic palaeogeography and biogeography: Oxford, United Kingdom, p. 1-21.

—, 1991, Ordovician plate tectonic reconstructions, in Barnes, C.R., and Williams, S.H., eds., Advances in Ordovician geology: Geological Survey of Canada Paper 90-9, p. 225-234.

Sepkoski, J.J., 1996, Patterns of Phanerozoic extinction: a perspective from global databases, in Walliser, O.H., ed., Global Events and Event Stratigraphy in the Phanerozoic: Berlin, Springer, p. 35-51.

Servais, T., Li, J., Molyneux, S., and Raevskaya, E., 2003, Ordovician organic-walled microphytoplankton (acritarch) distribution: the global scenario: Palaeogeography, Palaeoclimatology, Palaeoecology, v. 195, p. 149-172.

Sheehan, P.M., 1973, The relation of Late Ordovician glaciation to the Ordovician-Silurian changeover in North American brachiopod faunas: Lethaia, v. 6, p. 147-154.

Sheehan , P.M., and Coorough, P.J., 1990, Brachiopod zoogeography across the Ordovician-Silurian extinction event, in Scotese, C.R., ed., Palaeozoic palaeogeography and biogeography: Oxford, United Kingdom, p. 181-187.

Shi, G.R., 1993, Multivariate data analysis in palaeoecology and palaeobiogeography: Palaeogeography, Palaeoclimatology, Palaeoecology, v. 105, p. 199-234.

Skevington, D., 1974, Controls influencing the composition and the distribution of Ordovician graptolite faunal provinces: Special papers in Palaeontology, v. 13, p. 59-73.

—, 1976, A discussion of the factors responsible for the provincialism displayed by graptolite faunas during the Early Ordovician, in Kaljo, D., and Koren, T., eds., Graptolites and Stratigraphy: Tallinn, Academy of Sciences of Estonia SSR, p. 180-200.

Stanley, S.M., 1984, Temperature and biotic crises in the marine realm: Geology, v. 12, p. 205-208.

Taylor, M.E., 1977, Late Cambrian of western North America: Trilobite biofacies, environmental significance and biostratigraphic implications, in Kauffman, E.G., and Hazel, J.E., eds., Concepts and Methods of Biostratigraphy: Dowden, Hutchison and Ross, p. 397-426.

Tuckey, M.E., 1990, Biogeography of Ordovician bryozoans: Palaeogeography, Palaeoclimatology, Palaeoecology, v. 77, p. 91-126.

van der Pluijm, B.A., van der Voo, R., and Torsvik, T.H., 1995, Convergence and subduction at the Ordovician margin of Laurentia, in Hibbard, J.P., van Staal, C.R., and Cawood, P.A., eds., Current Perspectives in the Appalachian-Caledonian Orogen, Volume Geological Association of Canada, Special Paper 41, p. 127-136.

Vannier, J., Racheboeuf, P.R., Brussa, E.D., Williams, M., Rushton, A.W.A., Servais, T., and Siveter, D.J., 2003, Cosmopolitan arthropod zooplankton in the Ordovician seas: Palaeogeography, Palaeoclimatology, Palaeoecology, v. 195, p. 173-191.

Wang, K., Chatterton, B.D.E., Attrep, M., and Orth, C.J., 1992, Iridium abundance maxima at the latest Ordovician mass extinction horizon, Yangtze Basin, China: Terrestrial or Extraterrestrial: Geology, v. 20, p. 39-42.

Webby, B.D., 1984, Ordovician reefs and climate: a review, in Bruton, D.L., ed., Aspects of the Ordovician System, Volume 295: Oslo, Universitetsforlaget - Palaeontological Contributions from the University of Oslo, p. 89-100.

—, 1992, Global biogeography of Ordovician corals and stromatoporoids, in Webby, B.D., and Laurie, J.R., eds., Global perspectives on Ordovician geology: Rotterdam - Brookfield, Netherlands (NLD), A.A. Balkema, p. 261-276.

—, 2002, Patterns of Ordovician reef development, in Kiessling, W., Flügel, E., and Golonka, J., eds., Phanerozoic Reef Patterns, Volume SEPM Special Publication 72.

Whittington, H.B., 1966, Phylogeny and distribution of Ordovician trilobites: Journal of Paleontology, v. 40, p. 696-737.

—, 1973, Ordovician trilobites, in Hallam, A., ed., Atlas of Palaeobiogeography: Amsterdam, Elsevier, p. 13-18.

Whittington, H.B., and Hughes, C.P., 1973, Ordovician trilobite distribution and geography, in Hughes, N.F., ed., Organisms and Continents through time, Volume Special Papers in Palaeontology 12, p. 235-240.

Wilde, P., 1991, Oceanography in the Ordovician, in Barnes, C.R., and Williams, S.H., eds., Advances in Ordovician geology: Geological Survey of Canada Paper 90-9, p. 225-234.

Wilde, P., Berry, W.B.N., Quinby-Hunt, M.S., Orth, C.J., Quitana, L.R., and Gilmore, J.S., 1986, Iridium abundances across the Ordovician-Silurian stratotype: Science, v. 233, p. 339-341.

Williams, A., 1973, Distribution of brachiopod assemblages in relation to Ordovician palaeogeography: Special Papers in Palaeontology, v. 12, p. 241-269.

Wyatt, A.R., 1993, Phanerozoic shallow water diversity driven by changes in sea-level: Geologische Rundschau, v. 83, p. 203-211.

—, 1995, Late Ordovician extinctions and sea-level change: Journal of the Geological Society, v. 152, p. 899-902.

Yapp, C.H., and Poths, H., 1992, Ancient atmospheric CO_2 inferred from natural geothites: Nature, v. 355, p. 342-344.

Young, T.P., 1990, Ordovician sedimentary facies and faunas of Southwest Europe: palaeogeographic and tectonic implications, in McKerrow, W.S., and Scotese, C.R., eds., Palaeozoic palaeogeography and biogeography: The Geological Society Memoir No. 12: London, The Geological Society.

Chapter 6

Conclusions, limitations, and future work

Due to its association with a major glaciation and absence of evidence for extraterrestrial causes, the Late Ordovician mass extinction has generally been attributed to environmental perturbations that were the result of this glaciation. However, the nearly complete subduction of Ordovician oceanic crust limits the data set of proxies from deep ocean sea floor sediments that can be used to study the Late Ordovician climate system. In particular we are left with mostly geochemical data from shallow epeiric seas that might not reflect the global climate characteristics. Numerical models of Earth's atmosphere-ocean interactions therefore provide a tool to constrain those geochemical results within reasonable boundary conditions and assess the response of the climate system to different perturbations. I used numerical models to investigate the response of the Late Ordovician climate system to different perturbations. More specifically, I evaluated changes in sea level, solar insolation cycles (obliquity cycles), paleogeography and atmospheric pCO_2. I also compared the results of the numerical simulations to the geographic distribution of 490 genera and previous paleobiogeographic studies to see whether the observed faunal patterns corroborate gradients hindcasted by the models.

Factors affecting the ocean-climate system

The atmospheric general circulation model (AGCM) results indicate that the paleogeographic evolution coupled with an ice-albedo feedback and/or a drop in atmospheric pCO_2 can only be regarded as pre-conditioning factors for the Late Ordovician glaciation. This is in contrast to previous studies that suggested that these were the main climate drivers during this time period. This study shows that with a high sea level and a normal heat transport (i.e., a value that replicates the modern climate) ice sheets do not form, even with atmospheric pCO_2 levels as low as 8x PAL, which is the lower limit of proposed pCO_2 values for the Ordovician. If atmospheric pCO_2 did not drop below these estimates, then either sea level must be lowered from its generally high Late Ordovician levels, or poleward ocean heat transport must be reduced to cause glaciation. The results of the ocean general circulation model (OGCM) results also support the results of the AGCM simulations that changes in atmospheric pCO_2 alone were not sufficient to initiate the Late Ordovician glaciation. These results also indicate that sea level might have played a critical role in the Late Ordovician climate system.

Sea level

The Late Ordovician record of sea level change is not well understood and my results underline the importance of better constraining sea level change in the future. The proposed range of sea level change and the timing of sea level changes vary widely between research groups. However, environmental changes associated with sea level changes are not only important for global cooling due to the increased exposed land area

in higher latitudes, but also could play a key role in the mass extinction event because of reduced area of shallow marine environments. In addition to the magnitude of sea level change, the precise timing of sea level change is also important. The combined results of the AGCM and OGCM simulations indicate that sea level change might be the cause, not the result, of the glaciation. One of the goals of a newly proposed IGCP project (personal communication, T. Servais, August 2003) is to study level changes in the Ordovician in greater detail. This could give further insight whether sea level changes were the result of, or the cause for, global cooling during the Late Ordovician.

Poleward ocean heat transport

The asymmetrically coupled OGCM and AGCM results indicate that poleward ocean heat transport might have changed due to paleogeographic change and a drop in sea level. This could have led to a positive feedback that may have led to the amplification or initiation of the glaciation. However, because the models are not fully coupled, there are no direct feedbacks between the atmospheric and oceanic general circulation model. Therefore, this modeling strategy contributes some uncertainty to the model results. Specifically, the uncoupled methodology prevents the ocean surface climate from evolving much beyond the atmospheric surface forcing attained from GENESIS and paleoward ocean heat transport feedbacks can not be fully explored. Therefore, future investigations need to take advantage of evolving fully coupled climate-ocean models (e.g., the community climate system model) to further test various

hypotheses concerning the poleward ocean heat transport during the Ordovician and other time periods.

Atmospheric pCO_2

Assuming that pCO_2 did not fall below 8x PAL, a minimum value for the Late Ordovician based on geochemical modeling and geochemical data from paleosols, a drop in pCO_2 can only be regarded as a pre-conditioning event. Therefore, other environmental changes must have played a crucial role in initiating the growth of extensive ice-sheets (i.e., sea level or paleogeographic changes). This interpretation, which I follow in this thesis, supports the growing view that there is an uncertainty about CO_2 as the major climate driver. Alternatively, CO_2 might have dropped below the proposed lower limits. The time steps of geochemical models are millions of years and are therefore not able to capture perturbations at the time scale of the Late Ordovician glaciation (i.e., <1 Mys). More geochemical studies are therefore needed to better determine the range of pCO_2 values during the Late Ordovician and test whether pCO_2 was lower than predicted by these models.

Vegetation

The AGCM simulations were conducted with bare land surfaces and prescribed median soil values following earlier climate models. This is because the Ordovician is characterized by a lack of vascular land plants and no detailed information on Late

Ordovician soil types is available. However, the reflectivity, and thus the albedo, of the Earth is partly determined by the soil color. In the presence of moisture, early mosses and lichens, which would not leave a full fossil record of their presence, could have covered exposed rock surfaces. In addition, during early stages of a sea level fall, the exposed equatorial carbonate platforms could have enhanced the global albedo due to the generally light color of limestones. However, during later stages those limestones could have covered by mosses and lichens, and thus darkening the exposed carbonate platforms. A wide range of potential soil colors during the Ordovician therefore could have existed. Further sensitivity studies should aim at investigating the potential impact of these very light (e.g., exposed equatorial carbonate platforms) or dark (e.g., moss-covered rocks) end members of soil colors.

Topography

Because no topographic maps for the Late Ordovician have been published, the approach a uniform land elevation of 500 m for all land grid points and 250 m for all coastal areas was specified. Earlier models indicated showed that this topographic elevation was sufficient to generate permanent summer snow cover, which is essential for the formation of ice. However, the elevation of polar land is important for the inception and maintenance of ice sheets. For example, under the present climate, which is considered interglacial, elevated Greenland is glaciated. Future work therefore needs to focus on generating paleoaltitude maps in order to overcome these simplifications.

Paleobiogeography

The paleobiogeographic data provide an important corroboration of the global ocean-climate models. In particular, the interpretation of the paleobiogeographic pattern supports the OGCM results, which indicate warm equatorial temperatures and cool higher latitude temperatures. This temperature gradient would have led to strong thermohaline circulation and consequently the oxygenation of the deep ocean before the onset of the major phase of the Late Ordovician glaciation. This finding is in contrast with the so-called "overturning hypothesis" for the Late Ordovician mass extinction which calls for the upwelling of oxygen depleted deep ocean waters from a previously stagnant ocean due to the inception of the Late Ordovician glaciation.

Problems associated with the Paleobiology Database

The presence-absence matrix that was assembled from the Paleobiology database contains a large amount of data (Appendix 2), more than any other previously assembled data matrix of previos paleogeographic studies for the Ordovician. However, despite its large size, the database is not perfect. For example, some locations are not well represented the database (e.g., Baltic localities), while other regions have a large amount of data entries (e.g., North America) (Appendix 3). In addition, key localities are not represented at all in the database. For instance, there is a large data gap along the western continental margin of Gondwana between the Chinese and South Central European localities. In order to further test the presence of a latitudinal gradient in faunal

composition, these gaps need to be filled in future studies by adding more data into the Paleobiology database in these regions.

Appendix A

Download location for model results

The ocean general circulation model results can be accessed via:

http://www.essc.psu.edu/~/achim/ogcm

The atmospheric general circulation model results can be accessed via:

http://www.essc.psu.edu/~achim/agcm

The ice sheet model results can be accessed via

http://www.essc.psu.edu/~achim/ism

Appendix B

Data matrix used for the multivariate analyses

The following data matrix was used for the multivariate analysis in chapter five. The matrix is in a format that can be directly imported into PC-ORD. The matrix is the absence-presence matrix of genera – '1' for presence and '0' for absence.

PC-ORD Data matrix

490,Genera

42,Localities

Australia - New South Wales, Australia - Tasmania, Canada - District of Mackenzie, Canada - Nunavut, Canada - Ontario, Candada - Quebec, China - GanSu, China - Guizhui, China - Hubei, China - ShaanXi, China - Sichuan, China - XinJiang, Norway, Russia, US - Colorado, US - Minnesota, US - Nevada, US - New York, US - Ohio, US - Tennessee, US - Virginia, Venezuela, Argentina, Bolivia, Czech Republic,France, Morrocco, Portugal, Spain, Sweden, United Kingdom, US - Illinois, US - Iowa, US - Kentucky, US - Wisconsin, Canada - Northwest Territories, China - Anhui, China - Jiangsu, China - Yunnan, China - Zhejiang, US - Oklahoma, China - Hunan

Acidolites,1,1,0,0,0,0,0,0,0,0,0,0,0,0,0,0,0,0,0,0,0,0,0,0,0,0,0,0,0,0,0,0,0,0,0,0,0,0,0,0,0,0

Aulopora,1,0,0,0,0,0,0,0,0,0,0,0,0,0,0,0,0,0,0,0,1,0,0,0,0,0,0,0,0,0,0,0,0,0,0,0,0,0,0,0,0,0

Bajgolia,1,1,0,0,0,0,0,0,0,0,0,0,0,0,0,0,0,0,0,0,0,0,0,0,0,0,0,0,0,0,0,0,0,0,0,0,0,0,0,0,0,0

Billingsaria,1,1,0,0,0,0,0,0,0,0,0,0,0,0,0,0,0,0,0,0,0,0,0,0,0,0,0,0,0,0,0,0,0,0,0,0,0,0,0,0,0,0

Catenipora,1,1,1,0,1,0,0,0,0,1,0,1,0,0,0,0,0,0,0,0,0,0,0,0,0,0,0,0,0,0,0,0,0,0,0,0,0,0,0,0,0,0

Coccoseris,1,1,0,0,0,0,0,0,0,0,0,0,0,0,0,0,0,0,0,0,0,0,0,0,0,0,0,0,0,0,0,0,0,0,0,0,0,0,0,0,0,0

Eofletcheria,1,1,0,0,0,0,0,0,0,0,0,1,1,0,0,0,0,0,0,0,0,0,0,0,0,0,0,0,0,0,0,0,0,0,0,0,0,0,0,0,0,0

Favistina,1,1,0,0,0,0,0,0,0,0,0,0,0,0,0,0,0,0,0,0,0,0,0,0,0,0,0,0,0,0,0,0,0,0,0,0,0,0,0,0,0,0

Fletcheria,1,0,0,0,0,0,0,0,0,0,0,0,0,0,0,0,0,0,0,1,0,0,0,0,0,0,0,0,0,0,0,0,0,0,0,0,0,0,0,0,0,0

Halysites,1,0,0,1,0,0,0,0,0,0,0,0,0,0,1,0,0,0,0,0,0,0,0,0,0,0,0,0,0,0,0,0,0,0,0,0,0,0,0,0,0,0

Heliolites,1,0,0,0,0,0,0,0,0,1,0,1,0,0,0,0,0,0,0,0,0,0,0,0,0,0,0,0,0,0,0,0,0,0,0,0,0,0,0,0,0,0

Hillophyllum,1,1,0,0,0,0,0,0,0,0,0,0,0,0,0,0,0,0,0,0,0,0,0,0,0,0,0,0,0,0,0,0,0,0,0,0,0,0,0,0,0,0

Lichenaria,1,1,0,0,1,1,0,0,0,1,0,0,0,1,0,0,0,0,0,1,0,0,0,0,0,0,0,0,0,0,0,0,0,0,0,0,0,0,0,0,0,0

Nyctopora,1,1,0,0,1,0,0,0,0,0,0,1,0,0,0,0,0,0,0,0,0,0,0,0,0,0,0,0,0,0,0,0,0,0,0,0,0,0,0,0,0,0

Palaeophyllum,1,1,1,0,1,0,0,0,0,0,0,0,0,0,0,0,0,0,0,0,0,0,0,0,0,0,0,0,0,0,0,0,0,0,0,0,0,0,0,0,0,0

Paleofavosites,1,1,0,0,0,0,0,0,0,0,0,0,0,0,0,0,0,0,0,0,0,0,0,0,0,0,0,0,0,0,0,0,0,0,0,0,0,0,0,0,0,0

Plasmoporella,1,1,0,0,0,0,0,1,1,1,1,1,0,0,0,0,0,0,0,0,0,0,0,0,0,0,0,0,0,0,0,0,0,0,0,0,0,0,0,0,0,0

Propora,1,1,0,0,0,0,0,0,0,1,0,1,0,0,0,0,0,0,0,0,0,0,0,0,0,0,0,0,0,0,0,0,0,0,0,0,0,0,0,0,0,0

Saffordophyllum,1,0,0,0,1,0,0,0,0,0,0,0,0,0,1,0,0,0,0,0,0,0,0,0,0,0,0,0,0,0,0,0,0,0,0,0,0,0,0,0,0,0

Streptelasma,1,0,1,1,1,0,1,0,0,0,0,0,1,0,1,1,1,1,1,1,0,1,0,0,0,0,0,0,0,0,0,0,0,0,0,0,0,0,0,0,0,0

Tetradium,1,1,0,0,1,0,0,0,0,0,0,0,0,0,0,0,0,1,0,1,0,0,0,0,0,0,0,0,0,0,0,0,0,0,0,0,0,0,0,0,0,0

Wormsipora,1,0,0,0,0,0,0,0,0,0,0,1,0,0,0,0,0,0,0,0,0,0,0,0,0,0,0,0,0,0,0,0,0,0,0,0,0,0,0,0,0,0

Calapoecia,0,1,1,1,1,0,0,0,0,0,0,0,0,0,1,0,0,0,0,0,0,0,0,0,0,0,0,0,0,0,0,0,0,0,0,0,0,0,0,0,0,0

Cyathophylloides,0,1,0,0,0,0,0,0,0,0,0,1,0,0,0,0,0,0,0,0,0,0,0,0,0,0,0,0,0,0,0,0,0,0,0,0,0,0,0,0,0,0

Diploepora,0,1,0,0,0,0,0,0,0,1,0,1,0,0,0,0,0,0,0,0,0,0,0,0,0,0,0,0,0,0,0,0,0,0,0,0,0,0,0,0,0,0

Favosites,0,1,1,0,0,0,0,0,0,0,0,0,0,0,0,0,0,0,0,0,0,0,0,0,0,0,0,0,0,0,0,0,0,0,0,0,0,0,0,0,0,0

Foerstephyllum,0,1,0,0,1,0,0,0,0,0,0,0,0,0,0,0,0,0,0,0,0,0,0,0,0,0,0,0,0,0,0,0,0,0,0,0,0,0,0,0,0,0

Lyopora,0,1,0,0,0,0,0,0,0,0,0,0,1,0,0,0,0,0,0,0,0,0,0,0,0,0,0,0,0,0,0,0,0,0,0,0,0,0,0,0,0,0

Protaraea,0,1,0,0,0,0,0,1,0,0,0,1,0,0,0,0,0,0,1,0,0,0,0,0,0,0,0,0,0,0,0,0,0,0,0,0,0,0,0,0,0,0

Bighornia,0,0,1,0,0,1,0,0,0,0,0,0,0,0,0,0,1,0,0,0,0,0,0,0,0,0,0,0,0,0,0,0,0,0,0,0,0,0,0,0,0,0

Lobocorallium,0,0,1,0,1,0,0,0,0,0,0,0,0,0,0,0,1,0,0,0,0,0,0,0,0,0,0,0,0,0,0,0,0,0,0,0,0,0,0,0,0,0

Plasmopora,0,0,0,1,1,0,0,0,0,0,0,0,0,0,0,0,0,0,0,0,0,0,0,0,0,0,0,0,0,0,0,0,0,0,0,0,0,0,0,0,0,0

Columnaria,0,0,0,0,1,0,0,0,0,0,0,0,0,0,0,0,0,1,0,1,0,0,0,0,0,0,0,0,0,0,0,0,0,0,0,0,0,0,0,0,0,0

Grewingkia,0,0,0,0,1,0,0,0,0,0,0,0,0,0,0,1,0,0,0,1,0,0,0,0,0,0,0,0,0,0,0,0,0,0,0,0,0,0,0,0,0,0

Lambeophyllum,0,0,0,0,1,0,0,0,0,0,0,0,0,0,0,0,0,0,0,0,1,0,0,0,0,0,0,0,0,0,0,0,0,0,0,0,0,0,0,0,0

Paratetradium,0,0,0,0,0,1,0,0,0,0,0,1,0,0,0,0,0,0,0,0,0,0,0,0,0,0,0,0,0,0,0,0,0,0,0,0,0,0,0,0,0

Agetolites,0,0,0,0,0,0,0,0,0,1,0,1,0,0,0,0,0,0,0,0,0,0,0,0,0,0,0,0,0,0,0,0,0,0,0,0,0,0,0,0,0

Neowormsipora,0,0,0,0,0,0,0,0,0,1,0,1,0,0,0,0,0,0,0,0,0,0,0,0,0,0,0,0,0,0,0,0,0,0,0,0,0,0,0,0,0

Tryplasma,0,0,0,0,0,0,0,0,0,1,0,1,1,0,0,0,0,0,0,0,0,0,0,0,0,0,0,0,0,0,0,0,0,0,0,0,0,0,0,0,0

Concavodonta,0,0,0,0,0,0,0,0,0,0,0,0,0,0,0,0,0,0,0,0,0,1,0,0,1,0,1,0,0,0,0,0,0,0,0,0,0,0,0,0,0

Ctenodonta,1,1,0,0,1,1,0,0,0,1,0,0,1,0,1,1,0,1,1,1,1,1,0,1,1,1,1,0,0,0,1,0,1,1,1,0,0,0,0,0,0,0,0

Modiolopsis,0,1,0,0,1,1,0,0,0,0,0,0,0,0,1,1,0,0,1,1,1,0,1,0,1,1,1,0,1,1,1,1,1,1,1,0,0,0,0,0,0,0,0

Palaeoconcha,0,0,0,0,0,0,0,0,0,0,0,0,0,0,0,0,0,0,0,0,0,0,0,0,1,0,0,0,0,0,0,0,0,0,0,1,0,0,0,0,0,0,0

Praenucula,0,0,0,0,0,0,0,0,0,0,0,0,0,0,0,1,0,0,0,0,0,1,0,1,0,1,0,1,0,1,0,0,0,1,0,1,0,0,0,0,0,0,0

Pterinea,0,1,0,0,0,0,0,0,0,0,0,0,0,0,0,1,0,0,1,1,1,0,0,1,0,0,0,0,0,0,0,1,1,0,1,0,0,0,0,0,0,0,0

Arca,0,0,0,0,0,0,0,0,0,0,0,0,0,0,0,0,0,0,0,0,0,0,0,1,0,0,0,0,0,0,1,0,0,0,0,0,0,0,0,0,0,0,0

Goniophorina,0,0,0,0,0,0,0,0,0,0,0,0,0,0,0,0,0,0,0,0,0,0,0,1,1,0,0,0,0,0,1,0,0,0,0,0,0,0,0,0,0,0,0

Grammysia,0,0,0,0,0,0,0,0,0,0,0,0,0,0,0,0,0,0,0,0,0,0,0,1,1,0,0,0,0,0,0,0,0,0,0,0,0,0,0,0,0,0,0

Nucula,0,0,0,0,0,0,0,0,0,0,0,0,0,0,0,0,0,0,0,0,0,0,0,1,0,0,0,0,0,1,0,0,0,0,0,0,0,0,0,0,0,0,0

Ambonychia,0,0,0,0,1,0,0,0,0,0,0,0,0,0,0,1,0,0,1,1,1,0,0,0,0,0,0,0,0,0,0,1,1,1,1,1,0,0,0,0,0,0,0

Cuneamya,0,0,0,0,1,0,0,0,0,0,0,0,0,0,0,1,0,0,1,0,1,0,0,0,0,0,0,0,0,0,0,1,1,1,0,0,0,0,0,0,0,0,0

Cymatonota,0,0,0,0,1,1,0,0,0,0,0,0,1,0,0,1,0,0,1,0,1,0,0,0,0,0,0,0,0,0,0,1,1,1,0,0,0,0,0,0,0,0,0

Cyrtodonta,0,0,0,0,1,0,0,0,0,0,0,0,0,0,1,1,0,0,0,1,1,0,0,0,0,0,0,0,0,0,0,1,1,1,1,1,0,0,0,0,0,0,0

Cyrtodontula,0,0,0,0,1,0,0,0,0,0,0,0,0,1,0,0,1,0,1,0,0,1,0,0,0,0,0,0,0,0,0,0,1,1,1,1,0,0,0,0,0,0,0

Goniophora,0,0,0,0,1,0,0,0,0,0,0,0,0,0,0,1,0,0,0,0,0,0,0,0,0,0,0,0,0,0,1,1,1,0,0,0,0,0,0,0,0,0,0

Lyrodesma,0,0,0,0,1,0,0,0,0,0,0,0,0,0,0,1,0,1,1,1,0,0,0,0,0,1,0,0,0,0,1,1,1,0,0,0,0,0,0,0,0,0,0

Matheria,0,0,0,0,1,0,0,0,0,0,0,0,0,0,0,1,0,0,0,0,0,0,0,0,0,0,0,0,0,0,1,1,0,0,0,0,0,0,0,0,0,0,0

Nuculites,0,0,0,0,1,0,0,0,0,0,0,0,0,0,0,1,0,0,1,0,1,0,0,0,0,0,1,0,0,0,1,1,1,1,1,1,0,0,0,0,0,0,0

Plethocardia,0,0,0,0,1,0,0,0,0,0,0,0,0,0,0,1,0,0,0,0,0,0,0,0,0,0,0,0,0,0,1,1,0,0,0,0,0,0,0,0,0,0,0

Prolobella,0,0,0,0,1,0,0,0,0,0,0,0,0,0,0,1,0,0,0,0,0,0,0,0,0,0,0,0,0,0,1,1,0,0,0,0,0,0,0,0,0,0,0

Rhytimya,0,0,0,0,1,0,0,0,0,0,0,0,0,0,0,1,0,1,1,0,1,0,0,0,0,0,0,0,0,0,0,1,1,0,0,0,0,0,0,0,0,0,0

Saffordia,0,0,0,0,1,0,0,0,0,0,0,0,0,0,0,1,0,0,0,0,0,0,0,0,0,0,0,0,0,0,0,0,1,1,0,1,0,0,0,0,0,0,0

Tancrediopsis,0,0,0,0,1,0,0,0,0,0,0,0,0,0,0,1,0,0,0,0,1,0,0,0,0,0,0,0,0,0,0,1,1,1,0,0,0,0,0,0,0,0,0

Vanuxemia,0,0,0,0,1,0,0,0,0,0,0,0,0,0,1,1,0,1,0,1,0,0,0,0,0,0,0,0,0,0,0,1,1,1,1,1,0,0,0,0,0,0,0

Whiteavesia,0,0,0,0,1,0,0,0,0,0,0,0,0,0,0,1,0,0,1,1,0,0,0,0,0,0,0,0,0,0,0,1,1,0,1,0,0,0,0,0,0,0

Colpomya,0,0,0,0,0,1,0,0,0,0,0,0,0,0,0,1,0,1,0,0,1,0,0,0,0,0,0,0,0,0,0,1,0,0,1,0,0,0,0,0,0,0,0

Allodesma,0,0,0,0,0,0,0,0,0,1,0,0,0,0,0,1,0,0,0,0,0,0,0,0,0,0,0,0,0,0,0,1,1,0,0,0,0,0,0,0,0,0

Similodonta,0,0,0,0,0,0,0,0,0,1,0,0,0,0,0,1,0,0,1,0,0,0,0,0,0,0,0,0,0,0,0,1,1,1,0,1,0,0,0,0,0,0,0

Deceptrix,0,0,0,0,0,0,0,0,0,0,0,0,0,0,0,1,0,0,1,0,0,0,0,0,1,1,0,0,0,0,0,1,1,1,0,0,0,0,0,0,0,0,0

Myoplusia,0,0,0,0,0,0,0,0,0,0,0,0,0,0,0,0,0,0,0,0,0,0,0,0,0,0,0,1,1,0,1,1,0,0,0,0,0,0,0,0,0,0,0

Palaeoneilo,0,0,0,0,0,0,0,0,0,0,0,0,0,0,0,1,0,0,0,0,0,0,0,0,1,1,1,0,0,0,1,1,1,0,1,0,0,0,0,0,0,0,0

Sluha,0,0,0,0,0,0,0,0,0,0,0,0,0,0,0,0,0,0,0,0,0,0,0,0,0,0,0,1,1,0,1,0,0,0,0,0,0,0,0,0,0,0,0

Redonia,0,0,0,0,0,0,0,0,0,0,0,0,0,0,0,0,0,0,0,0,0,0,0,0,0,0,0,1,0,0,1,0,0,0,0,0,0,0,0,0,0,0,0

Ambonychiopsis,0,0,0,0,0,0,0,0,0,0,0,0,0,0,0,1,0,0,0,0,0,0,0,0,0,0,0,0,0,0,0,1,1,0,1,0,0,0,0,0,0,0

Cleionychia,0,0,0,0,0,0,0,0,0,0,0,0,0,0,1,0,0,1,0,0,0,0,0,0,0,0,0,0,0,0,0,1,1,0,1,0,0,0,0,0,0,0

Glyptarca,0,0,0,0,0,0,0,0,0,0,0,0,0,0,0,0,0,0,0,0,0,0,0,0,0,0,0,1,1,1,0,0,0,0,0,0,0,0,0,0,0,0,0

Cardiolaria,0,0,0,0,0,0,0,0,0,0,0,0,0,0,0,0,0,0,0,0,0,0,0,0,0,0,0,1,0,1,0,0,0,0,0,0,0,0,0,0,0,0,0

Eurymya,0,0,0,0,0,0,0,0,0,0,0,0,0,0,0,1,0,0,1,0,0,0,0,0,0,0,0,0,0,0,0,1,1,0,1,0,0,0,0,0,0,0,0

Modiolodon,0,0,0,0,0,0,0,0,0,0,0,0,0,0,0,1,0,0,1,1,0,0,0,0,0,0,0,0,0,0,0,1,1,1,0,0,0,0,0,0,0,0,0

Allonychia,0,0,0,0,0,0,0,0,0,0,0,0,0,0,0,0,0,0,1,0,0,1,0,0,0,0,0,0,0,0,0,0,0,0,0,0,0,0,0,0,0,0,0

Ischyrodonta,0,0,0,0,0,0,0,0,0,0,0,0,0,0,0,0,0,0,0,1,0,1,0,0,0,0,0,0,0,0,0,0,0,0,0,0,0,0,0,0,0,0,0

Bicuspina,0,0,0,0,0,1,0,0,0,1,0,0,0,0,0,0,0,0,0,0,0,1,1,0,1,1,1,0,0,0,1,0,0,0,0,0,0,0,0,0,0,0,0

Camerella,0,0,1,0,1,0,1,0,0,0,0,0,0,0,0,0,0,0,0,1,0,0,1,0,0,0,0,0,0,0,0,0,0,0,0,0,1,0,0,0,0,1,0

Campylorthis,0,0,0,0,0,0,0,0,0,0,0,0,0,0,0,1,0,0,0,0,0,0,1,0,0,0,0,0,0,0,0,1,1,0,1,0,0,0,0,0,0,0,0

Dinorthis,1,1,1,0,1,0,1,0,0,0,0,1,1,0,0,1,1,1,0,1,1,0,1,1,0,0,0,0,0,0,0,1,1,1,0,0,0,0,0,0,0,1,0

Lingula,1,0,0,0,1,1,0,0,0,1,0,0,0,0,0,1,1,0,1,1,0,1,1,1,1,1,1,1,0,0,0,1,1,1,1,0,0,0,0,0,0,0,1,0

Ptychoglyptus,0,0,0,0,0,0,0,0,0,0,0,0,0,0,0,1,0,0,0,0,0,0,0,1,0,1,0,0,0,0,0,0,0,0,0,0,0,0,0,0,0,0,0

Sowerbyella,1,1,0,1,1,1,1,0,0,1,1,1,1,0,0,1,1,1,1,1,1,1,1,0,0,0,0,0,0,1,1,1,1,1,0,1,0,0,1,0,1,0

Tissintia,0,0,0,0,0,0,0,0,0,0,0,0,0,0,0,0,0,0,0,0,0,0,1,0,0,1,0,0,0,0,0,0,0,0,0,0,0,0,0,0,0,0

Anazyga,1,1,0,0,1,0,0,0,0,1,0,0,0,0,0,0,0,0,1,0,1,0,0,0,0,0,0,0,0,0,0,0,0,0,0,0,0,0,0,0,0,0

Anoptambonites,1,0,0,0,0,0,0,0,1,0,1,0,0,0,0,0,0,0,0,0,0,0,0,0,0,0,0,0,0,0,0,0,0,0,0,0,0,0,0,0,0,0

Bellimurina,1,0,0,0,0,0,0,0,0,0,0,0,0,1,0,1,0,0,0,0,0,0,0,0,0,0,0,0,0,0,0,1,1,0,0,0,0,0,1,0,1,0

Catazyga,1,0,0,0,1,1,0,0,0,0,0,0,0,0,0,0,0,0,1,0,0,0,0,0,0,0,0,0,0,0,0,0,0,0,0,0,0,0,1,0,0

Christiania,1,0,0,0,0,0,0,0,1,1,1,0,1,0,0,0,0,0,0,0,1,0,0,0,0,0,0,0,0,1,1,0,0,0,0,0,0,1,0,1,0,0

Conotreta,1,0,0,0,0,0,0,0,0,0,0,0,0,0,0,0,0,0,0,0,0,1,0,0,0,0,0,0,0,0,1,0,0,1,0,0,0,0,0,0,0,0

Cyclospira,1,0,1,1,1,0,0,0,0,0,0,0,1,0,0,1,0,0,0,0,1,0,0,0,0,0,0,0,0,0,1,1,1,0,0,0,0,0,0,0,1,0

Didymelasma,1,0,0,0,0,0,0,0,0,1,0,0,0,0,0,0,0,0,0,0,0,0,0,0,0,0,0,0,0,0,0,0,0,0,0,0,0,0,0,0,0,0

Doleroides,1,0,1,0,1,0,0,0,0,0,0,0,0,0,0,0,1,0,1,0,1,1,0,0,0,0,0,0,0,0,0,0,1,1,0,0,1,0,0,0,0,1,0

Eodinobolus,1,0,0,0,0,0,0,0,0,0,0,0,0,1,0,0,0,0,0,0,0,0,0,0,0,0,0,0,0,0,0,0,0,0,0,0,0,0,0,0,0,0

Eridorthis,1,0,0,0,0,0,0,0,0,0,0,0,0,0,0,0,0,0,0,0,1,0,0,0,0,0,0,1,0,0,0,0,0,0,0,0,0,0,0,0,0,0

Furcitella,1,0,0,0,0,0,0,0,0,0,0,0,0,0,1,0,0,0,0,0,0,0,0,0,0,0,0,0,0,1,1,0,0,1,0,0,0,0,0,0,0,0

Hesperorthis,1,0,1,1,1,0,0,0,0,0,0,0,0,1,0,1,1,1,0,1,1,0,0,0,0,0,0,0,0,1,0,1,1,1,1,1,0,0,0,1,1,0

Holtedahlina,1,0,0,0,0,0,0,0,0,0,0,0,0,0,1,0,0,1,0,0,0,0,0,0,0,0,0,0,0,0,1,1,0,0,1,0,0,0,0,0,0,0

Leptellina,1,1,0,0,0,0,1,0,0,0,0,0,1,1,0,0,1,0,0,0,1,0,0,0,0,0,0,0,0,0,0,0,0,0,0,0,0,0,1,0,0,0

Leptestiina,1,0,0,0,0,0,0,0,0,0,0,0,1,0,0,0,0,0,0,0,0,0,0,0,0,1,0,0,1,0,1,0,0,0,0,0,0,1,0,0,0,0

Obolus,1,0,0,0,0,0,0,0,0,0,0,0,0,0,0,0,0,0,0,0,0,0,0,0,0,0,1,0,0,0,1,1,0,0,0,0,0,0,0,0,0,0

Oepikina,1,0,1,0,1,0,1,0,0,0,0,0,1,1,0,1,1,1,0,1,1,0,0,0,0,0,0,0,0,1,0,1,1,0,1,1,0,0,0,0,1,0

Paterula,1,0,0,0,0,0,0,0,0,0,0,0,0,0,0,0,0,0,1,0,0,0,0,0,0,1,0,0,0,0,1,1,0,0,0,0,0,0,0,0,0,0

Plectorthis,1,0,0,1,1,0,0,0,0,0,0,0,0,1,0,0,1,1,1,1,0,1,1,0,0,0,0,0,0,0,0,0,1,1,0,0,0,0,0,1,0,1,0

Protozyga,1,0,0,0,0,0,0,0,0,0,0,0,0,1,0,0,1,0,1,0,0,1,0,0,0,0,0,0,0,0,0,0,1,1,1,0,0,0,0,0,0,0,1,0

Ptychopleurella,1,1,0,0,0,0,0,0,0,1,0,0,0,0,0,0,0,0,0,0,0,0,1,0,0,0,0,0,0,0,0,0,0,0,0,0,0,0,1,0,0,0,0,0

Rhynchotrema,1,0,1,1,1,0,0,0,0,1,0,0,0,0,1,1,0,1,1,1,0,0,0,0,0,0,0,0,0,0,0,0,1,1,1,0,1,0,0,0,0,0,0

Scaphorthis,1,0,0,0,0,0,0,0,0,0,0,0,0,0,0,0,0,0,1,0,0,0,0,0,0,0,0,0,0,0,0,0,0,0,0,0,0,0,0,0,0,0

Sericoidea,1,0,0,0,0,0,0,0,0,0,0,0,0,1,0,0,0,0,0,0,0,0,0,0,0,1,0,0,0,0,1,1,0,0,0,0,0,0,0,0,0,0

Skenidioides,1,1,0,1,1,1,0,0,1,0,0,0,1,0,0,1,1,0,0,0,1,0,0,0,0,0,0,0,0,0,1,1,1,1,0,1,1,0,1,0,0,1,0

Sowerbyites,1,1,0,0,0,0,0,0,0,0,0,0,0,0,0,0,0,1,0,0,0,0,0,0,0,0,0,0,0,0,0,0,0,0,0,0,0,0,0,0,0,1,0

Strophomena,1,1,1,1,1,0,1,0,0,1,0,1,1,1,1,1,1,1,1,1,1,0,0,0,0,1,0,0,1,0,1,1,1,0,1,1,0,0,1,0,1,0

Trigrammaria,1,0,0,0,0,0,0,0,0,0,0,0,0,0,0,0,1,0,1,1,0,0,0,0,0,0,0,0,0,0,0,0,0,1,1,0,0,0,0,0,0,0,0

Zygospira,1,0,1,1,1,0,0,0,0,0,0,0,1,0,1,1,0,1,1,1,1,0,0,0,0,0,0,0,0,0,0,1,1,1,1,0,1,0,0,0,0,0,0

Clitambonites,0,1,0,0,0,0,1,0,0,0,0,0,0,0,0,0,0,0,0,0,0,0,0,0,0,0,0,0,0,0,0,0,0,0,0,0,0,0,0,0,0,0

Kjerulfina,0,1,0,0,0,0,0,0,0,0,0,0,1,0,0,0,0,0,0,0,0,0,0,0,0,0,0,0,0,0,1,0,0,0,0,0,0,0,0,0,0,0

Lepidocyclus,0,1,1,0,0,0,0,0,0,0,0,0,0,0,1,1,0,0,1,0,0,0,0,0,0,0,0,0,0,0,0,1,1,0,0,1,0,0,0,0,0,0

Onniella,0,1,0,0,0,0,0,0,0,0,0,0,1,0,0,1,0,0,1,0,1,1,0,0,1,0,0,1,0,1,1,1,1,1,1,0,0,0,0,0,0,1,0

Drabovinella,0,0,0,0,0,0,0,0,0,0,0,0,0,0,0,0,0,0,0,0,0,0,0,0,0,0,0,0,1,1,1,1,0,1,0,0,0,0,0,0,0,0,0,0,0

Heterorthis,0,0,0,0,0,0,0,0,0,0,0,0,0,0,0,0,0,0,0,0,0,1,0,0,0,1,1,1,1,1,0,1,0,1,0,0,0,0,0,0,0,0,0,0,0

Kjaerina,0,0,0,0,0,0,0,0,0,0,0,0,1,0,0,0,0,0,0,0,0,0,0,1,0,0,0,0,0,0,1,0,0,0,0,0,0,0,0,0,0,0

Orbiculoidea,0,0,0,0,1,0,1,0,0,0,1,0,1,0,0,1,0,1,1,1,1,1,0,0,1,1,0,0,0,0,1,1,1,1,1,0,0,0,0,0,0,0,1,0

Rostricellula,0,0,1,0,0,1,1,0,0,0,0,0,1,1,0,1,0,0,0,1,1,1,0,1,1,0,1,1,1,1,0,1,1,1,1,0,0,1,0,0,0,0,1,0

Schizocrania,0,0,0,0,0,0,0,0,0,0,0,0,0,0,0,0,0,1,0,1,1,0,0,0,0,1,0,0,0,0,0,0,0,1,1,1,0,0,0,0,0,0,0,0

Chaulistomella,0,0,1,0,0,0,0,0,0,0,0,0,0,0,0,0,0,0,0,0,0,0,0,0,0,0,0,0,0,0,0,0,0,0,0,0,0,0,0,0,0,1,0

Diceromyonia,0,0,1,0,1,0,0,0,0,0,0,0,0,0,0,0,1,1,0,0,0,0,0,0,0,0,0,0,0,0,0,0,1,1,0,0,0,0,0,0,0,0,0

Eoplectodonta,0,0,1,0,1,0,0,0,1,0,0,0,1,0,0,1,1,0,1,0,1,0,0,0,0,0,0,0,1,1,1,1,1,0,0,1,0,0,0,1,0,0

Glyptorthis,0,0,1,1,1,0,0,0,1,1,0,0,1,1,0,1,0,0,0,1,1,1,0,0,0,1,0,0,0,0,0,1,1,0,0,1,0,0,0,0,1,0

Mimella,0,0,1,0,0,0,0,0,0,0,0,0,0,1,0,0,0,0,0,1,1,0,0,0,0,0,0,0,0,0,0,0,0,0,0,1,0,0,0,0,1,0

Ancistrorhyncha,0,0,0,0,0,0,0,0,0,0,0,0,0,0,0,0,0,0,0,0,0,0,0,0,0,0,0,0,0,0,0,0,0,0,0,0,0,0,0,1,0,0,0,0,1,0

Boreadorthis,0,0,0,0,0,0,0,0,0,0,0,0,0,0,1,0,0,0,0,0,0,0,0,0,0,0,0,0,0,0,0,0,0,0,0,0,0,1,0,0,0,0,0,0

Megamyonia,0,0,0,0,1,0,0,0,0,0,0,0,0,0,0,1,0,0,0,0,0,0,0,0,0,0,0,0,0,0,0,0,1,1,0,0,1,0,0,0,0,0,0

Paucicrura,0,0,0,0,1,0,0,0,0,0,0,0,0,0,0,1,1,1,0,0,1,1,0,0,0,1,0,0,1,0,0,1,1,0,0,1,0,0,0,0,0,0

Pionodema,0,0,0,0,1,0,0,0,0,0,0,0,0,0,0,1,0,0,0,1,0,1,0,0,0,0,0,0,0,0,0,0,1,1,0,1,1,0,0,0,0,0,0

Plaesiomys,0,0,0,0,0,0,1,0,0,0,0,0,0,0,1,1,0,0,1,1,1,0,0,0,0,0,0,0,0,0,0,0,1,1,0,0,1,0,0,0,0,0,0

Platystrophia,0,0,0,1,1,0,1,0,0,0,0,0,1,0,0,1,0,1,1,1,0,1,0,0,0,0,0,0,0,1,1,1,1,1,1,0,1,0,0,0,0,0,0

Rafinesquina,0,0,0,1,1,0,0,0,0,0,0,0,1,1,0,0,1,1,1,1,1,1,1,1,0,0,1,1,1,0,1,0,0,1,1,1,0,1,1,0,0,0,0,0

Tetraphalerella,0,0,0,0,0,0,0,0,0,0,0,0,0,0,0,0,1,0,0,0,0,0,0,0,0,0,0,0,0,0,0,0,1,1,0,0,1,0,0,0,0,0,0

Triplesia,0,0,0,0,0,0,0,0,0,0,0,0,1,1,1,0,0,0,1,0,0,0,0,0,0,1,1,1,1,1,0,1,0,0,0,0,1,0,0,0,0,0,0

Austinella,0,0,0,1,0,0,0,1,0,0,0,0,0,0,0,0,1,0,0,0,0,0,0,0,0,0,0,0,0,0,0,0,1,1,0,0,0,0,0,0,0,0,0

Dalmanella,0,0,0,1,1,1,0,0,0,0,0,0,0,1,0,0,1,0,0,0,1,1,1,0,0,1,1,1,0,1,1,1,1,1,1,1,0,0,1,0,0,0,0,0

Parastrophinella,0,0,0,1,0,0,0,0,0,0,0,0,0,1,0,0,0,0,0,0,0,0,0,0,0,0,0,1,0,0,0,0,0,0,0,0,0,0,0,0,0,0,0

Ectenoglossa,0,0,0,0,1,0,0,0,0,0,0,0,0,0,0,0,0,0,0,0,0,0,0,0,0,0,0,0,0,0,0,0,0,0,0,0,0,0,0,0,1,0

Hebertella,0,0,0,0,1,1,0,0,0,0,0,0,0,0,0,1,0,0,0,1,1,1,0,0,0,0,0,0,0,1,0,0,0,0,1,0,0,0,0,0,0,0,0

Hypsiptycha,0,0,0,0,1,0,0,0,0,0,0,0,0,0,0,1,1,0,0,0,0,0,0,0,0,0,0,0,0,0,0,1,1,0,0,0,0,0,0,0,0,0,0

Leptaena,0,0,0,0,1,1,1,0,0,1,0,0,1,0,0,0,0,0,0,1,0,1,0,0,0,0,1,0,0,0,0,1,0,0,0,0,0,0,0,1,0,0,0

Leptobolus,0,0,0,0,1,0,0,0,0,0,0,1,0,0,0,0,0,0,1,1,1,0,1,0,0,0,0,0,0,0,0,0,1,0,0,1,0,0,0,0,0,0,0,0

Microtrypa,0,0,0,0,1,0,0,0,0,0,0,0,0,0,0,0,1,0,0,0,0,0,0,0,0,0,0,0,0,0,0,0,0,0,0,0,0,0,0,0,0,0,0

Parastrophina,0,0,0,0,1,0,0,0,0,0,0,0,0,1,0,0,1,0,1,0,0,0,0,0,0,0,0,0,0,0,0,0,0,1,1,0,0,0,0,0,0,0,0

Pseudolingula,0,0,0,0,1,0,0,0,0,0,0,0,1,0,0,0,1,0,0,0,0,0,0,0,0,0,0,0,0,0,1,0,0,1,1,1,0,0,0,0,0,0,1,0

Resserella,0,0,0,0,1,0,0,0,0,0,0,0,1,0,0,0,0,0,1,0,0,0,1,0,0,0,0,0,0,0,0,0,0,0,0,0,0,0,0,0,0,0,0

Trematis,0,0,0,0,1,0,0,0,0,0,0,0,0,0,0,0,1,0,1,1,0,0,0,0,0,1,0,0,0,0,0,0,1,1,0,0,0,0,0,0,0,0,0

Valcourea,0,0,0,0,1,0,0,0,0,0,0,0,1,0,0,0,0,1,0,0,1,0,0,0,0,0,0,0,0,0,0,0,0,0,0,0,0,0,0,0,0,1,0

Vellamo,0,0,0,0,1,0,0,0,0,0,0,0,0,1,0,0,1,0,0,0,0,0,0,0,0,0,0,0,0,0,0,1,1,1,1,0,0,0,0,0,0,0,0

Lingulella,0,0,0,0,0,1,0,0,0,0,0,0,0,0,0,0,0,0,0,0,0,0,0,0,0,0,0,1,0,0,0,0,0,1,0,0,0,0,0,0,0,0,1,0

Atrypa,0,0,0,0,0,0,0,0,0,0,0,0,1,0,0,0,0,0,0,0,0,0,0,0,0,1,0,0,0,0,0,0,0,0,0,0,0,0,0,0,0,0,0

Dolerorthis,0,0,0,0,0,0,0,0,0,0,0,0,0,1,0,0,0,0,0,0,0,0,0,0,0,0,0,1,0,0,0,0,1,0,0,0,0,0,0,0,0,0,0

Bilobia,0,0,0,0,0,0,0,0,0,0,0,0,0,0,0,0,1,0,0,0,1,0,0,0,0,0,0,0,0,1,0,0,0,0,0,0,1,0,0,0,0,0,0

Anisopleurella,0,0,0,0,0,0,0,1,0,0,0,0,0,1,0,0,0,0,0,0,0,0,0,0,0,0,0,0,0,0,0,0,1,1,0,0,0,0,0,0,1,0,0,0,0

Cliftonia,0,0,0,0,0,0,0,1,0,0,0,0,0,0,0,0,0,0,0,0,0,0,0,0,0,0,0,0,0,0,0,0,1,1,0,0,0,0,0,0,0,0,0,0,0,0

Leptelloidea,0,0,0,0,0,0,0,1,0,0,1,0,1,0,0,0,0,0,0,0,0,0,0,0,0,0,0,0,0,0,0,0,0,0,0,0,0,0,0,0,1,0,0,0

Nicolella,0,0,0,0,0,0,0,1,0,0,0,0,0,0,1,0,0,0,0,0,0,0,0,0,0,0,0,0,0,1,0,0,1,1,1,0,0,0,0,0,0,0,0,0,0

Plectatrypa,0,0,0,0,0,0,0,1,0,0,1,0,0,0,0,0,0,0,0,0,0,0,0,0,0,0,0,0,0,0,0,0,0,0,0,0,0,0,0,0,0,0,0

Multicostella,0,0,0,0,0,0,0,0,0,0,0,0,0,0,0,0,0,0,0,1,0,0,1,1,0,0,0,0,0,0,0,0,0,0,0,0,0,0,0,0,0,1,0

Orthis,0,0,0,0,0,0,0,0,0,1,0,0,0,0,0,0,1,0,1,0,0,0,0,0,1,1,0,0,0,0,0,0,0,0,0,0,0,0,0,0,0

Acrotreta,0,0,0,0,0,0,0,0,1,1,0,0,0,0,0,0,0,0,0,0,0,0,0,0,0,0,0,0,0,0,1,0,0,0,0,0,0,0,0,0,0

Leangella,0,0,0,0,0,0,0,0,1,0,0,0,0,0,0,0,0,0,0,0,0,0,0,0,0,0,0,0,0,1,0,0,0,0,0,0,0,0,0,0,0

Idiospira,0,0,0,0,0,0,0,0,0,0,0,0,0,0,0,1,0,0,0,0,0,0,0,0,0,0,0,0,0,0,0,1,1,0,0,0,0,1,0,0,0,0

Paracraniops,0,0,0,0,0,0,0,0,0,0,0,0,0,0,0,0,0,0,0,0,0,0,0,0,0,0,0,0,0,0,0,1,0,0,0,0,0,0,1,0,0,0,0

Gunnarella,0,0,0,0,0,0,0,0,0,1,0,0,1,0,0,0,0,0,0,0,0,0,0,0,0,0,0,0,0,0,0,0,0,0,0,0,0,0,0,0,0

Porambonites,0,0,0,0,0,0,0,0,0,1,1,0,1,0,0,0,0,0,0,0,0,0,0,0,0,0,1,0,0,0,0,0,0,0,0,0,0,0,0,0,0

Bimuria,0,0,0,0,0,0,0,0,0,0,1,0,1,0,0,0,1,0,0,0,0,0,0,0,0,0,0,0,1,1,0,0,0,0,0,0,0,0,0,0,0

Paurorthis,0,0,0,0,0,0,0,0,0,0,1,0,0,0,0,0,0,0,0,0,1,0,0,0,0,0,0,0,0,0,0,0,0,0,0,0,0,0,1,0

Diorthelasma,0,0,0,0,0,0,0,0,0,0,0,0,0,0,0,1,0,0,0,0,0,0,0,0,0,0,0,0,0,1,1,0,0,0,0,0,1,0,0,0

Howellites,0,0,0,0,0,0,0,0,0,0,0,0,1,0,0,0,0,0,0,0,0,0,0,1,0,1,1,0,0,1,0,0,0,0,0,0,1,0,0,0

Aegiria,0,0,0,0,0,0,0,0,0,0,0,0,0,0,0,0,0,0,0,0,0,0,0,0,1,0,0,0,0,1,0,0,0,0,0,0,0,0,0,0,0

Cryptothyris,0,0,0,0,0,0,0,0,0,0,0,0,0,0,0,0,0,0,0,0,0,0,0,0,1,1,0,0,0,0,1,0,0,0,0,0,0,0,0,0,0

Drabovia,0,0,0,0,0,0,0,0,0,0,0,0,0,0,0,0,0,0,0,0,0,0,0,0,1,1,1,1,1,1,0,0,0,0,0,0,0,0,0,0,0

Gelidorthis,0,0,0,0,0,0,0,0,0,0,0,0,0,0,0,0,0,0,0,0,0,0,0,0,1,0,1,1,1,0,0,0,0,0,0,0,0,0,0,0,0

Heterorthina,0,0,0,0,0,0,0,0,0,0,0,0,0,0,0,0,0,0,0,0,1,0,0,1,0,0,1,1,0,1,1,0,1,0,0,1,0,0,0,0,0,0,0

Horderleyella,0,0,0,0,0,0,0,0,0,0,0,0,1,0,0,0,0,0,0,0,0,0,0,0,1,0,0,1,1,0,1,0,0,0,0,0,0,0,0,0,0

Jezercia,0,0,0,0,0,0,0,0,0,0,0,0,0,0,0,0,0,0,0,0,0,0,0,0,1,0,0,0,1,0,0,0,0,0,0,0,0,0,0,0,0

Petrocrania,0,0,0,0,0,0,0,0,0,0,0,0,1,0,0,1,0,1,1,0,0,0,0,0,1,0,0,1,0,0,0,1,1,1,0,0,0,0,0,0,1,0

Plectoglossa,0,0,0,0,0,0,0,0,0,0,0,0,0,0,0,0,0,0,0,0,0,0,0,0,1,0,0,0,0,0,0,0,0,0,0,0,0,0,1,0

Reuschella,0,0,0,0,0,0,0,0,0,0,0,0,0,0,0,0,0,0,0,0,0,0,0,0,1,0,0,0,1,0,1,0,0,0,0,0,0,0,0,0,0

Saukrodictya,0,0,0,0,0,0,0,0,0,0,0,0,0,0,0,0,0,0,0,0,0,0,0,0,1,0,0,1,1,0,0,0,0,0,0,0,0,0,0,0,0

Schizotreta,0,0,0,0,0,0,0,0,0,0,0,0,0,0,0,0,0,0,0,1,0,0,0,0,0,1,0,0,0,0,0,1,0,0,0,0,0,0,0,0,0

Svobodaina,0,0,0,0,0,0,0,0,0,0,0,0,0,0,0,0,0,0,0,0,0,0,0,0,1,1,0,1,1,0,0,0,0,0,0,0,0,0,0,0,0

Aegiromena,0,0,0,0,0,0,0,0,0,0,0,0,0,0,0,0,0,0,0,0,0,0,0,0,1,1,1,1,0,0,0,0,0,0,0,0,0,0,0,0,0

Bancroftina,0,0,0,0,0,0,0,0,0,0,0,0,0,0,0,0,0,0,0,0,0,0,0,0,1,0,0,0,0,1,0,0,0,0,0,0,0,0,0,0,0

Hedstroemina,0,0,0,0,0,0,0,0,0,0,0,0,1,0,0,0,0,0,0,0,0,0,0,0,1,0,1,1,0,1,0,0,0,0,0,0,0,0,0,0,0

Iberomena,0,0,0,0,0,0,0,0,0,0,0,0,0,0,0,0,0,0,0,0,0,0,0,0,0,1,0,0,1,0,0,0,0,0,0,0,0,0,0,0,0,0

Portranella,0,0,0,0,0,0,0,0,0,0,0,0,0,0,0,0,0,0,0,0,0,0,0,0,0,1,0,0,1,0,0,0,0,0,0,0,0,0,0,0,0,0

Tafilaltia,0,0,0,0,0,0,0,0,0,0,0,0,0,0,0,0,0,0,0,0,0,0,0,0,0,1,1,0,1,0,0,0,0,0,0,0,0,0,0,0,0,0

Kiaeromena,0,0,0,0,0,0,0,0,0,0,0,0,1,0,0,0,0,0,0,0,0,0,0,0,0,0,1,0,0,0,1,0,0,0,0,0,0,0,0,0,0,0

Cremnorthis,0,0,0,0,0,0,0,0,0,0,0,0,1,0,0,0,0,0,0,0,0,0,0,0,0,0,0,0,0,1,0,0,0,0,0,0,0,0,0,0,0,0

Hisingerella,0,0,0,0,0,0,0,0,0,0,0,0,1,0,0,0,0,0,0,0,0,0,0,0,0,0,0,0,0,1,0,0,0,0,0,0,0,0,0,0,0,0

Kullervo,0,0,0,0,0,0,0,0,0,0,0,0,1,0,0,0,0,0,0,0,0,0,0,0,0,0,0,0,0,1,1,0,0,0,0,0,0,0,0,0,0,0,0

Oxoplecia,0,0,0,0,0,0,0,0,0,0,0,0,1,0,0,1,1,0,0,0,1,0,0,0,0,0,0,0,0,0,1,1,1,1,0,0,0,0,0,0,0,1,0

Rhactorthis,0,0,0,0,0,0,0,0,0,0,0,0,1,0,0,0,0,0,0,0,0,0,0,0,0,0,0,0,0,1,0,0,0,0,0,0,0,0,0,0,0,0

Orthambonites,0,0,0,0,0,0,0,0,0,0,0,0,0,0,0,0,0,0,0,0,0,0,0,0,0,1,0,0,0,0,0,0,1,0,0,0,0,0,0,0,0,0,0,0

Cyrtonotella,0,0,0,0,0,0,0,0,0,0,0,0,0,0,0,0,0,0,0,0,0,0,0,0,0,0,0,0,0,0,0,0,1,1,0,0,0,0,0,0,0,0,0,0

Palaeostrophomena,0,0,0,0,0,0,0,0,0,0,0,0,0,0,0,0,0,0,0,0,0,0,0,0,0,0,0,0,0,0,0,0,0,0,1,1,0,0,0,0,0,0,0,0,0,0

Schizambon,0,0,0,0,0,0,0,0,0,0,0,0,0,0,0,0,1,0,0,1,0,1,0,0,0,0,0,0,0,0,1,0,1,1,0,0,0,0,0,0,0,1,0

Lingulasma,0,0,0,0,0,0,0,0,0,0,0,0,0,0,0,0,1,0,0,0,0,0,0,0,0,0,0,0,0,0,1,1,1,0,0,0,0,0,0,0,1,0

Macrocoelia,0,0,0,0,0,0,0,0,0,0,0,0,0,0,0,0,0,0,0,0,0,0,0,0,0,0,0,0,0,0,0,0,1,0,0,0,0,0,0,0,1,0

Palaeoglossa,0,0,0,0,0,0,0,0,0,0,0,0,0,0,0,0,1,0,0,0,0,0,0,0,0,0,0,0,0,1,1,1,0,0,0,0,0,0,0,0,0,0

Acanthocrania,0,0,0,0,0,0,0,0,0,0,0,0,0,0,0,0,1,0,0,0,1,1,0,0,0,0,0,0,0,0,0,0,1,1,0,0,0,0,0,0,0,1,0

Craniops,0,0,0,0,0,0,0,0,0,0,0,0,0,0,0,0,1,0,0,0,0,1,0,0,0,0,0,0,0,0,0,1,1,0,0,0,0,0,0,0,1,0

Eremotrema,0,0,0,0,0,0,0,0,0,0,0,0,0,0,0,0,1,0,0,0,0,0,0,0,0,0,0,0,0,0,1,1,0,0,0,0,0,0,0,0,0,0

Lingulops,0,0,0,0,0,0,0,0,0,0,0,0,0,0,0,0,1,0,0,0,1,0,0,0,0,0,0,0,0,0,0,1,1,0,0,0,0,0,0,0,0,0

Pachyglossella,0,0,0,0,0,0,0,0,0,0,0,0,0,0,0,0,1,0,0,0,0,0,0,0,0,0,0,0,0,0,1,1,0,0,0,0,0,0,0,0,0,0

Philhedra,0,0,0,0,0,0,0,0,0,0,0,0,0,0,0,0,1,0,0,0,0,0,0,0,0,0,0,0,0,1,0,0,0,0,0,0,0,0,1,0,0,0

Plectambonites,0,0,0,0,0,0,0,0,0,0,0,0,0,0,0,0,1,0,0,0,0,0,0,0,0,0,0,0,0,0,0,0,0,0,0,0,0,0,0,1,0

Crania,0,0,0,0,0,0,0,0,0,0,0,0,0,0,0,0,1,0,0,0,1,0,0,0,0,0,0,0,0,0,0,0,0,0,0,0,0,0,0,0,0,0

Camarotoechia,0,0,0,0,0,0,0,0,0,0,0,0,0,0,0,0,1,0,1,0,0,0,0,0,0,0,0,0,0,0,0,0,0,0,0,0,0,0,0,0,0,0

Orthorhyncula,0,0,0,0,0,0,0,0,0,0,0,0,0,0,0,0,1,1,0,0,0,0,0,0,0,0,0,0,0,0,0,0,0,0,0,0,0,0,0,0,0,0

Bactroceras,1,0,0,0,0,0,0,0,1,0,0,0,0,0,0,0,0,0,0,0,0,0,0,0,0,0,0,0,0,0,0,0,0,0,0,0,0,1,0,0,0,0

Gorbyoceras,1,1,0,0,0,0,0,0,0,0,0,0,1,0,0,1,0,0,0,0,0,0,0,0,0,0,0,0,0,0,0,0,1,1,0,1,0,0,0,0,0,0,0

Kionoceras,1,0,0,1,0,0,0,0,0,0,0,0,1,0,1,1,0,0,0,0,0,0,0,0,0,0,0,0,0,0,0,0,1,1,0,1,1,0,0,0,0,0,1

Orthoceras,1,0,0,0,1,0,1,1,1,1,1,0,0,0,0,1,0,1,1,1,0,0,0,0,0,0,0,0,0,0,0,0,1,1,0,1,1,1,1,1,1,0,1

Trocholites,1,0,0,0,1,0,0,1,0,0,0,1,0,0,0,0,0,0,1,1,0,0,0,0,0,0,0,0,0,0,0,0,0,0,0,1,0,0,0,0,1,0,0,0

Anaspyroceras,0,1,0,0,0,0,0,0,0,0,0,0,0,0,0,1,0,0,0,0,0,0,0,0,0,0,0,0,0,0,0,0,0,0,1,1,0,1,0,0,0,0,0,0,0

Beloitoceras,0,1,0,1,1,0,0,0,0,0,1,0,0,1,0,1,1,0,0,0,0,0,0,0,0,0,0,0,0,0,0,0,0,0,1,1,0,1,0,0,0,0,0,0,0

Discoceras,0,1,0,0,0,0,0,1,1,1,1,1,1,1,0,0,0,0,0,0,0,0,0,0,0,0,0,0,0,0,0,0,0,0,0,0,1,0,1,0,0,0,1

Actinoceras,0,0,0,0,1,1,0,0,0,0,0,0,0,0,0,0,1,1,0,0,0,1,0,0,0,0,0,0,0,0,0,0,0,0,0,1,1,0,1,1,0,0,0,0,0

Armenoceras,0,0,0,0,0,0,0,0,0,0,1,0,0,0,0,0,0,1,0,0,0,0,0,0,0,0,0,0,0,0,0,0,0,0,0,1,1,0,1,1,0,0,0,0,0

Billingsites,0,0,0,0,0,1,0,0,0,0,0,0,0,0,0,0,0,0,0,0,0,1,0,0,0,0,0,0,0,0,0,0,0,0,0,0,0,1,0,0,0,0,0,0

Charactoceras,0,0,0,0,1,1,0,0,0,0,0,0,0,0,0,0,1,1,0,0,0,0,0,0,0,0,0,0,0,0,0,0,0,0,0,1,1,0,1,1,0,0,0,0,0

Cycloceras,0,0,0,0,0,1,0,0,0,0,0,0,0,0,0,0,0,0,0,0,0,0,0,0,0,0,0,0,0,0,0,0,0,0,0,0,0,0,1,0,0,0,0,0,0

Cyrtogomphoceras,0,0,0,0,1,1,0,0,0,0,0,0,0,0,0,0,0,1,0,0,0,0,0,0,0,0,0,0,0,0,0,0,0,0,0,0,0,0,1,0,0,0,0,0,0

Deiroceras,0,0,0,0,0,0,0,0,0,0,0,0,0,0,0,0,0,1,0,0,0,0,0,0,0,0,0,0,0,0,0,0,0,0,0,1,1,0,1,1,0,0,0,0,0

Diestoceras,0,0,0,0,1,0,0,0,0,0,0,0,0,0,1,0,1,1,0,0,1,0,0,0,0,0,0,0,0,0,0,0,0,0,0,1,1,0,1,1,0,0,0,0,0

Lambeoceras,0,0,0,0,0,1,0,0,0,0,0,0,0,0,0,0,1,1,0,0,0,0,0,0,0,0,0,0,0,0,0,0,0,0,0,1,1,0,1,1,0,0,0,0,0

Narthecoceras,0,0,0,0,0,1,0,0,0,0,0,0,0,0,0,0,0,0,0,0,0,0,0,0,0,0,0,0,0,0,0,0,0,0,0,0,0,0,0,1,0,0,0,0,0

Ormoceras,0,0,0,0,1,1,0,1,0,0,0,0,0,0,0,0,1,1,0,0,0,0,0,0,0,0,0,0,0,0,0,0,0,0,0,1,1,0,1,1,0,0,0,0,0

Paractinoceras,0,0,0,0,0,1,0,0,0,0,0,0,0,0,0,0,0,0,0,0,0,1,0,0,0,0,0,0,0,0,0,0,0,0,0,0,0,0,0,1,0,0,0,0,0

Spyroceras,0,0,0,0,1,1,0,0,0,0,0,0,0,0,0,0,0,1,1,0,1,1,1,1,0,0,0,0,0,0,0,0,0,0,0,0,0,1,1,0,1,1,0,0,0,0,0

Westonoceras,0,0,0,0,1,1,0,0,0,0,0,1,0,0,0,0,0,1,1,0,0,1,0,0,0,0,0,0,0,0,0,0,0,0,0,0,1,1,0,1,1,0,0,0,0,0

Winnipegoceras,0,0,0,0,1,1,0,0,0,0,0,0,0,0,0,0,0,0,0,0,0,0,0,0,0,0,0,0,0,0,0,0,0,0,0,0,0,0,0,0,0,1,0,0,0,0,0

Endoceras,0,0,0,0,1,1,0,0,0,0,0,0,0,0,0,0,1,0,1,1,0,1,1,0,0,0,0,0,0,0,0,0,0,0,0,0,1,1,0,1,0,0,0,0,1,0,0

Ephippiorthoceras,0,0,0,0,1,1,0,0,0,0,0,0,0,0,0,1,0,1,1,0,0,0,0,0,0,0,0,0,0,0,0,0,0,0,0,1,1,0,1,0,0,0,0,0,0,0

Kochoceras,0,0,0,0,1,1,0,0,0,0,0,0,0,0,0,0,0,0,0,0,0,0,0,0,0,0,0,0,0,0,0,0,0,0,0,0,0,0,0,0,0,0,0,0,0,0,0

Neumatoceras,0,0,0,0,1,1,0,0,0,0,0,0,0,0,0,0,1,0,0,0,0,0,0,0,0,0,0,0,0,0,0,0,0,0,0,0,0,0,0,0,0,0,0,0,0,0,0

Cameroceras,0,0,0,0,0,1,0,0,0,0,0,0,0,0,0,0,0,1,0,1,0,0,0,0,0,0,0,0,0,0,0,0,0,0,0,1,1,0,1,0,0,0,0,0,0,0,0

Geisonoceras,0,0,0,0,1,1,0,0,0,0,0,0,0,0,1,0,1,0,0,0,0,0,0,0,0,0,0,0,0,1,1,0,1,0,0,0,0,0,0,0

Gonioceras,0,0,0,0,1,0,0,0,0,0,0,0,0,0,0,1,0,0,0,1,0,0,0,0,0,0,0,0,0,0,0,1,1,0,1,0,0,0,0,0,0,0

Probillingsites,0,0,0,0,1,0,0,0,0,0,0,0,1,0,1,1,0,0,0,0,0,0,0,0,0,0,0,0,0,0,0,1,1,0,1,0,0,0,0,0,0,0

Protokionoceras,0,0,0,0,1,0,0,0,0,0,0,0,1,0,0,0,0,0,0,0,0,0,0,0,0,0,0,0,0,0,0,0,0,0,0,0,0,0,0,0,0,0

Whiteavesites,0,0,0,0,1,0,0,0,0,0,0,0,0,0,0,1,0,0,0,0,0,0,0,0,0,0,0,0,0,0,0,1,1,0,1,0,0,0,0,0,0,0

Michelinoceras,0,0,0,0,0,1,1,1,1,1,1,1,0,0,0,1,0,0,1,0,0,0,0,0,0,0,0,0,0,0,0,1,1,0,1,0,1,1,1,1,0,1

Dideroceras,0,0,0,0,0,0,0,1,1,0,0,0,0,0,0,0,0,0,0,0,0,0,0,0,0,0,0,0,0,0,0,0,0,0,0,0,0,0,1,0,1,0,0,1

Lituites,0,0,0,0,0,0,0,0,0,1,1,1,1,0,0,0,0,0,0,0,0,0,0,0,0,0,0,0,0,0,0,0,0,0,0,0,0,0,1,1,1,0,0,1

Protocycloceras,0,0,0,0,0,0,0,0,0,1,0,0,0,0,0,0,0,0,0,0,0,0,0,0,0,0,0,0,0,0,0,0,0,0,0,0,0,0,1,0,0,0,0,0

Sinoceras,0,0,0,0,0,0,0,1,1,1,1,1,1,0,0,0,0,0,0,0,0,0,0,0,0,0,0,0,0,0,0,0,0,0,0,0,0,0,1,1,1,1,0,1

Trilacinoceras,0,0,0,0,0,0,0,0,0,1,0,0,1,0,0,0,0,0,0,0,0,0,0,0,0,0,0,0,0,0,0,0,0,0,0,0,0,0,1,0,0,0,0,1

Vaginoceras,0,0,0,0,0,0,0,1,0,1,0,0,0,0,0,0,0,0,0,0,0,0,0,0,0,0,0,0,0,0,0,0,0,0,0,0,0,0,1,0,1,1,0,1

Centrocyrtoceras,0,0,0,0,0,0,0,1,0,0,0,0,0,0,0,0,1,0,0,0,0,0,0,0,0,0,0,0,0,0,0,0,0,0,0,1,1,0,1,0,0,0,0,0,0,0

Richardsonoceras,0,0,0,0,0,0,0,1,1,0,1,1,1,0,0,0,1,0,0,0,0,0,0,0,0,0,0,0,0,0,0,0,0,0,0,1,1,0,1,0,0,1,0,0,0,1

Eosomichelinoceras,0,0,0,0,0,0,0,0,1,1,0,1,0,0,0,0,0,0,0,0,0,0,0,0,0,0,0,0,0,0,0,0,0,0,0,0,0,0,0,1,1,0,0,0

Ancistroceras,0,0,0,0,0,0,0,0,0,1,0,0,1,0,0,0,0,0,0,0,0,0,0,0,0,0,0,0,0,0,0,0,0,0,0,0,0,0,0,0,0,0,0,0

Cyclolituites,0,0,0,0,0,0,0,0,0,1,0,0,1,0,0,0,0,0,0,0,0,0,0,0,0,0,0,0,0,0,0,0,0,0,0,0,0,0,0,0,0,0,0,0

Ctenoceras,0,0,0,0,0,0,0,0,0,0,1,0,1,1,0,0,0,0,0,0,0,0,0,0,0,0,0,0,0,0,0,0,0,0,0,0,0,0,0,0,0,0,0,0

Cyrtorizoceras,0,0,0,0,0,0,0,0,0,0,0,1,0,0,0,1,0,1,0,0,0,0,0,0,0,0,0,0,0,0,0,1,1,0,1,0,0,0,0,0,0,0

Polygrammoceras,0,0,0,0,0,0,0,0,0,0,0,0,1,0,0,1,0,0,0,0,0,0,0,0,0,0,0,0,0,0,0,1,1,0,1,0,0,0,0,0,0,0

Allumettoceras,0,0,0,0,0,0,0,0,0,0,0,0,0,1,1,0,0,0,0,0,0,0,0,0,0,0,0,0,0,0,0,1,1,0,1,0,0,0,0,0,0,0

Antiplectoceras,0,0,0,0,0,0,0,0,0,0,0,0,0,0,1,0,0,0,0,0,0,0,0,0,0,0,0,0,0,0,0,1,1,0,1,0,0,0,0,0,0,0

Bodeiceras,0,0,0,0,0,0,0,0,0,0,0,0,0,0,1,0,0,0,0,0,0,0,0,0,0,0,0,0,0,0,0,1,1,0,1,0,0,0,0,0,0,0

Chidleyenoceras,0,0,0,0,0,0,0,0,0,0,0,0,0,0,1,0,0,0,0,0,0,0,0,0,0,0,0,0,0,0,0,1,1,0,1,0,0,0,0,0,0,0

Cyrtocerina,0,0,0,0,0,0,0,0,0,0,0,0,0,0,1,0,0,0,0,0,0,0,0,0,0,0,0,0,0,0,0,1,1,0,1,0,0,0,0,0,0,0

Deckeroceras,0,0,0,0,0,0,0,0,0,0,0,0,0,0,1,0,0,0,0,0,0,0,0,0,0,0,0,0,0,0,0,1,1,0,1,0,0,0,0,0,0,0

Fayettoceras,0,0,0,0,0,0,0,0,0,0,0,0,0,0,1,0,0,0,0,0,0,0,0,0,0,0,0,0,0,0,0,1,1,0,1,0,0,0,0,0,0,0

Hebetoceras,0,0,0,0,0,0,0,0,0,0,0,0,0,0,0,1,0,0,0,0,0,0,0,0,0,0,0,0,0,0,0,1,1,0,1,0,0,0,0,0,0,0

Isorthoceras,0,0,0,0,0,0,0,0,0,0,0,0,0,0,0,1,0,0,0,0,0,0,0,0,0,0,0,0,0,0,0,1,1,0,1,0,0,0,0,0,0,0

Kentlandoceras,0,0,0,0,0,0,0,0,0,0,0,0,0,0,0,1,0,0,0,0,0,0,0,0,0,0,0,0,0,0,0,1,1,0,1,0,0,0,0,0,0,0

Loganoceras,0,0,0,0,0,0,0,0,0,0,0,0,0,0,0,1,0,0,0,0,0,0,0,0,0,0,0,0,0,0,0,1,1,0,1,0,0,0,0,0,0,0

Manitoulinoceras,0,0,0,0,0,0,0,0,0,0,0,0,0,0,0,1,0,0,0,0,0,0,0,0,0,0,0,0,0,0,0,1,1,0,1,0,0,0,0,0,0,0

Metaspyroceras,0,0,0,0,0,0,0,0,0,0,0,0,0,0,0,1,0,0,0,0,0,0,0,0,0,0,0,0,0,0,0,1,1,0,1,0,0,0,0,0,0,0

Nanno,0,0,0,0,0,0,0,0,0,0,0,0,0,0,0,1,0,0,0,0,0,0,0,0,0,0,0,0,0,0,0,1,1,0,1,0,0,0,0,0,0,0

Oncoceras,0,0,0,0,0,0,0,0,0,0,0,0,0,0,0,1,0,0,0,0,0,0,0,0,0,0,0,0,0,0,0,1,1,0,1,0,0,0,0,0,0,0

Plectoceras,0,0,0,0,0,0,0,0,0,0,0,0,0,0,0,1,0,0,0,1,0,0,0,0,0,0,0,0,0,0,0,1,1,0,1,0,0,0,0,0,0,0

Reedsoceras,0,0,0,0,0,0,0,0,0,0,0,0,0,0,0,1,0,0,0,0,0,0,0,0,0,0,0,0,0,0,0,1,1,0,1,0,0,0,0,0,0,0

Schuchertoceras,0,0,0,0,0,0,0,0,0,0,0,0,0,0,0,1,0,0,0,0,0,0,0,0,0,0,0,0,0,0,0,1,1,0,1,0,0,0,0,0,0,0

Scofieldoceras,0,0,0,0,0,0,0,0,0,0,0,0,0,0,0,1,0,0,0,0,0,0,0,0,0,0,0,0,0,0,0,1,1,0,1,0,0,0,0,0,0,0

Staufferoceras,0,0,0,0,0,0,0,0,0,0,0,0,0,0,0,1,0,0,0,0,0,0,0,0,0,0,0,0,0,0,0,1,1,0,1,0,0,0,0,0,0,0

Teichertoceras,0,0,0,0,0,0,0,0,0,0,0,0,0,0,0,1,0,0,0,0,0,0,0,0,0,0,0,0,0,0,0,1,1,0,1,0,0,0,0,0,0,0

Tripteroceras,0,0,0,0,0,0,0,0,0,0,0,0,0,0,0,1,0,0,0,0,0,0,0,0,0,0,0,0,0,0,0,1,1,0,1,0,0,0,0,0,0,0

Ulrichoceras,0,0,0,0,0,0,0,0,0,0,0,0,0,0,0,1,0,0,0,0,0,0,0,0,0,0,0,0,0,0,0,1,1,0,1,0,0,0,0,0,0,0

Valcouroceras,0,0,0,0,0,0,0,0,0,0,0,0,0,0,0,1,0,0,0,0,0,0,0,0,0,0,0,0,0,0,0,1,1,0,1,0,0,0,0,0,0,0

Whitfieldoceras,0,0,0,0,0,0,0,0,0,0,0,0,0,0,0,1,0,0,0,0,0,0,0,0,0,0,0,0,0,0,0,1,1,0,1,0,0,0,0,0,0,0

Zittelloceras,0,0,0,0,0,0,0,0,0,0,0,0,0,0,0,1,0,0,0,0,0,0,0,0,0,0,0,0,0,0,0,1,1,0,1,0,0,0,0,0,0,0

Treptoceras,0,0,0,0,0,0,0,0,0,0,0,0,0,0,0,1,0,0,0,0,0,0,0,0,0,0,0,0,0,0,0,1,0,0,0,0,0,0,0,0,0,0

Ectomaria,1,0,0,0,0,0,0,0,0,0,0,0,0,0,0,1,0,0,0,1,0,0,0,0,0,0,0,0,0,0,0,1,1,0,0,0,0,0,0,0,0,0

Hormotoma,1,0,0,1,1,0,1,0,0,0,0,0,1,0,0,1,0,1,1,1,0,0,0,0,0,0,0,0,0,0,0,1,1,0,1,0,0,0,0,0,0,0

Lophospira,1,0,0,1,1,0,0,0,0,0,0,1,0,0,1,1,0,0,1,1,1,0,0,0,1,0,0,0,0,0,1,1,1,1,1,0,0,0,0,0,1,0

Loxoplocus,1,0,0,0,0,0,0,0,0,0,0,0,0,0,0,1,1,1,0,0,0,0,0,0,0,0,0,0,0,0,0,1,1,0,0,0,0,0,0,0,0,0

Maclurites,1,0,0,1,1,0,1,0,0,1,0,1,0,0,0,1,0,0,0,1,0,0,0,0,0,0,0,0,0,0,0,1,1,0,0,0,1,0,0,0,1,1

Raphistomina,1,0,0,0,1,0,0,0,0,0,0,0,0,0,0,1,0,0,0,1,0,0,0,0,0,0,0,0,0,0,0,1,0,1,1,0,0,0,0,0,0,0

Trochonema,1,0,0,1,1,0,0,0,0,0,0,0,0,0,0,1,1,0,0,1,1,0,0,0,0,1,0,0,0,0,0,0,1,1,0,0,0,0,0,0,0,0

Eotomaria,0,0,0,1,1,0,0,0,0,0,0,0,1,0,0,1,0,0,0,0,0,0,0,0,0,0,0,0,0,0,0,1,1,1,0,0,0,0,0,0,1,0

Holopea,0,0,0,1,1,0,0,0,0,0,0,0,1,0,0,1,0,1,0,0,0,0,0,0,1,1,0,0,1,0,0,1,1,0,1,0,0,0,0,0,1,0

Archinacella,0,0,0,0,1,0,0,0,0,0,0,0,0,0,0,1,0,0,1,1,0,0,0,0,1,0,0,0,1,0,1,1,1,1,0,0,0,0,0,0,0,0

Bucania,0,0,0,0,1,0,0,0,0,0,0,0,0,0,0,1,0,0,0,1,0,0,0,0,0,0,0,0,0,0,0,1,1,1,0,0,0,0,0,0,0,0

Carinaropsis,0,0,0,0,1,0,0,0,0,0,0,0,0,0,0,0,0,0,0,0,0,0,0,0,0,0,0,0,0,0,0,1,0,0,1,0,0,0,0,0,0,0

Clathrospira,0,0,0,0,1,0,0,0,0,0,0,0,0,0,0,1,0,0,1,0,0,0,0,0,0,0,0,0,0,1,1,1,1,1,0,0,0,0,0,0,0,0

Cyclonema,0,0,0,0,1,0,1,0,0,0,0,0,1,0,0,1,0,1,1,1,0,0,0,0,0,0,0,0,0,0,0,1,1,1,1,0,0,0,0,0,0,1,0

Fusispira,0,0,0,0,1,0,0,0,0,0,0,0,0,0,0,1,0,1,1,0,0,0,0,0,0,0,0,0,0,0,0,1,1,1,0,0,0,0,0,0,0,0

Helicotoma,0,0,0,0,1,0,0,0,0,0,0,0,0,0,0,1,1,0,0,0,1,0,0,0,0,0,0,0,0,0,0,0,1,1,0,0,0,0,0,0,0,0

Liospira,0,0,0,0,1,0,0,0,0,0,0,0,0,1,0,1,1,0,1,1,1,1,0,0,0,0,0,0,0,0,0,0,1,1,1,1,0,0,0,0,0,0,1,0

Omospira,0,0,0,0,1,0,0,0,0,0,0,0,0,0,0,1,0,0,0,1,0,0,0,0,0,0,0,0,0,0,0,1,1,0,0,0,0,0,0,0,0,0

Phragmolites,0,0,0,0,1,0,0,0,0,0,0,0,1,0,0,1,0,1,1,1,0,0,0,0,0,0,0,0,0,0,0,1,1,0,0,0,1,0,0,1,1,0

Pleurotomaria,0,0,0,0,1,0,0,0,0,0,0,0,0,0,0,0,0,0,0,0,0,0,0,0,0,0,0,0,1,0,0,0,0,0,0,0,0,0,0,0,0,0

Pterotheca,0,0,0,0,1,0,0,0,0,0,0,0,0,0,0,1,0,0,1,1,0,0,0,0,0,0,0,0,0,0,0,1,1,0,0,0,0,0,0,0,0,0

Salpingostoma,0,0,0,0,1,0,0,0,0,0,0,0,0,0,0,1,0,0,0,0,0,0,0,0,0,0,0,0,0,0,0,1,1,0,0,0,0,0,0,0,0,0

Sinuites,0,0,0,0,1,0,0,0,0,0,0,0,1,0,0,1,1,1,1,0,0,0,0,0,0,0,0,0,1,0,1,1,1,1,1,0,0,0,0,0,0,0

Subulites,0,0,0,0,1,0,0,0,0,0,0,0,0,0,0,1,0,1,0,1,0,0,0,0,0,0,0,0,0,0,0,1,1,0,0,0,0,0,0,0,0,0

Tetranota,0,0,0,0,1,0,0,0,0,0,0,0,0,0,0,1,0,0,1,1,0,0,0,0,0,0,0,0,0,0,0,1,1,0,0,0,0,0,0,0,0,0

Tropidodiscus,0,0,0,0,1,0,1,0,0,0,0,0,0,0,0,1,0,0,0,0,0,0,0,0,0,0,0,0,0,0,0,1,1,1,0,0,0,0,0,0,0,0

Ecculiomphalus,0,0,0,0,0,0,1,0,0,1,0,1,0,0,1,1,0,0,0,0,0,0,0,0,0,0,0,0,0,0,0,1,1,0,0,0,1,0,0,1,0,1

Euomphalus,0,0,0,0,0,0,1,0,0,0,0,0,0,0,0,0,0,0,0,0,0,0,0,0,0,0,0,0,0,0,0,1,0,0,0,0,0,0,0,0,0,0

Ruedemannia,0,0,0,0,0,0,0,0,0,0,0,0,0,0,0,0,0,0,0,0,0,0,0,0,0,0,0,0,0,0,0,0,0,0,0,0,0,0,0,0,0,1

Loxonema,0,0,0,0,0,0,0,0,0,1,0,0,1,0,0,0,0,0,0,0,0,0,0,0,0,0,0,0,0,0,0,0,0,0,0,0,0,0,0,0,0,0

Bucanella,0,0,0,0,0,0,0,0,0,0,0,0,0,1,0,0,0,0,0,0,0,0,0,1,0,0,0,0,1,0,0,1,0,0,0,0,0,0,0,0,0,0

Bucanopsis,0,0,0,0,0,0,0,0,0,0,0,0,0,0,0,0,0,0,0,1,0,0,0,0,0,1,0,0,0,0,0,1,0,1,1,0,0,0,0,0,0,0

Bellerophon,0,0,0,0,0,0,0,0,0,0,0,0,0,0,0,1,0,0,1,1,0,0,0,0,0,1,0,0,0,0,1,1,1,0,0,0,0,0,0,0,0,0

Cymbularia,0,0,0,0,0,0,0,0,0,0,0,0,1,0,0,0,0,0,0,0,0,0,0,0,0,0,0,0,0,0,0,1,0,0,0,0,0,0,0,0,0,0

Kokenospira,0,0,0,0,0,0,0,0,0,0,0,0,1,0,0,1,0,0,0,0,0,0,0,0,0,0,0,0,0,0,1,1,1,0,0,0,0,0,0,0,0

Lytospira,0,0,0,0,0,0,0,0,0,0,0,0,1,0,0,0,0,0,0,0,0,0,0,0,0,0,0,0,0,0,1,0,0,0,0,0,0,0,0,0,0

Murchisonia,0,0,0,0,0,0,0,0,0,0,0,0,1,0,0,0,0,0,0,0,0,0,0,0,0,0,0,0,0,1,0,1,1,0,0,0,0,0,0,0,0

Temnodiscus,0,0,0,0,0,0,0,0,0,0,0,0,0,0,0,0,0,0,0,0,0,0,0,0,0,0,0,0,0,0,1,1,0,0,0,0,0,0,0,0,0,0

Seelya,0,0,0,0,0,0,0,0,0,0,0,0,0,0,0,0,0,0,1,0,0,0,0,0,0,0,0,0,0,0,0,1,0,0,0,0,0,0,0,0,0,0

Cyrtospira,0,0,0,0,0,0,0,0,0,0,0,0,0,0,0,1,0,0,0,1,0,0,0,0,0,0,0,0,0,0,0,1,1,0,0,0,0,0,0,0,0,0

Gyronema,0,0,0,0,0,0,0,0,0,0,0,0,0,0,0,1,0,0,0,0,0,0,0,0,0,0,0,0,0,0,0,1,1,0,0,0,0,0,0,0,1,0

Horiostomella,0,0,0,0,0,0,0,0,0,0,0,0,0,0,0,1,0,0,0,0,0,0,0,0,0,0,0,0,0,0,0,1,1,0,0,0,0,0,0,0,0,0

Meekospira,0,0,0,0,0,0,0,0,0,0,0,0,0,0,0,1,0,0,0,0,0,0,0,0,0,0,0,0,0,0,0,1,1,0,0,0,0,0,0,0,0,0

Michelia,0,0,0,0,0,0,0,0,0,0,0,0,0,0,0,1,0,0,0,0,0,0,0,0,0,0,0,0,0,0,0,1,1,0,0,0,0,0,0,0,0,0

Ophileta,0,0,0,0,0,0,0,0,0,0,0,0,0,0,0,1,0,0,0,0,0,0,0,0,0,0,0,0,0,0,0,1,1,0,0,0,0,0,0,0,0,0

Ophiletina,0,0,0,0,0,0,0,0,0,0,0,0,0,0,0,1,0,0,0,1,0,0,0,0,0,0,0,0,0,0,0,1,1,0,0,0,0,0,0,0,0,0

Platyceras,0,0,0,0,0,0,0,0,0,0,0,0,0,0,0,1,0,0,0,0,0,0,0,0,0,0,0,0,0,0,0,1,1,0,0,0,0,0,0,0,0,0

Plethospira,0,0,0,0,0,0,0,0,0,0,0,0,0,0,0,1,0,0,0,0,0,0,0,0,0,0,0,0,0,0,0,1,1,0,0,0,0,0,0,0,0,0

Raphistoma,0,0,0,0,0,0,0,0,0,0,0,0,0,0,0,1,0,0,1,1,0,0,0,0,0,0,0,0,0,0,0,1,1,0,0,0,0,0,0,0,1,0

Strophostylus,0,0,0,0,0,0,0,0,0,0,0,0,0,0,0,1,0,0,0,0,0,0,0,0,0,0,0,0,0,0,0,1,1,0,0,0,0,0,0,0,0,0

Amphilichas,1,1,1,0,1,0,1,0,0,0,0,0,0,1,0,1,0,0,1,1,0,0,1,0,0,0,0,0,0,0,0,1,1,0,1,1,0,0,0,0,1,0

Ampyx,0,1,0,0,0,0,1,0,1,0,0,0,1,0,0,0,0,0,0,0,1,0,1,0,0,0,0,0,0,1,0,0,0,0,0,1,0,1,0,0,0,0

Calymenella,0,0,0,0,0,0,0,0,0,0,0,0,0,0,0,0,0,0,0,0,0,0,0,0,1,0,1,1,1,1,1,0,0,0,0,0,0,0,0,0,0,0,0,0,0

Encrinurus,0,1,0,1,1,0,0,0,0,0,0,0,1,0,0,0,0,1,0,0,0,0,1,0,0,0,0,0,0,0,0,0,0,0,0,0,0,0,0,0,0,0

Illaenus,1,0,0,1,1,0,1,1,1,1,1,1,0,0,0,1,1,0,0,0,0,0,1,0,0,1,0,0,0,1,1,1,1,0,1,0,1,1,1,1,0,1

Porterfieldia,0,0,0,0,0,0,0,0,0,0,0,0,0,0,0,0,0,0,0,0,0,0,0,0,1,1,0,0,0,0,0,0,0,0,0,0,0,0,0,0,0,0,0,0,0

Pseudobasilicus,1,1,0,0,0,0,1,0,0,0,0,0,0,0,0,0,0,0,0,0,0,0,1,0,0,0,0,0,0,0,0,0,0,0,0,0,0,0,1,0,0,0

Telephina,0,1,0,0,0,0,1,0,1,1,1,0,1,0,0,0,0,0,0,0,0,0,1,0,0,0,0,0,0,1,0,0,0,0,0,0,1,1,1,1,0,0

Toernquistia,1,0,0,0,0,0,1,0,0,0,0,0,0,0,1,0,1,0,0,0,0,0,1,0,0,0,0,0,0,0,0,0,0,0,0,0,0,0,0,0,0,0

Eobronteus,1,1,0,0,1,0,0,0,0,0,0,0,0,0,0,0,0,0,0,0,0,0,0,0,0,0,0,0,0,0,0,1,0,1,0,1,0,0,0,0,0,0,0

Eokosovopeltis,1,1,0,0,0,0,0,0,0,0,0,0,0,0,0,0,0,0,0,0,0,0,0,0,0,0,0,0,0,0,0,0,0,0,0,0,0,0,0,0,0,0,0,0

Geragnostus,1,0,0,0,0,0,1,0,1,1,0,1,0,0,0,0,0,0,0,0,0,0,0,0,0,0,0,0,0,0,0,0,0,0,0,0,0,0,1,0,1,1,0,1

Pliomerina,1,1,0,0,0,0,1,0,0,1,0,0,0,0,0,0,0,0,0,0,0,0,0,0,0,0,0,0,0,0,0,0,0,0,0,0,0,0,0,0,0,0,0,0

Remopleurides,1,1,1,1,0,1,1,1,1,1,1,1,1,0,0,0,0,0,0,0,1,0,0,0,0,0,0,0,0,1,1,0,0,0,0,1,1,1,1,1,1,1

Shumardia,1,1,0,0,0,0,1,0,1,0,0,0,0,0,0,0,0,0,0,0,0,0,0,0,0,0,0,0,0,0,0,0,0,0,0,0,0,0,0,0,1,0,0

Sphaerocoryphe,1,0,1,0,1,1,0,0,0,0,0,0,1,0,0,0,0,0,0,0,1,0,0,0,0,0,0,0,0,0,1,1,0,0,0,0,1,0,0,0,0,1,0

Bumastoides,0,1,1,0,1,0,0,0,0,0,0,0,0,0,0,1,0,0,0,0,0,0,0,0,0,0,0,0,0,0,0,0,1,1,0,1,1,0,0,0,0,1,0

Bumastus,0,1,0,1,1,0,1,0,0,0,1,0,0,1,0,1,1,1,0,0,1,0,0,0,0,0,0,0,0,0,0,0,1,1,0,0,0,0,0,1,0,0,0

Homotelus,0,1,0,0,1,0,0,0,0,0,0,0,0,0,0,0,1,0,0,0,1,0,0,0,0,0,0,0,0,0,0,0,1,0,0,0,0,0,0,0,0

Neseuretus,0,1,0,0,0,0,0,0,0,1,0,1,0,0,0,0,0,0,0,0,0,0,0,0,0,0,1,0,0,1,0,0,0,0,0,0,0,0,0,0,0

Nileus,0,1,0,0,0,0,1,0,1,1,0,1,1,0,0,0,0,0,0,0,0,0,0,0,0,0,0,0,0,0,1,0,0,0,0,0,0,1,1,1,1,0,1

Brongniartella,0,0,0,0,0,0,0,0,0,0,0,0,0,0,0,0,0,0,0,0,0,0,0,0,0,0,1,0,0,0,0,0,0,1,0,0,0,0,0,0,0,0,0

Acanthoparypha,0,0,1,0,0,0,0,0,0,0,0,0,0,0,0,1,0,0,0,0,0,0,0,0,0,0,0,0,0,0,0,1,1,0,0,1,0,0,0,0,0,0

Ampyxina,0,0,1,0,0,0,0,0,0,0,0,0,1,0,0,0,1,0,0,0,1,0,0,0,0,0,0,0,0,0,0,0,0,0,0,1,0,0,0,0,0

Anataphrus,0,0,1,0,0,0,0,0,0,0,0,0,0,0,0,0,1,0,0,0,0,0,0,0,0,0,0,0,0,0,0,0,0,1,0,0,1,0,0,0,0,0

Apianurus,0,0,1,0,0,0,0,0,0,0,0,0,1,0,0,0,0,0,0,0,0,0,0,0,0,0,0,0,0,0,0,0,0,0,1,0,0,0,0,1,0

Bathyurus,0,0,1,0,1,0,0,0,0,0,0,0,0,0,0,0,0,0,1,0,0,0,0,0,0,0,0,0,0,0,0,0,0,1,0,0,0,0,1,0

Borealaspis,0,0,1,0,0,0,0,0,0,0,0,0,0,0,0,0,0,0,0,0,0,0,0,0,0,0,0,0,0,0,0,0,0,0,1,0,0,0,0,0

Calyptaulax,0,0,1,1,1,0,0,0,0,0,0,0,1,0,0,0,1,0,0,0,0,0,0,0,0,0,0,0,0,0,1,0,1,0,1,1,0,0,0,0,1,0

Ceratocephala,0,0,1,0,0,0,0,0,0,0,0,0,0,0,0,0,0,0,1,0,0,0,0,0,0,0,0,0,0,0,0,0,0,0,0,1,0,0,0,0,1,0

Ceraurinella,0,0,1,0,0,0,0,0,0,0,0,0,0,0,0,0,1,0,0,0,0,0,0,0,0,0,0,0,0,0,0,0,1,1,0,1,1,0,0,0,0,0

Ceraurus,0,0,1,1,1,0,0,0,0,0,0,0,0,0,0,1,0,1,1,1,1,0,0,0,0,0,0,0,0,0,0,1,1,0,1,1,0,0,0,0,1,0

Chasmops,0,0,1,0,1,0,0,0,0,0,0,0,0,0,0,0,0,0,0,0,0,0,0,0,0,0,0,0,0,0,0,0,1,1,0,0,0,0,1,0,0,0,0,0

Cnemidopyge,0,0,1,0,0,0,0,0,0,0,0,0,0,0,0,0,0,0,0,0,0,0,0,0,0,0,0,0,0,0,0,0,0,0,1,0,0,0,0,0,0,0,0

Cryptolithoides,0,0,1,0,0,0,0,0,0,0,0,0,0,0,0,0,1,0,0,0,0,0,0,0,0,0,0,0,0,0,0,0,0,0,0,0,0,0,0,0,0

Cryptolithus,0,0,1,0,1,1,0,0,0,0,0,0,0,0,0,0,1,1,0,1,1,0,0,0,1,1,0,0,0,0,0,0,0,0,1,0,0,0,0,0,0

Cybeloides,0,0,1,0,0,0,0,0,0,0,0,0,0,0,0,0,0,0,0,0,0,0,0,0,0,0,0,0,0,0,0,0,0,0,1,0,1,1,0,0,0,0,1,0

Dimeropyge,0,0,1,0,0,0,0,0,0,0,0,0,0,0,0,0,0,0,0,0,0,0,0,0,0,0,0,0,0,0,0,0,0,0,1,0,0,0,0,0,0

Dolichoharpes,0,0,1,0,0,0,0,0,0,0,0,0,0,0,0,1,0,0,0,0,0,0,0,0,0,0,0,0,0,0,0,1,0,1,1,0,0,0,0,1,0

Encrinuroides,0,0,1,0,1,0,0,0,1,0,1,0,0,0,0,1,0,0,0,0,0,0,0,0,0,0,0,0,0,0,0,1,1,0,1,1,0,0,0,0,1,1

Hemiarges,0,0,1,0,1,0,0,0,0,0,0,0,0,0,0,0,1,0,0,0,0,0,0,0,0,0,0,0,0,0,0,1,0,1,1,0,0,0,0,0,0

Holia,0,0,1,0,0,0,0,0,0,0,0,0,0,0,0,0,0,0,0,0,0,0,0,0,0,0,0,0,0,0,0,0,0,0,0,1,0,0,0,0,0,0

Hypodicranotus,0,0,1,0,0,0,0,0,0,0,0,0,0,0,0,0,0,1,0,0,0,0,0,0,0,0,0,0,0,0,0,0,0,0,0,1,0,1,1,0,0,0,0,0,0

Isotelus,0,0,1,1,1,1,0,0,0,0,0,1,0,1,0,1,1,1,1,1,1,0,0,0,0,0,0,0,0,0,0,0,1,1,0,1,1,0,0,0,0,0,0

Lonchodomas,0,0,1,0,0,1,1,0,1,1,1,1,1,0,0,0,0,0,0,0,1,0,0,0,1,0,0,0,0,1,1,0,0,0,0,0,1,1,0,1,1,0

Nahannia,0,0,1,0,0,0,0,0,0,0,0,0,0,0,0,0,0,0,0,0,0,0,0,0,0,0,0,0,0,0,0,0,0,0,0,0,0,1,0,0,0,0,0,0

Nanillaenus,0,0,1,0,0,0,0,0,0,0,0,0,0,0,0,0,0,0,0,0,0,0,0,0,0,0,0,0,0,0,0,0,0,0,0,0,0,1,0,0,0,0,1,0

Pandaspinapyga,0,0,1,0,0,0,0,0,0,0,0,0,0,0,0,0,0,0,0,0,0,0,0,0,0,0,0,0,0,0,0,0,0,0,0,0,0,0,0,0,0,1,0

Robergia,0,0,1,0,0,0,0,0,0,0,0,0,1,0,0,0,1,0,0,0,1,0,0,0,0,0,0,0,0,1,0,0,0,0,0,0,0,0,0,0,0,0,0

Sphaerexochus,0,0,1,0,0,0,1,0,1,1,0,0,0,0,0,0,0,0,0,0,1,0,0,0,0,0,0,0,0,0,0,0,0,0,0,1,0,0,0,0,0,1

Triarthrus,0,0,1,0,1,1,0,0,0,0,0,0,0,0,0,0,0,1,1,0,0,1,0,0,0,0,0,0,0,1,1,0,0,0,0,1,0,0,0,0,0,0

Whittakerites,0,0,1,0,0,0,0,0,0,0,0,0,0,0,0,0,0,0,0,0,0,0,0,0,0,0,0,0,0,0,0,0,0,0,0,0,0,1,0,0,0,0,0,0

Ceraurinus,0,0,0,1,1,0,1,0,0,0,0,0,0,1,1,1,0,0,0,1,0,0,0,0,0,0,0,0,0,0,0,1,1,0,0,1,0,0,0,0,0,0

Cyphoproetus,0,0,0,0,0,0,0,0,0,0,0,0,0,0,0,0,0,0,0,0,0,0,0,0,0,0,0,0,0,0,0,0,0,0,0,1,0,0,0,0,1,0,0,0,0,0,0

Eomonorachus,0,0,0,1,0,0,0,0,0,0,0,0,0,0,0,0,1,0,0,0,0,0,0,0,0,0,0,0,0,0,0,0,0,0,0,1,1,0,1,1,0,0,0,0,1,0

Lichida,0,0,0,0,0,0,0,0,0,0,0,0,0,0,0,0,0,0,0,0,0,0,0,0,0,0,0,0,0,0,0,0,0,0,0,1,0,0,0,0,0,1,0,0,0,0,0,0

Otarion,0,0,0,0,0,1,0,0,1,0,0,0,0,0,0,0,0,0,0,0,0,0,0,0,0,0,0,0,0,0,0,0,0,0,0,1,0,0,0,0,1,0,1,0,0,1,1

Pseudogygites,0,0,0,0,1,0,0,0,0,0,0,0,0,0,0,0,0,0,0,0,0,0,0,0,0,0,0,0,0,0,0,0,0,0,0,0,0,1,0,0,0,0,0,0

Calymene,0,0,0,1,0,1,0,0,0,0,0,0,0,0,0,1,0,0,0,1,1,0,0,0,0,1,0,0,0,0,0,1,1,0,0,0,0,0,0,0,0,0

Pterygometopus,0,0,0,1,1,0,0,0,0,0,0,0,0,0,0,0,0,0,0,1,0,0,0,0,0,0,0,0,0,0,0,0,0,0,0,0,0,0,0,0,0,0,0

Achatella,0,0,0,0,1,0,0,0,0,0,0,0,0,0,0,0,0,0,0,1,0,0,0,0,0,0,0,0,0,0,0,0,0,0,0,0,0,0,0,0,0,0,0

Calliops,0,0,0,0,1,0,0,0,0,0,0,0,0,0,0,0,0,0,1,0,0,1,0,0,0,0,0,0,0,0,0,0,0,0,0,0,0,0,0,0,0,0,0

Flexicalymene,0,0,0,0,1,0,0,0,0,0,0,0,1,0,0,1,1,1,1,1,0,1,0,0,1,0,1,0,0,1,1,1,1,1,0,0,0,0,0,0,0,0

Proetus,0,0,0,0,1,0,0,0,0,1,0,0,0,1,0,0,0,0,0,1,1,0,0,0,0,0,0,0,0,0,0,1,0,0,0,0,0,0,0,0,0,0,0

Raymondites,0,0,0,0,1,0,0,0,0,0,0,0,0,0,0,1,0,0,0,0,0,0,0,0,0,0,0,0,0,0,0,1,1,0,1,0,0,0,0,0,0,0

Dionide,0,0,0,0,0,1,0,0,0,1,0,1,1,0,0,0,0,0,0,0,1,0,0,0,1,0,0,0,0,0,0,0,0,0,0,0,0,1,1,1,1,0,0

Gravicalymene,0,0,0,0,0,1,0,0,0,0,0,0,1,0,0,0,0,0,0,0,0,0,0,0,0,0,0,0,0,0,1,0,0,0,0,0,0,0,0,0,0

Primaspis,0,0,0,0,0,1,0,0,0,0,0,0,1,0,0,0,1,1,0,0,0,0,0,0,1,0,0,0,0,0,1,0,0,0,0,0,0,0,0,0,0

Tretaspis,0,0,0,0,0,1,0,0,0,0,0,0,1,0,0,0,0,0,0,0,1,0,0,0,0,0,0,0,0,1,1,0,0,0,0,0,0,0,0,0,0

Atractopyge,0,0,0,0,0,0,0,1,0,1,0,0,0,1,0,0,0,0,0,0,0,0,0,0,0,0,0,0,0,0,0,0,0,0,0,0,0,0,1,1,0,0,0,0

Basilicus,0,0,0,0,0,0,0,1,0,0,0,0,0,0,0,0,0,0,0,0,0,0,0,0,0,0,0,0,0,0,0,0,0,0,0,0,0,0,1,0,0,0,0,0

Birmanites,0,0,0,0,0,0,0,1,0,1,1,1,1,0,0,0,0,0,0,0,0,0,0,0,0,0,0,0,0,0,0,0,0,0,0,0,0,0,1,0,0,1,0,0

Calymenesum,0,0,0,0,0,0,0,0,1,1,1,0,0,0,0,0,0,0,0,0,0,0,0,0,0,0,0,0,0,0,0,0,0,0,0,0,0,0,1,1,1,1,0,0

Cheirurus,0,0,0,0,0,0,0,1,0,0,0,0,0,0,0,0,0,0,0,0,0,0,0,0,0,0,0,0,0,0,0,0,0,0,0,0,0,0,1,0,0,0,0,0

Corrugatagnostus,0,0,0,0,0,0,0,0,0,0,1,1,0,0,0,0,0,0,0,0,0,0,0,0,0,0,0,0,0,0,0,0,0,0,0,0,0,0,1,1,1,1,0,0

Cyclopyge,0,0,0,0,0,0,0,1,0,1,1,1,1,0,0,0,0,0,0,0,0,0,0,0,0,1,0,0,0,0,0,0,0,0,0,0,0,0,1,1,1,1,0,1

Dalmanitina,0,0,0,0,0,0,0,0,1,0,0,0,0,0,0,0,0,0,0,0,0,0,0,0,0,1,1,1,1,1,0,0,0,0,0,0,0,1,0,0,1,0,1

Encrinurella,0,0,0,0,0,0,0,0,0,0,0,0,0,0,0,0,0,0,0,0,0,0,0,0,0,0,0,0,0,0,0,0,0,0,0,0,0,0,1,1,0,0,0,0

Hammatocnemis,0,0,0,0,0,0,0,1,1,1,1,1,1,0,0,0,0,0,0,0,0,0,0,0,0,0,0,0,0,0,0,0,0,0,0,0,0,0,1,1,1,1,0,1

Nankinolithus,0,0,0,0,0,0,0,1,1,1,1,1,1,0,0,0,0,0,0,0,0,0,0,0,0,0,0,0,0,0,0,0,0,0,0,0,0,0,1,1,1,1,0,1

Paraphillipsinella,0,0,0,0,0,0,0,0,0,1,1,0,0,0,0,0,0,0,0,0,0,0,0,0,0,0,0,0,0,0,0,0,0,0,0,0,0,0,1,1,0,1,0,0

Sphaeragnostus,0,0,0,0,0,0,0,0,0,0,0,0,0,0,0,0,0,0,0,0,0,0,0,0,0,0,0,0,0,0,0,0,0,0,0,0,0,0,1,1,0,1,0,0

Trinodus,0,0,0,0,0,0,0,1,0,1,1,1,1,1,1,0,0,0,0,0,0,0,0,0,0,0,1,0,0,0,0,1,0,0,0,0,0,0,1,1,1,1,0,0

Asaphus,0,0,0,0,0,0,1,0,0,0,0,1,1,0,0,0,0,0,0,0,0,0,0,0,0,0,0,0,0,0,1,0,0,0,0,0,0,0,0,0,0,0,0,0

Basiliella,0,0,0,0,0,0,0,1,0,0,1,0,0,0,0,0,0,1,0,0,0,0,0,0,0,0,0,0,0,0,0,0,0,0,0,0,1,1,0,1,0,0,0,1,1,0,0

Bronteopsis,0,0,0,0,0,0,0,1,0,0,1,0,0,1,0,0,0,0,0,0,0,0,1,0,0,0,0,0,0,0,0,0,1,0,0,0,0,0,0,0,0,0,0,0

Isoteloides,0,0,0,0,0,0,0,1,0,0,1,0,0,0,0,0,0,0,0,0,0,0,0,0,0,0,0,0,0,0,0,0,0,0,0,0,0,0,0,0,0,0,0,0

Oedicybele,0,0,0,0,0,0,0,1,0,0,0,0,0,0,0,0,0,0,0,0,0,0,0,0,0,0,0,0,0,0,0,0,0,0,1,0,0,0,0,0,0,0,0,0

Paraceraurus,0,0,0,0,0,0,0,1,0,1,1,1,0,0,0,0,0,0,0,0,0,0,0,0,0,0,0,0,0,0,0,0,0,0,1,0,0,0,0,0,0,0,0,0

Pliomera,0,0,0,0,0,0,0,1,0,0,1,0,0,0,0,0,0,0,0,0,0,0,0,0,0,0,0,0,0,0,0,0,0,0,0,0,0,0,0,0,0,0,0,0

Pliomerops,0,0,0,0,0,0,0,1,0,0,0,0,0,0,0,0,0,0,0,0,0,0,0,0,0,0,0,0,0,0,0,0,0,0,0,0,0,0,0,0,0,0,1,0

Scutellum,0,0,0,0,0,0,0,1,0,0,0,0,0,1,0,0,0,0,0,0,0,0,0,0,0,0,0,0,0,0,0,0,0,0,0,0,0,0,0,0,0,0,1,0,0

Staurocephalus,0,0,0,0,0,0,1,0,1,0,0,0,1,0,0,0,0,0,0,0,0,0,0,0,0,0,0,0,0,0,0,0,0,0,0,0,0,0,0,0,1

Symphysurus,0,0,0,0,0,0,1,0,0,1,0,0,0,0,0,0,0,0,0,0,0,0,0,0,0,0,0,0,0,0,0,0,0,0,0,0,0,0,0,0,1

Amphitryon,0,0,0,0,0,0,0,0,1,0,0,0,0,0,0,0,0,0,0,0,0,0,0,0,0,0,0,0,0,0,0,0,0,0,0,0,0,1,0,1,0,1

Geragnostella,0,0,0,0,0,0,0,0,1,0,0,0,0,0,0,0,0,0,0,0,0,0,0,0,1,0,0,0,0,0,0,0,0,0,0,0,0,0,0,0,1

Eccoptochile,0,0,0,0,0,0,0,0,0,0,0,0,0,0,0,0,0,0,0,0,0,0,0,0,0,1,0,1,1,1,0,0,0,0,0,0,0,0,0,0,1

Ampyxinella,0,0,0,0,0,0,0,0,0,0,0,0,0,0,0,0,0,0,0,0,0,0,0,0,0,0,0,0,0,0,0,0,0,0,0,0,0,1,0,1,0,0

Raphiophorus,0,0,0,0,0,0,0,0,0,0,0,0,0,0,0,0,0,0,0,0,0,0,0,0,0,0,0,0,0,0,0,1,0,0,0,0,0,0,1,0,0,0,0

Phillipsinella,0,0,0,0,0,0,0,0,0,1,0,0,1,0,0,0,0,0,0,0,0,0,0,0,0,0,0,0,0,0,1,1,0,0,0,0,0,1,0,0,0,0

Ampyxella,0,0,0,0,0,0,0,0,0,1,0,1,1,0,0,0,0,0,0,0,0,0,0,0,0,0,0,0,0,0,1,0,0,0,0,0,0,0,0,0,0

Cekovia,0,0,0,0,0,0,0,0,0,1,0,0,0,0,0,0,0,0,0,0,0,0,0,0,1,0,0,0,1,0,0,0,0,0,0,0,0,0,0,0,0

Miaopopsis,0,0,0,0,0,0,0,0,0,1,1,0,0,0,0,0,0,0,0,0,0,0,0,0,0,0,0,0,0,0,0,0,0,0,0,0,0,0,0,0,0

Phorocephala,0,0,0,0,0,0,0,0,0,1,0,0,1,0,0,0,0,0,0,0,0,0,0,0,0,0,0,0,0,0,0,0,0,0,0,0,0,0,0,0,0

Pseudoasaphus,0,0,0,0,0,0,0,0,0,1,0,0,0,0,0,0,0,0,0,0,0,0,0,0,0,0,0,0,0,0,1,0,0,0,0,0,0,0,0,0,0

Actinopeltis,0,0,0,0,0,0,0,0,0,0,0,1,0,0,0,0,0,0,0,0,0,0,0,0,1,0,1,1,1,0,0,0,0,0,0,0,0,0,0,0,0

Pharostoma,0,0,0,0,0,0,0,0,0,0,0,0,1,0,0,0,0,0,0,0,0,0,0,0,1,0,0,0,0,1,0,0,0,0,0,0,0,0,1,0,0,0

Zbirovia,0,0,0,0,0,0,0,0,0,0,0,0,0,0,0,0,0,0,0,0,0,0,0,0,0,1,0,0,0,0,0,0,0,0,0,0,0,1,1,0,0

Stenopareia,0,0,0,0,0,0,0,0,0,0,0,0,0,1,1,0,0,0,0,0,0,0,0,0,0,1,0,0,0,0,1,0,0,0,0,0,0,0,0,1,0,0

Colpocoryphe,0,0,0,0,0,0,0,0,0,0,0,0,0,0,0,0,0,0,0,0,0,0,0,0,0,0,0,0,0,0,1,1,1,1,1,0,0,0,0,0,0,0,0,0,0

Deanaspis,0,0,0,0,0,0,0,0,0,0,0,0,0,0,0,0,0,0,0,0,0,0,0,0,0,0,0,0,0,0,1,0,0,1,0,0,0,0,0,0,0,0,0,0,0

Eudolatites,0,0,0,0,0,0,0,0,0,0,0,0,0,0,0,0,0,0,0,0,0,0,0,0,0,0,0,0,0,0,1,1,1,1,1,0,0,0,0,0,0,0,0,0,0

Kloucekia,0,0,0,0,0,0,0,0,0,0,0,0,0,0,0,0,0,0,0,0,0,0,0,0,0,0,0,0,0,0,1,1,1,0,1,0,1,0,0,0,0,0,0,0,0

Marrolithus,0,0,0,0,0,0,0,0,0,0,0,0,0,0,0,0,0,0,0,0,0,0,0,0,0,0,0,0,0,0,1,0,0,1,1,0,0,0,0,0,0,0,0,0,0

Nobiliasaphus,0,0,0,0,0,0,0,0,0,0,0,0,0,0,0,0,0,0,0,0,0,0,0,0,0,0,0,0,0,0,1,0,0,0,1,0,0,0,0,0,0,0,0,0,0

Onnia,0,0,0,0,0,0,0,0,0,0,0,0,0,0,0,0,0,0,0,0,0,0,0,0,0,1,0,0,1,1,0,1,1,0,1,0,0,0,0,0,0,0,0,0,0

Phacopidina,0,0,0,0,0,0,0,0,0,0,0,0,0,0,0,0,0,0,0,0,0,0,0,0,0,1,0,0,1,1,0,0,0,0,0,0,0,0,0,0,0

Placoparia,0,0,0,0,0,0,0,0,0,0,0,0,0,0,0,0,0,0,0,0,0,0,0,0,0,1,1,0,0,1,0,0,0,0,0,0,0,0,0,0,0

Plaesiacomia,0,0,0,0,0,0,0,0,0,0,0,0,0,0,0,0,0,0,0,0,0,0,0,0,0,1,1,0,1,1,0,0,0,0,0,0,0,0,0,0,0

Prionocheilus,0,0,0,0,0,0,0,0,0,0,0,0,1,0,0,0,0,0,0,0,0,0,0,0,0,1,0,1,1,1,0,0,0,0,0,0,0,0,0,0,0,0,0

Selenopeltis,0,0,0,0,0,0,0,0,0,0,0,0,0,0,0,0,0,0,0,0,0,0,0,0,0,0,0,1,0,1,1,1,0,0,0,0,0,0,0,0,0,0,0,0

Zeliszkella,0,0,0,0,0,0,0,0,0,0,0,0,0,0,0,0,0,0,0,0,0,0,0,0,0,0,0,1,0,0,0,1,0,0,0,0,0,0,0,0,0,0,0,0

Eodalmanitina,0,0,0,0,0,0,0,0,0,0,0,0,0,0,0,0,0,0,0,0,0,0,0,0,0,0,0,1,0,0,1,0,0,0,0,0,0,0,0,0,0,0,0

Ogmasaphus,0,0,0,0,0,0,0,0,0,0,0,0,0,0,0,0,0,0,0,0,0,0,0,0,0,0,0,1,0,0,1,0,0,0,0,0,0,0,0,0,0,0,0

Broeggerolithus,0,0,0,0,0,0,0,0,0,0,0,0,1,0,0,0,0,0,0,0,0,0,0,0,0,0,0,1,0,0,0,0,0,0,0,0,0,0,0,0,0

Deacybele,0,0,0,0,0,0,0,0,0,0,0,0,1,0,0,0,0,0,0,0,0,0,0,0,0,0,0,1,0,0,0,0,0,0,0,0,0,0,0,0,0

Decoroproetus,0,0,0,0,0,0,0,0,0,0,0,0,1,0,0,0,0,0,0,0,0,0,0,0,0,0,0,1,0,0,0,0,0,0,0,0,0,0,0,0,0

Diacanthaspis,0,0,0,0,0,0,0,0,0,0,0,0,1,0,0,0,0,0,0,0,0,0,0,0,0,0,0,1,0,0,0,0,0,0,0,0,0,0,0,0,0

Hemisphaerocoryphe,0,0,0,0,0,0,0,0,0,0,0,0,1,0,0,0,0,0,0,0,0,0,0,0,0,0,0,1,0,0,0,0,0,0,0,0,0,0,0,0,0

Miraspis,0,0,0,0,0,0,0,0,0,0,0,0,1,0,0,0,0,0,0,0,0,0,0,0,0,0,0,1,0,0,0,0,0,0,0,0,0,0,0,0,0

Nieszkowskia,0,0,0,0,0,0,0,0,0,0,0,0,1,0,0,0,0,0,0,0,0,0,0,0,0,0,0,1,0,0,0,0,0,0,0,0,0,0,0,0,0

Platylichas,0,0,0,0,0,0,0,0,0,0,0,0,1,0,0,0,0,0,0,0,0,0,0,0,0,0,0,1,1,0,0,0,0,0,0,0,0,0,0,0,0

Pseudosphaerexochus,0,0,0,0,0,0,0,0,0,0,0,0,1,0,0,0,0,0,0,0,0,0,0,0,0,0,0,1,1,0,0,0,0,0,0,0,0,0,0,0,0

Remopleurella,0,0,0,0,0,0,0,0,0,0,0,0,1,0,0,0,0,0,0,0,0,0,0,0,0,0,0,1,0,0,0,0,0,0,0,0,0,0,0,0,0

Stygina,0,0,0,0,0,0,0,0,0,0,0,0,1,0,0,0,0,0,0,0,0,0,0,0,0,0,0,1,0,0,0,0,0,0,0,0,0,0,0,0,0

Crozonaspis,0,0,0,0,0,0,0,0,0,0,0,0,0,0,0,0,0,0,0,0,0,0,0,0,0,0,0,1,1,0,0,0,0,0,0,0,0,0,0,0,0

Dysplanus,0,0,0,0,0,0,0,0,0,0,0,0,0,0,0,0,0,0,0,0,0,0,0,0,0,0,0,1,1,0,0,0,0,0,0,0,0,0,0,0,0

Eoharpes,0,0,0,0,0,0,0,0,0,0,0,0,0,0,0,0,0,0,0,0,0,0,0,1,0,0,0,0,0,0,1,0,0,0,0,0,0,0,0,0,0,0,0

Scotiella,0,0,0,0,0,0,0,0,0,0,0,0,0,0,0,0,0,0,0,0,0,0,0,0,0,0,0,1,1,0,0,0,0,0,0,0,0,0,0,0,0

Gabriceraurus,0,0,0,0,0,0,0,0,0,0,0,0,0,0,0,1,0,0,0,0,0,0,0,0,0,0,0,0,0,1,1,0,1,0,0,0,0,0,0,0,0

Sceptaspis,0,0,0,0,0,0,0,0,0,0,0,0,0,0,0,1,0,0,0,0,0,0,0,0,0,0,0,0,0,1,1,0,1,0,0,0,0,0,0,0,0

Thaleops,0,0,0,0,0,0,0,0,0,0,0,0,0,0,0,1,0,0,0,0,0,0,0,0,0,0,0,0,0,1,1,0,1,0,0,0,0,0,0,0,0

Odontopleura,0,0,0,0,0,0,0,0,0,0,0,0,0,0,0,0,0,0,0,0,1,0,1,0,0,0,0,0,0,0,0,0,0,0,0,0,0,0,0,0,0,0,0

Appendix C

Paleobiology database collections used by locality

Argentina: 8874, 8889, 9033, 9080, 13513, 8708, 8708, 8776, 8887, 8889, 9033, 9080

Australia – New South Wales: 2645, 2646, 2647, 2648, 2655, 2661, 2698, 2699, 2700, 2701. 2702, 2703, 2704, 2705, 2706, 2707, 2708, 2709, 2714, 2715, 2716, 2717, 2718, 2719, 2720, 2721, 2722, 2723, 2724, 2725, 2726, 2727, 2728, 2729, 2730, 2731, 2732, 2745, 2746, 2747, 2749, 2750, 2751, 2752, 2753, 2754, 2755

Australia – Tasmania: 2685, 2686, 2687, 2691, 2692, 2693, 2694, 2695, 24252, 26238

Bolivia: 8784. 8847, 8848, 8849, 8851, 8852, 8853, 8855, 8856, 9102, 8784, 8848, 8854, 9102

Canada – District of Mackenzie: 25172, 25173, 25174, 25175, 25176, 25177, 25178, 25179, 25303, 25304, 25305, 25308, 25309, 25310, 25311, 25312, 25313, 25314, 25315, 25316, 25317, 25318,25319, 25320, 25321, 25322, 25323, 25324, 25331, 25333, 25333, 25341, 25344, 25345, 25513, 25533, 25552, 25925, 25929, 25930, 25931, 26060

Canada – Northwest Territories: 312. 313, 314, 402, 24628, 24628, 24631, 24634, 24635, 24636, 24637, 26090, 26340, 26341, 26342

Canada – Nunavut: 24115, 24116

Canada – Ontario: 336, 401, 13652, 13654, 13655, 13656, 13657, 13658, 14120, 23009, 23010, 26172, 26174, 26175, 26188, 26191, 26192, 26263, 26267, 26268, 26269, 26270, 26271, 26272, 26273, 26274, 26275, 26276, 26277, 26290, 26293, 26294, 26295, 26296, 26297, 26298, 26299, 26302, 26303

Canada – Quebec: 318, 440, 13128, 13129, 25124, 27235, 28189

China – Anhui: 7817, 7828, 7835, 7836, 7837, 7848, 7849, 7850, 7858, 7859,

China – Gansu: 8545, 8547, 8548, 8550, 8551, 8552, 8561, 8565, 20762, 20763, 23585, 23590, 23592

China – Guizhou: 4745, 4751, 5137, 5138, 5139, 5140, 7335, 7336, 7337, 7338, 7383, 7637

China – Hubei: 4690, 4691, 4708, 7714, 7715, 7722, 7723

China – Hunan: 7688, 7689, 7697, 7698, 7714, 7715

China – Jaingsu: 7872, 7873, 7929, 7930, 7931, 7935, 7936, 7937, 7942, 7943, 7947

China – Shaanxi: 7882, 7883, 7884, 7885, 7917, 7918, 8007, 8009, 8533, 8534, 8539, 8540

China – Sichuan: 5338, 5339, 5340, 7254, 7255, 7256, 7644, 7645, 7655, 7656, 7667, 7668, 7675

China – Xinjiang: 8579, 20785, 20789, 20792, 20796, 20797, 20801, 20802

China – Yunan: 5424, 5425, 7262, 7334, 7743, 7744

China – Zhejiang: 7768, 7769, 7779, 7781, 7794, 7795, 7804, 7809, 7810

Czech Republic: 3861, 3862, 3863, 3864, 3865, 3866, 3871, 3872, 3873, 3874

France: 20846, 20847, 20848, 20849, 20850, 20851, 20857, 20869, 20871, 20882, 20922, 21005, 21006, 21007, 21014, 21087

Morocco: 20961, 20964, 20969, 20970, 20988, 21000, 21001

Norway: 2761, 2762, 2763, 2764, 2945, 2947, 2948, 3251, 3252, 3253, 3254, 3255

Portugal: 20874, 20876, 20931, 20935, 20954

Russian Federation: 9298, 9302, 9305, 9307, 9309, 9310, 9311, 24016

Spain: 20835, 20885, 20887, 20892, 20920, 20921, 20928, 21020, 21021, 21047, 21049, 21055, 21056, 21089, 21090, 21095, 21099, 21100, 21101

Sweden: 380, 2765, 2766, 2767, 2769, 2770, 2771, 2772, 2941

United Kingdom: 348, 434, 3301, 3302, 3303, 3304, 3305, 3362, 3363, 3368, 3369, 3370, 3371, 3372, 3373, 3648, 3649, 3650, 3651, 3652, 3653, 3654, 3655, 3656, 3657, 3658, 3659, 3661, 3662, 13832, 13834

United States – Colorado: 10338, 10380, 10389, 10390, 10391, 24166

United States – Illinois: 417, 23304, 23305, 23309, 23311, 23312, 23314, 23377, 23378, 23548, 23552, 23554, 23612, 23613, 23614, 23615, 23617, 23619, 23620, 23621, 23622, 23623, 23644, 23651, 23653, 23656, 23659, 23664, 23667, 23668, 23670, 23678, 23679, 23680, 23682, 23684, 23750, 23751, 23752, 23753, 23756, 23757, 23758, 23761, 23762, 23766, 23767, 23768, 23769, 23770, 23771, 23773, 23775, 23776, 23777, 23778, 23779, 23780, 23783, 23784, 23785, 23788, 23789, 23790, 23791, 23792, 23794, 23795, 23796, 23797, 23798, 23799, 23800, 23801, 23802, 23803, 23804, 23805, 23806, 23807, 23808, 23809, 23810, 23811

United States – Iowa: 330, 416, 417, 13261, 13262, 23116, 23117, 23118, 23119, 23120, 23121, 23304, 23305, 23309, 23311, 23312, 23314, 23377, 23378, 23379, 23552, 23554, 23612, 23613, 23614, 23615, 23617, 23619, 23620, 23621, 23622, 23623, 23644, 23651, 23653, 23656, 23659, 23664, 23667, 23668, 23670, 23678, 23679, 23680, 23682, 23684, 23750, 23751, 23752, 23753, 23756, 23757, 23758, 23761, 23762, 23766, 23767, 23768, 23769, 23770, 23771, 23773, 23775, 23776, 23777, 23778, 23779, 23780, 23783, 23784, 23785, 23788, 23789, 23790, 23791, 23792, 23794, 23795, 23796, 23797, 23798, 23799, 23800, 23801, 23802, 23803, 23804, 23805, 23806, 23807, 23808, 23809, 23810, 23811, 24170, 26683

United States – Kentucky: 369, 375, 10720, 10722, 10745, 10746, 10751, 10752, 10757, 10758, 23386, 23387, 23388

United States – Minnesota: 416, 417, 10754, 10767, 23081, 23083, 23085, 23088, 23092, 23273, 23274, 23276, 23277, 23278, 23279, 23280, 23281, 23282, 23283, 23290, 23309, 23311, 23312, 23314, 23377, 23378, 23379, 23547, 23548, 23550, 23552, 23554, 23555, 23556, 23557, 23558, 23579, 23584, 23588, 23597, 23603, 23607, 23689, 23690, 23691, 23708, 23711, 23717, 23724, 23738, 23741, 23744, 28017

United States – Nevada: 320, 321, 331, 418, 419, 420, 10669, 28161

United States – New York: 328, 332, 333, 334, 335, 337, 338, 340, 436, 23381, 23382, 23383, 23384, 23385

United States – Ohio: 349, 350, 351, 383, 384, 385, 386, 387, 388, 389, 390, 391, 5394, 27500

United States – Oklahoma: 10753, 13815, 13816, 23889, 23892, 23893, 23895, 23896, 23898, 23899, 24105

United States – Tennessee: 1685, 1686, 1687, 1688, 1689, 1690, 1691, 1692, 1693, 1694, 1695, 1696, 1697, 1698, 1700, 1701, 1702, 1703, 1704, 1705, 1706, 1707, 1708, 1709, 1710, 1711, 1892, 1893, 1894, 1895, 1896, 1902, 1905, 1908, 1913, 1916, 1918, 1919, 1921, 1922, 1923, 1924, 1925, 1926, 1928, 1929, 1930, 1931, 1932, 1933, 1934, 1935, 1936, 1937, 1938, 1939, 1940, 1941, 1942, 1943, 1944, 1945, 1946, 1947, 1948, 1949, 1950, 1951, 1952, 1953, 1954, 1955, 1956, 1957, 1958, 1959, 1960, 1961, 1963, 1972, 1973, 1974, 1975, 1976, 1977, 1978, 1979, 5327, 5328, 5329, 5331, 5333, 5346, 5347, 5348, 5350, 5351, 5352, 5355, 5356, 5357, 5358, 5359, 5360, 5361, 5368, 5369, 5370, 5371, 5372, 5373, 5374, 6680, 6682,

6683, 6684, 6685, 6686, 6687, 6688, 6689, 6690, 6691, 6692, 6693, 6694, 6695, 6696, 6697, 6702, 6703, 6704, 6705, 6707, 6708, 6709

United States – Virginia: 326, 327, 343, 344, 5395, 5396, 5397, 5398, 5399, 6276, 6345, 6346, 6351, 6355, 6384, 6385, 6386, 6387, 6388, 6389, 6432, 6436, 6438, 6668, 6671, 6674, 6675, 6677, 6989, 6990, 6991, 7093, 7094, 7095, 7096, 7097

United States – Wisconsin: 416, 417, 23116, 23117, 23118, 23119, 23120, 23121, 23304, 23305, 23309, 23311, 23312, 23314, 23377, 23378, 23548, 23554, 23750, 23751, 23752, 23753, 23756, 23757, 23758, 23761, 23762, 23766, 23767, 23768, 23769, 23770, 23771, 23773, 23775, 23776, 23777, 23778, 23779, 23780, 23783, 23784, 23785

Venezuela: 8858

VITA

Achim D. Herrmann

Achim D. Herrmann was born in Stuttgart, Germany on October 8, 1970.

Education

The Pennsylvania State University, University Park, PA, USA
Ph.D. in Geosciences, 2004
Thesis advisor: Dr. Mark E. Patzkowsky
Thesis: "Late Ordovician ocean-climate system and paleobiogeography"
Universität Heidelberg, Heidelberg, Germany
Diplom in Geology and Paleontology, 1997
Thesis advisors: Dr. Peter Bengtson and Dr. Eduardo Koutsoukos
Thesis: "Geologische Kartierung und Faziesanalyse der Cenoman-Turon Grenzschichten nahe Japaratuba, Nordost-Brasilien"
University of Oregon, Eugene, OR, USA
One year exchange student 1995-1996
Universität Tübingen, Tübingen, Germany
Vordiplom in Geology and Paleontology, 1993

Teaching Experience

The George Washington University, Washington, DC, USA
Visiting Instructor, Fall semester 2003
Bloomsburg University, Bloomsburg, PA, USA
Visiting Instructor, Spring semester 2002
The Pennsylvania State University, University Park, PA, USA
Summer Graduate Lecturer, Summer 2001
Teaching Assistant, Fall 1999-Spring 2001

Selected Publications

Herrmann, A.D., Patzkowsky, M.E., and D. Pollard (2003) Obliquity forcing with 8-12x pre-industrial levels of atmospheric pCO_2 during the Late Ordovician glaciation. Geology, 31/6, 485-488.

Herrmann, A.D., Patzkowsky, M.E., and S.M. Holland (2003) BIOMODULE: A Java program to help model and interpret the stratigraphic record. Computers and Geosciences, 29/1 pp. 99-105.